2011

Conformation and ion transport of neuronal uncoupling proteins: UCP2, UCP4, and UCP5

Tuan Hoang

Wilfrid Laurier University, hoan4940@mylaurier.ca

CONFORMATION AND ION TRANSPORT OF NEURONAL UNCOUPLING PROTEINS: UCP2, UCP4, and UCP5

By

Tuan Hoang

B.Sc. Biochemistry/Biotechnology, Wilfrid Laurier University, 2009

THESIS

Submitted to the Department of Chemistry

In partial fulfillment of the requirements for

Master of Science in Chemistry

Wilfrid Laurier University

ABSTRACT

Located in the inner mitochondrial membrane of brown adipose tissue, uncoupling protein -1 (UCP1) dissipates the proton electrochemical gradient, causing reduction in the rate of ATP synthesis, and generates heat by non-shivering thermogenesis. Three other UCP homologs (UCP2, UCP4 and UCP5), expressed in neurons, are suggested to have potential roles in the function and protection of the central nervous system (CNS). Up to date, structural information for UCPs still remains limited. Extensive biochemical studies on UCP2 have provided adequate evidence for its participation in proton and anion transport. So far, no functional studies in proteoliposome systems have been performed on UCP4 and UCP5. Thus, the goals of this study are to gain further information on the conformations and functional properties of neuronal UCPs reconstituted in liposomes. The emphasis is on UCP4 and UCP5 and their comparison to UCP2. Recombinant versions of all neuronal UCPs were successfully expressed, purified and reconstituted in azolectin liposomes (with and without the supplement of 2.5 mol% cardiolipin). UCP2 and UCP4 showed a high α-helical content in liposomes, while UCP5 conformation was less helical, with conformations exhibiting β-sheet characteristics. Ion transport assays (proton and chloride) for reconstituted neuronal UCPs were successfully developed using anion-sensitive fluorescent probes. All neuronal UCPs displayed proton transport across the membrane with characteristics similar to the archetypical protein UCP1, which is activated by fatty acids and inhibited by purine nucleotides. Chloride anion transport is also shown for UCP2 and UCP4. In addition, it was observed that the mitochondrial lipid cardiolipin (CL) induced drastic changes in conformation and ion transport of reconstituted UCPs. A hypothesized interaction mechanism of UCPs and CL was drawn from experimental results and molecular modelling. Overall, this study has provided a detailed picture of the conformation and ion transport properties of neuronal UCPs in liposomes, and also emphasizes the crucial role of cardiolipin in UCP structure and function.

ACKNOWLEDGEMENTS

I want to acknowledge and appreciate the mentorship of my co-supervisors: Dr. Masoud Jelokhani-Niaraki and Dr. Matthew D. Smith. Being my supervisor for the last three years, Dr. Jelokhani has given me limitless support in both scientific work and personal life. Working for Dr. Smith has been my great pleasure. I see him not only as my mentor but also as my friend. I consider myself very fortunate to be able to continue working under the supervision of both Dr. Jelokhani and Dr. Smith for my PhD program in the coming years. I want to also acknowledge the support from Dr. Arthur Szabo and Dr. Frances Sharom. I cannot thank Marina V. Ivanova enough for her help throughout my undergraduate and graduate degrees. I also want to acknowledge the countless emails from Dr. Eva Urbánková, who contributed a great deal to my success in building the proton transport assay in proteoliposomes. I want to thank all the members in both the Jelokhani and Smith labs, especially Dr. Siddhartha Dutta, Dr. Geetika Patel, Kyle Weston, Tijana Matovic, Matthew Nichols, and Baindu Kosia for their company and help. My thanks go to Gena Braun and Dr. Jiangxiao Sun for their technical assistance. I am also very grateful for the mental support from all my close friends, especially Nguyen Vo, Gabriela Krnac, Payal Patel and Ashtina Appadu. Finally, I want to thank my sister Tu Hoang and my parents for being with me through all the fun and "not-so-fun" times in life. I could have never made it without your constant support and belief in me. This study was generously funded by NSERC CGS-M and OGS graduate scholarships.

DECLARATION OF WORK PERFORMED

All data presented and described in this thesis are the results of my own work. Furthermore, I hereby declare that I am the sole author of this thesis that includes all final revisions, as accepted by my examiners.

TABLE OF CONTENTS

LIST OF TABLES

MAIN TEXT

Table 1: Primary amino acid sequence homology of UCPs and ADP/ATP carrier (AAC)   36

Table 2: Sizes of UCP proteoliposomes determined by dynamic light-scattering   43

Table 3: Secondary structure composition of neuronal UCPs in lipid vesicles   59

APPENDICES

Table 4: Some common motifs among MCF members   92

LIST OF FIGURES

APPENDICES

LIST OF ABBREVIATIONS

AAC	ADP/ATP carrier
Arg	arginine
ADP	adenosine diphosphate
ATP	adenosine triphosphate
BAT	brown adipose tissue
BMCP1	brain mitochondrial carrier protein-1
BSA	bovine serum albumin
CAPS	N-cyclohexyl-3-aminopropanesulfonic acid
CATR	carboxyatractyloside
CoQ	Coenzyme Q
CD	circular dichroism
CL	cardiolipin
CMC	critical micelle concentration
CNS	central nervous system
CCCP	carbonylcyanide-3-chlorophenylhydrazone
DIC	dicarboxylate carrier
DNA	deoxyribose nucleic acid
EB	extraction buffer
EDTA	ethylenediaminetetraacetic acid
ETC	electron transport chain
FA	fatty acid
$FADH_2$	reduced flavin adenine dinucleotide
FCCP	carbonylcyanide-p-trifluoromethoxyphenylhydrazone
GDP	guanosine diphosphate
Glu	glutamic acid
GSIS	glucose-stimulated insulin secretion
GTP	guanosine triphosphate
His	histidine
IB	inclusion body

IMAC	immobilized metal affinity chromatography
IMS	Intermembrane space
IPTG	isopropyl-β-D-thiogalactoside
LA	lauric acid
LB	Luria-Bertani
LUV	large unilamellar vesicle
MCF	mitochondrial carrier protein family
NADH	nicotinamide adenine dinucleotide
NMR	nuclear magnetic resonance
OGMC	oxoglutarate/maleate carrier
ORD	optical rotary dispersion
P_i	inorganic phosphate
PC	phosphatidylcholine
POPC	1-palmitoyl-2-oleoyl-*sn*-glycero-3-phosphocholine
POPG	1-palmitoyl-2-oleoyl-*sn*-glycero-3-[phospho-*rac*-1-glycerol] (sodium salt)
RDC	residual dipolar coupling
ROS	reactive oxygen species
SDS-PAGE	sodium dodecyl sulfate polyacrylamide gel electrophoresis
SPQ	6-methoxy-N-(3-sulfopropyl) quinolinium
SUV	small unilamellar vesicle
TCA	trichloroacetic acid
TEA	Tetraethylammonium
TES	N-tris(hydroxymethyl)methyl-2-aminoethanesulfonic acid
TEV	tobacco etch virus
TM	transmembrane domain
UCP	uncoupling protein
UV	ultraviolet
val	valinomycin
λ_{max}	wavelength of fluorescence emission maximum

CHAPTER 1 – INTRODUCTION

1.1.Mitochondria: The power house of the cell and the source of degenerative diseases

1.1.1.   A brief introduction to the morphology and function of mitochondria

Mitochondria play an important role in being the main power plants in eukaryotic cells. They are the main production site of the cellular energy unit adenosine triphosphate (ATP). Thus, these organelles are found to be particularly abundant in tissues and cells with high metabolic activity such as muscle cells, where ATP is in high demand [1].

Mitochondria are rod-shaped organelles that are enclosed within two membranes – the outer membrane and the inner membrane [2]. The outer membrane contains a number of porins allowing non-specific transport of solutes with molecular weights up to 5000 Da [2]. This outer phospholipid membrane acts as a protective layer for the organelle. On the other hand, the inner mitochondrial membrane presents a permeability barrier to most solutes, thereby partitioning the intermembrane space and the interior matrix of the mitochondria. Composed of a more complex mixture of phospholipids, the inner membrane has high membrane protein content and is particularly rich in enzymes that are crucial for mitochondrial functions. In fact, proteins account for about 75% (by weight) of the inner membrane [1]. To better accommodate the respiration process and the membrane proteins embedded, the inner membranes of most mitochondria have many distinctive infoldings called cristae that greatly increase the inner membrane's surface area [1].

Another important feature of the inner mitochondrial membrane is the high content of cardiolipin (CL) [3]. In eukaryotes, CL is the only phospholipid that is synthesized in the mitochondria, where it remains until the cell dies [3]. Acting as a "double phospholipid", CL has two phosphatidylglycerols connected through a glycerol backbone in the centre to form a dimeric

structure (Appendix 1). Carrying two phosphates in the head group, CL can potentially hold

protons. Moreover, the two phosphate groups display different pK values (3 and 7.5), which

results in a net single negative charge of the phospholipid at physiological pH [3]. CL was also

shown to have a high binding affinity to many inner mitochondrial membrane proteins that are

actively involved in ATP synthesis and transport in mitochondria [4-9]. The proteins that CL has

been shown to interact with include cytochrome oxidases [4, 5], the ADP/ATP carrier (AAC)

[6], ATP synthases [7], orthophosphate transporters [8], and cytochrome bc_1 complexes [9]. The

strong binding between CL and these proteins is suggestive of an important role of this

phospholipid in mitochondrial metabolism and transport. Finally, an important characteristic of

the mitochondria is its genome. Human mitochondrial DNA was discovered in 1966 and contains

37 genes that encode two ribosomal mitRNA, 22 mitRNA carriers, and 13 polypeptide chains,

which are essential in electron transport chain complexes [1]. Other nuclear-encoded proteins

that are present in the organelle are imported through the cytosol from the nucleus.

1.1.2. Oxidative phosphorylation

Production of ATP through oxidative phosphorylation is the most important function

performed by the mitochondria. The mechanism of ATP formation in mitochondria was first

proposed by Mitchell in 1961 [10]. Electrons generated during substrate oxidation associated

with cellular metabolism are produced in the form of reduced hydrogen carriers such as NADH

and $FADH_2$, and carried through the respiratory chain located in the inner mitochondrial

membrane [11]. Electron carriers in the electron transport chain (ETC) are organized into four

large respiratory complexes. Complex I (NADH-coenzyme Q oxidoreductase) transfers electrons

from NADH to coenzyme Q (CoQ). Complex II (succinate-CoQ oxidoreductase) transfers

electrons from succinate to CoQ. The electrons from CoQ in both complex I and II are then

passed to cytochrome c in complex III (CoQ-cytochrome c oxidoreductase). Complex IV (cytochrome c oxidase) finally transfers electrons from cytochrome c to oxygen [11].

Concurrently with electron transport, protons are pumped from the mitochondrial matrix into the mitochondrial intermembrane space, which establishes a proton electrochemical gradient (Δp) across the inner mitochondrial membrane (Fig. 1). This proton motive force is dissipated when the protons travel back into the matrix, mainly through the F_0F_1 ATP synthase, an inner mitochondrial membrane protein that generates ATP from ADP and P_i [12]. Therefore, the crucial link between electron transport and ATP production is the electrochemical proton gradient. In the event that these processes occur at 100% efficiency, electron transport is perfectly coupled with ATP production [11].

However, the energy available in the electrochemical gradient is not entirely coupled with the ATP synthesis by ATP synthase. Evidence from different experiments suggests that uncoupling oxidative phosphorylation is another pathway of dissipating the energy via proton leak [13-15]. This uncoupling process can be mediated through the ADP/ATP carrier [13], the glutamate carrier [14], complexes such as the mitochondrial permeability transition pore [15], and the uncoupling protein (UCP) [16] (Fig. 1). The uncoupling effect can also occur through the introduction of synthetic uncouplers such as dinitrophenol, carbonylcyanide-*p*-trifluoromethoxyphenylhydrazone (FCCP), and carbonylcyanide-3-chlorophenylhydrazone (CCCP) [16]. Accounting for 25% of the basal metabolic rate, uncoupling is suggested to be an important process [17]. Some essential roles of uncoupling shown in different studies include thermogenesis, regulation of energy metabolism or carbon fluxes, control of body mass, glucose sensing, and attenuation of reactive oxygen species (ROS) production [16].
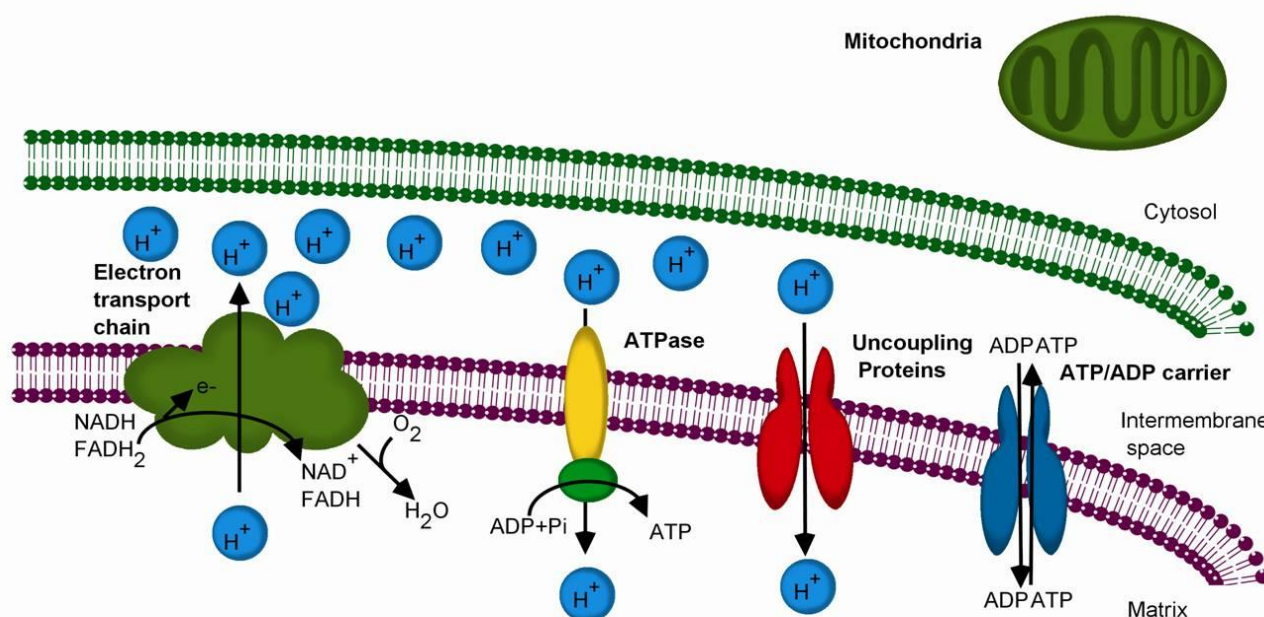
Figure 1 – **Oxidative phosphorylation and the proton leak pathway in mitochondria**

Electrons generated from oxidized substrates are transported through complex I- IV (all complexes together are represented as a green cloud) in the respiratory chain located in the mitochondrial inner membrane, and ultimately transported to molecular oxygen, which is reduced to water. Dissipation of the proton motive force is achieved through either coupling with ATP synthesis or uncoupling process via UCP. ADP and ATP are transported in and out of the matrix via the AAC .

1.1.3. Mitochondria: the major site for reactive oxygen species (ROS) production

Being the main ATP production factory, mitochondria are also the primary site for superoxide production, where superoxide anion ($O_2^{\bullet -}$) is the main precursor [16]. The production of ROS is a major cause of cellular oxidative damage that subsequently leads to degradative diseases and aging [16]. A recent study has suggested that complex I in the mitochondrial electron transport chain produces most of the superoxide, although the exact site(s) of superoxide production in this complex is still uncertain [13]. Other complexes in the ETC have also been shown to be capable of generating superoxide, especially in the presence of electron transport inhibitors [18]. Superoxide produced in the mitochondria is extremely reactive. They usually participate in fast chain reactions and result in degradative effects. Oxidative stress causes damage to cellular macromolecules such as nucleic acids, proteins, carbohydrates and lipids, and consequently leads to their loss in structure and function. These damages are the causative agent to many pathological conditions, including atherosclerosis, hypertension, ischemia-reperfusion, cystic fibrosis, cancer, diabetes, Parkinson's disease, and Alzheimer's disease [16]. Aging has also recently been proposed to be related closely to oxidative stress [16]. Thus, reduction of superoxide production is suggested to play an important role in cellular protection and survival. There are several mitochondrial antioxidant defence systems, including enzymes (i.e. catalase, superoxide dismutase, peroxidase), low molecular weight antioxidants (i.e. ascorbate, glutathione, phenolic compounds, tocopherols), and several electron carriers (i.e. Ubiquinone, CoQ) [16]. Mild uncoupling actions, which yield a small decrease in membrane potential, are also suggested to have a natural antioxidant effect [19].

1.2. Neuronal uncoupling proteins: Structure, function and physiology

1.2.1. Uncoupling proteins

UCPs, located in the inner mitochondrial membrane, are members of the mitochondrial carrier protein family (MCF) [20]. The proteins in this family were shown to share some common structural/topological characteristics [20]. All proteins in MCF are encoded by nuclear genes. The primary structures of these proteins are proposed to have a tripartite structure that consists of three repeat domains, each consisting of two hydrophobic transmembrane (TM) α-helical regions spanning across the inner mitochondrial membrane [6, 20]. The two attached helices that make up each repeated region are connected by a long hydrophilic loop oriented towards the matrix. In addition, both the N- and C-termini of these proteins are located on the mitochondrial intermembrane space [6, 20]. Finally, a common MCF motif, PxD/ExxK/RxK/R-(20-30 residues)-D/EGxxxxaK/RG, can be found in each repeated region with slight deviations on one or two signature sequences for some carriers [6, 20]. The proline residues located in the motif induce a kink that is responsible for the closed form towards the matrix, while charged amino acids such as arginine and lysine can form salt bridges that strengthen the closed conformation of the helix bundle [20].

There are five human UCP homologs identified to date, of which UCP1, 2, and 3 have been characterized most thoroughly [20]. UCPs have also been found in other vertebrates and invertebrates. Three isoforms of UCPs are also present in the model plant *Arabidopsis thaliana* (named PUMP or plant uncoupling mitochondrial proteins) [21]. Most molecular and structural studies on human UCPs have been hampered due to the lack of available crystal structures. Given the similarity in molecular weight (30-35 kDa) and primary sequence (~20% identity), the structure of the prototypical UCP1 and other UCPs have been assumed to resemble the crystal

structure of the ADP/ATP carrier (AAC) membrane protein [22]. The archetypal protein human UCP1 was found to be expressed predominantly in brown adipose tissue (BAT) [23]. UCP1-mediated proton leak, causing uncoupling effects, was confirmed to be activated by free fatty acids and inhibited by purine nucleotides (ATP, ADP, GTP, and GDP) [20]. Its physiological role has been determined to be in mediating a regulated, thermogenic proton leak in BAT. This excessive proton flux by UCP1 allows non-shivering thermogenesis in newborns, cold-acclimatized, hibernating mammals and overfed rodents [20, 23].

Among all human UCP homologs, UCP2 and UCP3 share the most common primary amino acid sequence with UCP1 (59% and 57% sequence identity to UCP1, respectively, and 73% to each other) [20]. These homologs, however, are expressed in different tissues. UCP3 is expressed primarily in skeletal muscle but may also be found in cardiac muscle and BAT [24-26]. UCP2 mRNA expression is ubiquitous in different tissues and cell types, varying from kidney to the nervous system [20]. It is important to note that despite the mRNA expression found in heart tissues, skeletal muscle and BAT, no UCP2 protein could be detected in these sites [27, 28]. This might be a strong implication for a translational regulation of UCP2 expression. Unlike other UCPs, UCP4 and UCP5 are expressed predominantly in the central nervous system (CNS) and share the lowest amino acid sequence identity with other members in the family [29, 30]. Thus, the amount of research on these two proteins has been minimal, which consequently leads to little biochemical information being available for UCP4 and UCP5.

1.2.2.   *UCP-mediated proton transport*

To date, extensive biochemical studies have been performed on UCP1, 2, and 3 due to their widespread expression and highly similar sequences [20]. All of these UCPs have been shown in proteoliposome systems to facilitate proton transport in the presence of fatty acids

(FAs), and this proton transport is inhibited by different types of purine nucleotides (ATP, ADP, GTP and GDP) to various degrees. UCP4 and UCP5 have been recently shown to have uncoupling effects in cells; however, their ion transport properties in proteoliposomes have not been investigated previously [29, 30].

1.2.2.1.UCP-mediated proton transport is activated by fatty acids

Although the activation of proton transport through UCP1-3 has been demonstrated, the activation mechanism by FA is still debated [20]. There are two main mechanisms proposed by different groups, including the flip-flop model and the cofactor model (Fig. 2) [20]. Inconsistent results from different studies have meant that a clear consensus mechanism has not been reached for FA-induced proton transport by UCP [31-36].

The flip-flop model (also known as the anion transport model) proposes that indirect proton transport through UCP1 is achieved by the transport of protonated FA across the membrane [20, 31-34]. In this model, protonated FA crosses the mitochondrial inner membrane into the matrix by a flip-flop action, dissociating a proton after which, the resulting FA anion is translocated out of the matrix through an unknown interaction with UCP. Several lines of evidence support this hypothesis [31-34]. First of all, UCP1 genetically belongs to the family of anion carriers [20]. Moreover, UCP1 is known to transport various anions such as Cl^-, NO_3^-, etc [31, 32]. Support for the anion transport model also comes from the ability of UCP1 to transport alkylsulfonates [33]. These FA analogs possess very low pKa values; thus, are unable to be protonated at physiological pH. Proton transport in the presence of alkylsulfonates was therefore not observed. Alkylsulfonates were also found to competitively inhibit FA-induced proton transport [34].

In the cofactor model (also known as the proton-buffering model), carboxyl groups from both FA (COO^-) and amino acid residues ($R\text{-}COO^-$) accept protons from the intermembrane space and transport them into the matrix through a channel in the UCP [20, 35, 36]. This proton transport is possible through proton donation by free FAs to proton-buffering amino acids in UCP. Strong evidence supporting this idea is the existence of the E167Q mutant in UCP1 expressed in *S.cerevisae,* which was reported to lose Cl^- transport capability while retaining proton transport activity [35]. In addition, the overall measured chloride transport rate in wild-type UCP1 was about an order of magnitude slower than proton transport, which partially supports the idea of UCP having separate mechanisms for transporting protons or anions across the inner membrane.
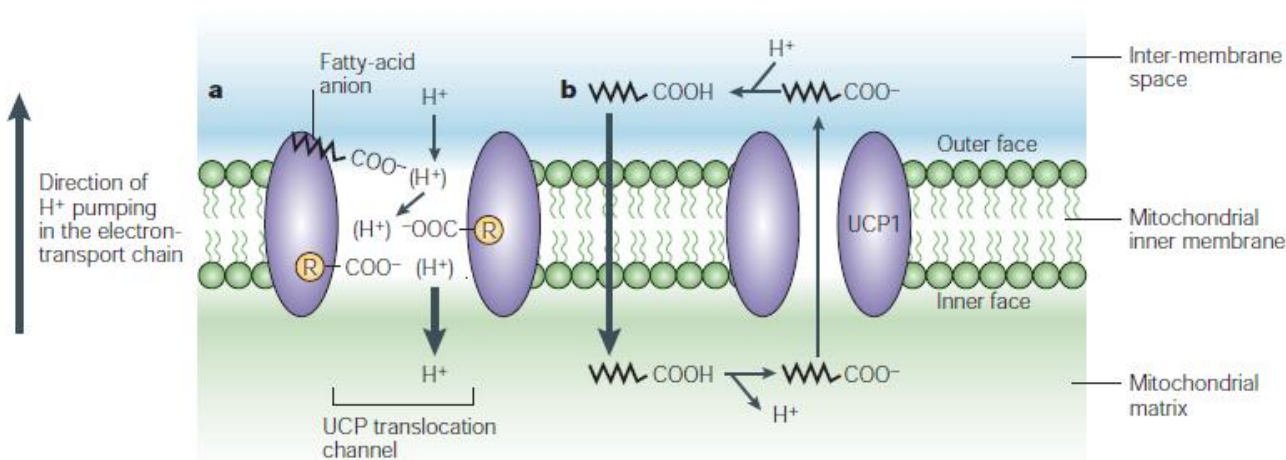
<u>Figure 2</u> – **Two proposed FA activation mechanisms of UCP1-mediated proton flux** [20]

The cofactor model (a) suggests the fatty acyl carboxyl groups (COO⁻) and the carboxyl groups from UCP1 (R-COO⁻) are the main tools providing a channel in transporting protons into the mitochondrial matrix. In the FA-cycling model (b), protonated FAs in the membrane space freely flip flop across the mitochondrial inner membrane into the matrix independent of UCP1. Due to pH difference in the matrix, protons are dissociated from the FAs and the resulting FA anions are being transported back into the intermembrane space by UCP1. Functional UCP1 was suggested to be in a dimeric form. Reprinted by permission from Macmillan Publishers Ltd: [Nature] (Krauss, S., Zhang, C.Y. and Lowell, B. B. (2005). The Mitochondrial Uncoupling Protein Homologues. *Nat. Rev. Mol. Cell. Bio.* **6**, 248-261), copyright (2005).

1.2.2.2.<u>*UCP-mediated proton transport is inhibited by purine nucleotides*</u>

The inhibitory role of purine nucleotides on proton transport mediated by UCPs (1-3) has been confirmed by many studies; however, the binding mechanism is still unresolved. The inhibitory effect was first shown by the reduced uncoupled respiration of BAT mitochondria after addition of purine nucleotides such as ATP, ADP, GTP, and GDP [37]. *In vitro* studies showed that binding of purine nucleotides to UCP1 occurs in the micromolar range, while physiological concentration of purine nucleotides is in the millimolar range [35]. This raised the question whether UCP can ever be released from nucleotide inhibition under normal cellular conditions. An explanation for this phenomenon is that binding only occurs between UCP1 and the free-form of purine nucleotides (non-Mg^{2+}-complexed) [38].

Site-directed mutagenesis studies have revealed some key UCP1 amino acid residues involved in purine nucleotide binding events. Consequently, a plausible three-stage binding mechanism for nucleotide binding was proposed (Fig. 3) [39-41]. In brief, the initial loose binding occurs between Arg182 and the sugar-based moiety of purine nucleotides. Following this step, the protonation of Glu190 leads to tight binding between Arg83 and the second charge on the β-phosphate (or the γ-phosphate) of diphosphates (or triphosphates). Finally, the inhibited conformation occurs once the nucleotide is firmLy bound to Arg276. It is suggested that this final step causes a change in the conformation of UCP1, which consequently inhibits proton transport [41]. The key amino acids in the proposed nucleotide binding mechanism are either the identical residues (R83, R182, and R276) or the conserved substitute (E190) in all UCP homologs. Another unique feature of the nucleotide binding to UCP1 is pH dependence. The plot of binding constant (pK_D) versus pH illustrated a reduced binding affinity between UCP1 and nucleotides when pH is increased [42].
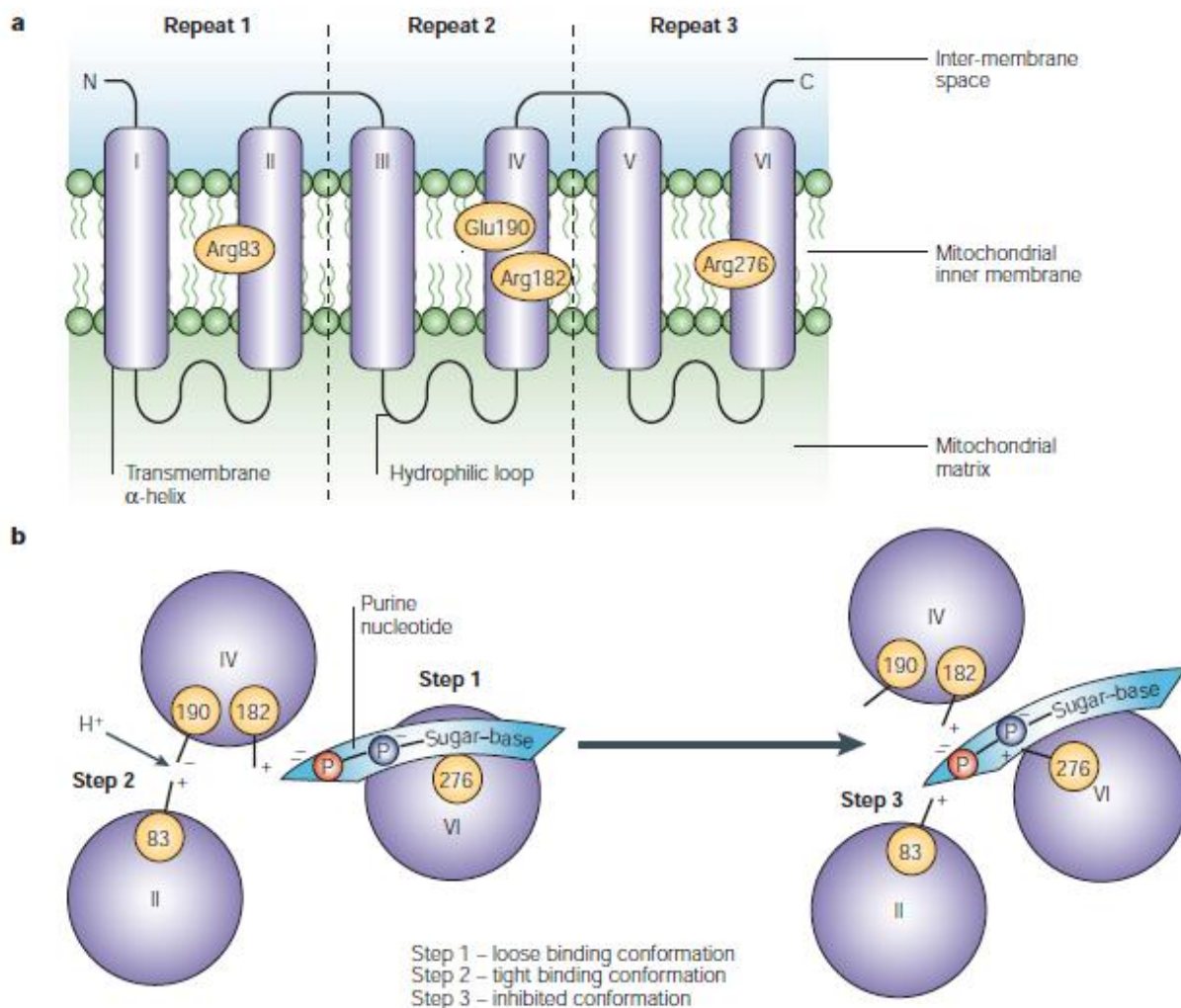
Figure 3- **Structural characteristics of UCP1 derived from biochemical studies** [20]

(a) Tripartite structure that UCP1 shares with ANT protein. (b) Proposed binding mechanism between UCP1 and purine nucleotides, including three stages of conformational changes – loose binding conformation, tight binding conformation, and inhibited conformation. Reprinted by permission from Macmillan Publishers Ltd: [Nature] (Krauss, S., Zhang, C.Y. and Lowell, B. B. (2005). The Mitochondrial Uncoupling Protein Homologs. *Nat. Rev. Mol. Cell. Bio.* **6**, 248-261), copyright (2005).

1.2.3. *UCP-mediated anion transport*

A patch-clamp study by Huang *et al.* in 1996 showed the ability of UCP1 to transport chloride anions [43]. The transport in this study was shown to be independent of pH and sensitive to purine nucleotides [43]. Later on, fluorescent probes were used to show transport of various anionic substrates by UCP1-3 [44]. The study of Ježek *et al.* in 1994 showed the interaction of FAs and anion transport through UCP1 [34]. Competitive inhibition of lauric acid (LA) on chloride transport, as well as the competitive inhibition of anions (nitrate and hexanesulfonate) on laurate-induced proton transport by UCP1 indicated a strong possibility of one common pathway for transport of anions [34]. Anion transport has been used very often as a strong argument for finding the mechanism of transport mediated by uncoupling proteins. A study by Garlid *et al.* in 1996 provided insight on chloride transport that further supported the FA cycling mechanism in UCP-catalyzed proton transport [45]. In this study, undecanesulfonate and LA both induced GDP-sensitive anion flux. However, undecanesulfonate did not induce any proton flux. In addition, both undecanesulfonate and LA inhibited transport of chloride and undecanesulfonate inhibited competitively lauric-induced proton flux of UCP1. Supporters of the cofactor model of UCP-mediated proton transport, on the other hand, used the differences between chloride and proton transport as a strong reasoning for their model [35, 42]. The distinction between the two types of transport was pointed out in their transport rate (proton transport was usually shown to be 10x faster than chloride transport), and the involvement of key amino acid residues in each transport (mutagenesis studies showed that a mutant E167Q of UCP1 abolished chloride transport, while maintaining proton flux) [35, 42]. The "Divide-and-conquer" method was used to determine the important anion transport site [46, 47]. While UCP2

and UCP3 were also shown to transport anions across the mitochondrial membrane, the relationships of anion and proton transport in all UCPs are still debated.

1.2.4. *Neuronal uncoupling protein homologs and their roles in the CNS*

Three of the five UCP homologs, namely UCP2, UCP4 and UCP5, are located in the CNS and are therefore believed to serve unique roles in neurons [48] (Fig. 4). However, no solid model for their roles in the CNS has been established. To date, UCP1 is the only UCP whose physiological role is well understood. Its thermogenic uncoupling function has been widely agreed upon among the scientific community [48]. Given a much lower concentration of other UCPs in the mitochondria of different tissues, it is unlikely that they play the same thermogenic role as UCP1. Expression of UCP2 mRNA can be found in heart, lung, white and brown adipose tissue, stomach, testis, and macrophages. High sequence homology to the prototypical UCP1 (59%) and ubiquitous expression have made UCP2 an attractive protein for many recent studies [20]. Currently, the most important focus on UCP2 is its ability to suppress ROS levels [20]. Numerous studies have focussed on the role of UCP2 in diseases such as cancer (chemoresistance marker), heart disease (myocardial ROS production during exercise), and obesity (food-induced thermogenesis) [49-53]. UCP2 is also expressed in β-cells, which triggered studies of UCP2 in β-cell dysfunction and type-2 diabetes [54, 55]. In a type-2 diabetes study, it was shown that UCP2 acts as a negative regulator of insulin secretion. Overexpression of UCP2 in pancreatic β-cells resulted in decreased ATP production (hence low ATP/ADP ratio), which subsequently led to the loss of glucose-stimulated insulin secretion (GSIS) [55]. In the brain, UCP2 mRNA is abundantly expressed in the hypothalamus, limbic system, cerebellum, choroids plexus, and brainstem [48, 56]. The abundance of UCP2 mRNA and protein in the hypothalamus indicates an important role of this protein in metabolic, autonomic and endocrine

regulation. Despite controversies in different studies, the proton transport activity regulation of UCP2 has been confirmed to be similar to that of UCP1, including fatty acid activation and purine nucleotide inhibition [57].

Although both UCP4 and UCP5 (also called brain mitochondrial carrier protein-1, BMCP1) are more widespread in the brain than UCP2, there is little known about these two proteins. UCP4 was found originally to be only expressed in the brain [29], but has been recently discovered also in adipocytes [58]. On the other hand, UCP5 has been expressed in diverse tissues and organs, including brain (cortex, hypothalamus, limbic system, cerebellum, basal ganglia, and spinal cords), testis, uterus, kidneys, lungs, stomach, liver and heart [16, 30, and 48]. There is also evidence for isoforms of UCP5 mRNA in fruit flies, supporting an important and evolutionarily retained function for this putative UCP in the CNS [59]. In humans, there are three isoforms of UCP5, including a "long" 325-amino acid form (UCP5L), a "short" 322-amino acid form (UCP5S) that lacks Val-Ser-Gly, and a "short-insert" 353-amino acid form (UCP5SI) that lacks the VSG sequence but has a 31-amino acid insertion between transmembrane domains III and IV [16, 60]. The presence of these isoforms suggests a complexity in function and regulation of UCP5 in the brain. UCP4 has also been reported to have isoforms of varying lengths [61].

There are suggestions that UCP4 and UCP5 do not even belong to the UCP family, due to their low protein sequence homology to the prototypical protein UCP1 (34% for UCP4 and 30% for UCP5), their distribution on the phylogenetic tree, and their slightly higher molecular weight compared to other UCPs (36-38 kDa for UCP4 and UCP5 compared to 31-34 kDa for UCP1-3) [16, 20]. In addition, transport properties of these proteins (i.e. proton transport being activated by FAs, and inhibited by purine nucleotides) have not yet been studied. Therefore, as pointed out

by many review articles, the question whether UPC4 and UCP5 are genuine mitochondrial UCPs remains to be answered [16, 20].

Although a thorough understanding has not yet been achieved for neuronal UCPs, their significance in cell metabolism and survival has been confirmed [48]. Cell culture studies showed that transfecting cells with UCP2, UCP4, or UCP5 resulted in a decrease in mitochondrial membrane potential, which indicates the uncoupling activity is consistent among all three neuronal UCPs [48]. These studies also proposed a mechanism through which neuronal UCPs can regulate neuronal functions. A list of physiological roles for neuronal UCPs has been suggested, including thermal synapses, calcium regulation, ROS production regulation, and pain tolerance (Fig. 4) [48]. These physiological functions of neuronal UCPs play an important part in neurodegenerative diseases such as epilepsy, Parkinson's disease, ischemia and traumatic brain injury, Alzheimer's disease, and aging [48].
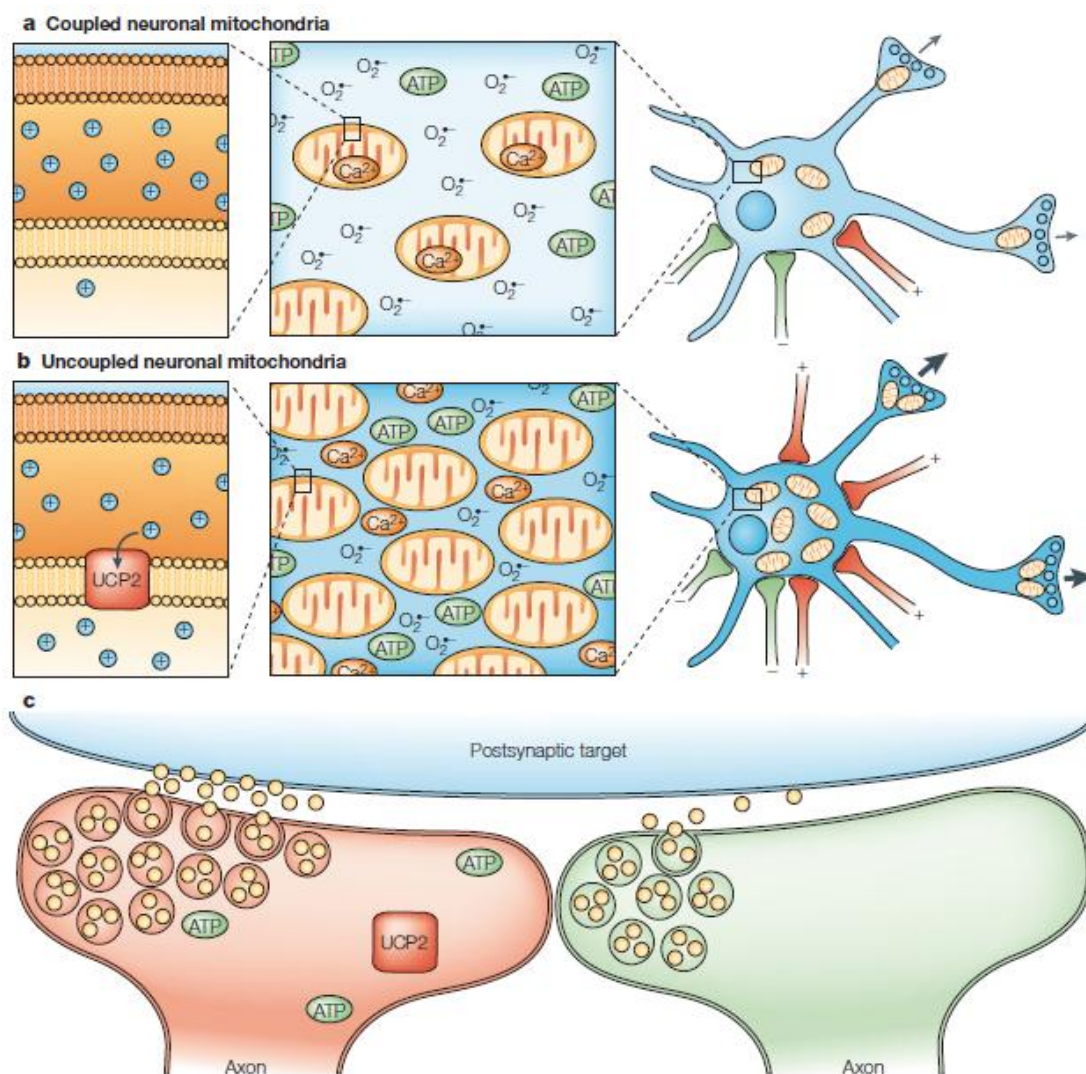
Figure 4 – **Proposed mechanism for neuronal UCPs in regulating neuronal functions** [48]

(a) Coupled neuronal mitochondria have a large membrane potential, which promotes a strong proton motive force across the inner membrane, thus driving the increased formation of ROS and calcium influx. These events are known to promote neuronal dysfunction and eventually limit synaptic plasticity and neurotransmission. (b) The presence of neuronal UCPs (UCP2 in this case) allows a proton leak to occur and hence decreases the mitochondrial membrane potential. This helps diminish the ROS production and mitochondrial calcium efflux is increased. (c) Enhanced neurotransmission is achieved through a UCP-induced mechanism. Local heat generated from uncoupling activity increases neurochemical diffusion through extracellular compartments to postsynaptic neuronal targets. Reprinted by permission from Macmillan Publishers Ltd: [Nature] (Andrews, Z. B., Diano, S. and Horvath, T.L. (2005). Mitochondrial Uncoupling Proteins in the CNS: In Support of Function and Survival. *Nat. Rev. Neurosci.* **6**, 829-840), copyright (2005).

CHAPTER 2 – BIOPHYSICAL TECHNIQUES for STUDYING STRUCTURE and FUNCTION of MEMBRANE PROTEINS

2.1. Detergent-mediated reconstitution of membrane proteins

In vitro studies offer an advantage compared to *in vivo* studies, by eliminating interfering signals contributed by other components of the system. An *in vitro* system is better defined, and therefore should present a "cleaner" system. These studies usually involve generating a chemical quantity of a biomolecule of interest and transferring it into a setting that mimics the *in vivo* environment. In order to study the biological functions of membrane proteins, building compartments in the form of synthetic phospholipid vesicles, called liposomes, is often used [62]. This allows the membrane proteins to assemble and fold correctly in an artificial membrane to carry out their functions. Liposome vesicles embedded with membrane proteins are called proteoliposomes [62]. Several methods can be used to produce proteoliposomes, including detergent-mediated reconstitution, direct incorporation into preformed vesicles, reversed phase evaporation, and others [63]. Since the detergent-mediated reconstitution method is the most commonly used technique and will be used in this study, it will be described in more detail here.

Generally, detergent-mediated reconstitution involves the solubilization of phospholipids with detergents, followed by incorporation of purified proteins into the lipid-detergent mixed micelles; proteoliposome formation is facilitated through detergent removal [63]. The reconstitution process is strongly dependent on different parameters, including the types of lipid bilayer structures, detergents, lipid composition, method of detergent removal, and ratios of macromolecule components in the system (i.e. proteins, lipids, and detergents) [63]. Modification of any of these parameters could lead to changes in the efficiency of reconstitution and in the final protein structure and function.

Large unilamellar vesicles (LUVs) are usually the liposome of choice for reconstitution of membrane proteins, due to their stability and homogeneity [64]. The diameters of LUVs are usually from 50 nm to 1 μm [64]. LUVs can be readily formed by the removal of detergent from lipid-detergent mixtures, thus allowing the simultaneous incorporation of the membrane protein that is solubilized in the detergent [64]. LUVs can also be generated using the freeze-thaw/extrusion method [63]. Due to the stability of LUVs, this type of phospholipid vesicle is very suitable for functional studies of membrane transporters. On the other hand, small unilamellar vesicles (SUVs), with a homogenous diameter of ~30 nm, are more advantageous for spectroscopic studies [64]. SUVs, however, are inherently unstable because of their high curvature [63]. Hence, they usually fuse to give larger vesicles of lower curvature over a certain time interval (24-48 h) [64].

Lipid composition is another important factor in any reconstitution process. The lipid components represent the micro-environment that surrounds the membrane proteins. Each type of lipid not only differs in its molecular weight and chemical properties, but also in curvature, which eventually leads to the different morphologies and organization of the liposomes. Some membrane proteins have a specific preference for certain lipids to promote their activity. For instance, the AAC was shown to require the presence of CL for its activity [65, 66]. Given the similarity between AAC and UCPs (~25%), it has been suggested that CL should be present in the lipid phase to yield UCPs' active form [67]. In this study, two systems of phospholipid will be examined (PC and PC supplemented with 2.5 mol% CL) to understand the role of CL in neuronal UCPs' conformation and transport activity.

Removal of detergents is the last step of protein reconstitution into liposomes and also one of the most important steps in the procedure [63]. Progressive removal of detergents results

in the spontaneous formation of lipid bilayer structures, which is the most energetically favoured arrangement for most phospholipids in water [64]. Ideally, detergents should be removed completely, since any traces of detergent may cause liposome leakage. To remove detergents, several methods have been used [63]. In general, if detergents have high critical micelle concentration (CMC), removal of detergents could be done through dialysis. On the other hand, detergents with a low CMC are usually removed via hydrophobic adsorption onto polystyrene beads. This method was introduced by Holloway in 1973 and has been used frequently since then [68]. The rate of detergent removal, which can be controlled by the amount of beads and the incubation temperature, is a key parameter in reconstitution studies [69]. Overall, reconstitution is a powerful tool for membrane protein studies. However, experimental parameters need to be controlled carefully to achieve reproducible and successful results.

2.2. Circular dichroism (CD) spectroscopic analysis of protein conformations

Circular dichroism (CD) spectroscopy is a tool for rapid determination of average secondary structure of purified proteins [70]. Optical rotation occurs when circularly-polarized light rays travel through an optically active medium with different velocities due to the different indices of refraction for right- and left-circularly polarized light [70]. The variation of optical rotation as a function of wavelength is called optical rotary dispersion (ORD). Based on the differential absorption between left- and right-handed circularly polarized radiation by chromophores, which either possess intrinsic chirality or are subject to a chiral environment, CD spectra provide information on the conformation of compounds [70]. ORD enables the chiral molecule to rotate the plane of polarized light. Therefore, ORD spectra are dispersive, while CD spectra are absorptive. The two phenomena are related by the so-called Konig-Kramers transform [70]. CD spectroscopy is commonly used to study biological macromolecules in two

ways. The first is to probe changes in the conformation of the macromolecules, and secondly, to monitor their interactions with small molecules [71].

Secondary structure of proteins is determined by the nature of the hydrogen bonding between the backbone amide and carboxyl groups. In the far-UV CD spectral region (190-260 nm), the absorbing group is principally the amide backbone, $n \rightarrow \pi^*$ or $\pi \rightarrow \pi^*$ transition. Therefore, studies using the far-UV region in CD spectroscopy can be used to assess quantitatively the overall conformational distribution of the protein (Fig. 5) [70]. Many proteins were shown to exhibit changes in secondary structures (for example α-helix to β-sheet) in different environments. Thus, far-UV CD spectra have been valuable for monitoring these transitions in such proteins/peptides [70].

On the other hand, the near-UV region (260-320 nm) can be used to monitor changes in disulfide bonds and aromatic side chain conformations in phenylalanine, tyrosine, and tryptophan [71]. The CD spectra of aromatic amino acids can be affected by a number of cofactors, including the rigidity of the protein, nature of the environment in terms of hydrogen bonding, polar groups and polarizability [70]. In addition, the near-UV region also provides information about the disulfide bonds (at ~260 nm) present in the proteins, as well as the environment of cofactors and other non-covalently bound ligands. Despite the fact that free ligands have little or even no CD signal, the observed CD signals in the complex could indicate their integral role in the biological activity of proteins.

Structure is an important aspect of protein research. Many advanced techniques have emerged to resolve the high resolution structures of proteins, such as X-ray crystallography, solid-state and solution nuclear magnetic resonance (NMR) spectroscopy. However, the process is not straightforward, especially for membrane proteins, owing to their stability depending

strongly on the surrounding environment. In the absence of high resolution structures of membrane proteins, CD spectroscopy, however, offers a quick and relatively easy means to estimate their conformational distribution. In addition, this technique also allows determination of the dynamics of protein conformations upon changes of environment and ligand interactions. Overall, CD spectroscopy is an accessible method to study the complexity of biological molecule structures and interactions.

2.3. Use of fluorescent probes as sensors for ion transport across membranes

Measurement of proton transport across reconstituted vesicles has been performed using different techniques. Originally, pH electrodes were used to directly measure the H^+ transport rate [72-74]. At a later stage, the fluorescent pH probe, pyranine, was developed for studying proton movement in reconstituted vesicles [36, 75]. Discovery of the buffer-dependent pH sensitivity of the fluorescent chloride-indicator dye 6-methoxy-N-(3-sulfopropyl) quinolinium (SPQ) allowed proton transport to be measured indirectly [76].

SPQ fluorescent dyes offer an advantage in measuring both anion (chloride, bromide, and iodide) and proton transport. During chloride transport measurements, the fluorescence intensity of SPQ is quenched by the presence of chloride anions [76]. On the other hand, proton transport is measured indirectly through the quenching of SPQ fluorescence by N-tris(hydroxymethyl)methyl-2-aminoethanesulfonic acid anion (TES$^-$) [76]. In a low pH environment, the TES anion will be fully protonated and will not affect SPQ's fluorescence. However, at high pH, the anionic form of TES is free to collisionally quench SPQ's fluorescence. The current study utilizes the fluorescent probe SPQ to track the UCP-mediated transport of chloride ions and protons across the membrane.
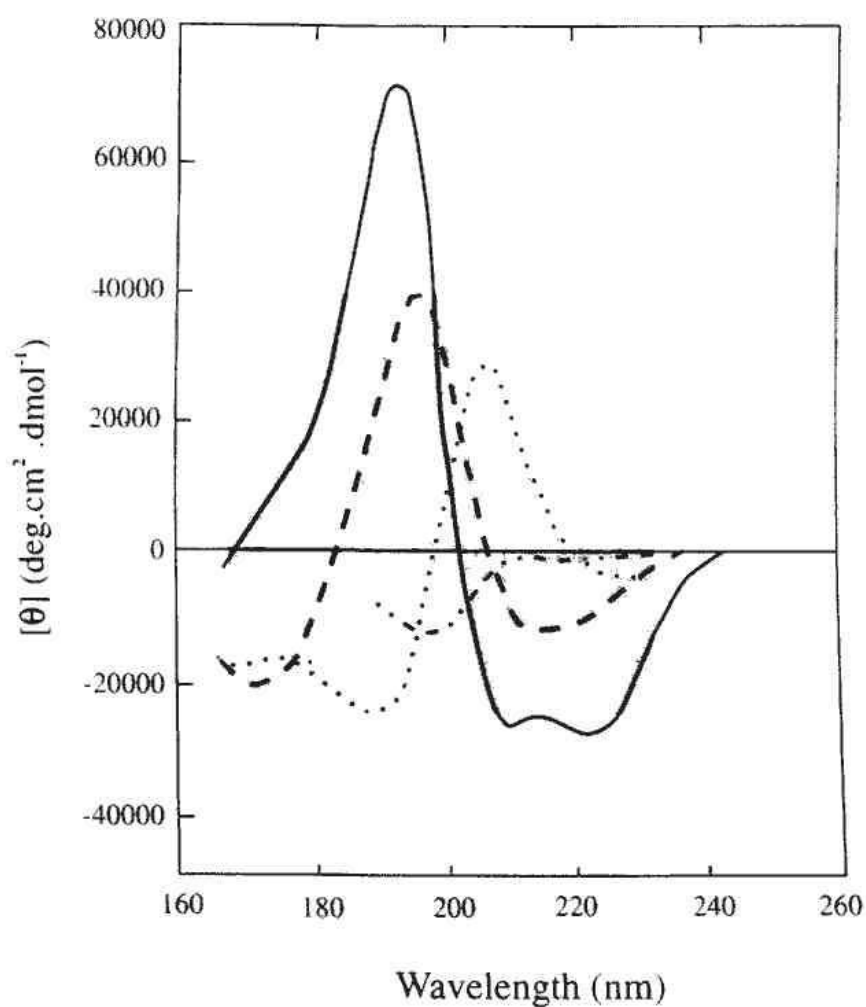
Figure 5 – **Computed circular dichroism spectra for the evaluation of protein conformation** [70]

The solid curve represents α-helix; the long dashes represents antiparallel β-sheet; the dots represents type I β-turn; the dots and short dashes represents irregular structure

CHAPTER 3 – MATERIALS, EXPERIMENTAL DESIGN, and METHODS

3.1. Materials

Detergent octyltetraoxyethylene (C_8E_4) was purchased from Bachem (Torrance, CA, USA). Triton X-100 (TX-100), Triton X-114 (TX-114) and N-lauroylsarcosine (sodium salt) (Sarcosyl) were from Calbiochem-EMD Biosciences. Egg yolk L-α-phosphatidylcholine (azolectin or L-α-lecithin) from Sigma (Catalogue # P5394), contained at least 60% phosphatidylcholine. The remaining 40% was comprised mostly phosphatidylethanolamine and to a lesser extent other lipids such as triglycerides and cholesterol. CL (1', 3'-bis[1,2-dioleoyl-*sn*-glycero-3-phospho]-*sn*-glycerol (sodium salt)) was purchased from Avanti Polar Lipids (Alabaster, AL, USA). Sodium dodecanoate (lauric acid), purine nucleotides (ATP, ADP) and other chemicals were from Sigma (Oakville, ON, Canada). The fluorescent probe SPQ (99%) was from Biotium Inc (Burlington, ON, Canada). Biobeads SM-2 were purchased from Bio-Rad (Missisauga, ON, Canada). Sephadex G25-300 resins were from GE Healthcare (QC, Canada). Sarcosyl was from BioShop. Valinomycin (val) and nigericin were purchased from Sigma (Oaskville, ON, Canada) and stored in 100% ethanol at $-20^{o}C$.

3.2. Experimental design and methods

3.2.1. Amino acid sequence analysis and modelling of neuronal UCPs

Sequence analysis was used to identify the signature sequence of UCPs through conserved residues in all UCPs, especially neuronal UCPs. The T-Coffee program (http://tcoffee.vital-it.ch/cgi-bin/Tcoffee/tcoffee_cgi/index.cgi) was used for primary sequence alignments [77, 78]. In addition, 3-D structural models of neuronal UCPs were obtained using

MODELLER 9.9 and Pymol programs based on the crystal structures of AAC reported in 2003 and 2005 (PDB IDs: 1OKC, 2C3E) [6, 22, 79, and 80].

3.2.2. Expression and extraction of neuronal UCPs

Neuronal UCPs were cloned into the pET21 expression vector and transformed into *E. coli* BL21 (DE) (with the exception of UCP4, which was introduced into *E. coli* BL21 CodonPlus (DE3) for expression), as described previously [81]. Overexpression of neuronal UCPs was achieved by inoculating 1 L Luria-Bertani (LB) broth containing 50 μg/mL ampicillin with 10 mL of an overnight culture. The cultures were grown at 37°C, with shaking at 240 rpm until they reached an OD_{600} of 0.6-0.8. Overexpression of recombinant proteins was achieved by induction with 1 mM isopropyl β-D-thiogalactoside (IPTG) for 3 h at 37ºC with shaking at 240 rpm. Cells were harvested by centrifugation at 8000 *g* for 15 min at 4°C (JLA-10.500 rotor, Beckman Coulter) and cell pellets were stored at -20°C.

Cell pellets were resuspended in ~20 mL extraction buffer (EB) (20 mM Tris/HCl, 500 mM NaCl, pH 8.0) and lysed using 200 μg/mL lysozyme (30 min incubation at 4°C) with the aid of tip sonication (output power ~6 W). Soluble proteins and inclusion bodies were separated by centrifugation at 86,876 *g* for 15 min at 4°C. Isolation of recombinant UCPs was adapted and modified from the work of Jabůrek *et al.* [82]. Inclusion bodies were carefully washed stepwise (3-4 times for each detergent) with 2% (w/v) TX-100, 2% (w/v) TX-114, and 0.1% (w/v) detergent sarcosyl in EB. During each wash, the pellet was resuspended in EB containing the desired detergent with appropriate concentration, tip sonicated (output power of ~8 W) for 10 min and ultracentrifuged at 86,876 *g* for 15 min at 4°C to collect the insoluble inclusion body proteins. The final pellet fraction was then resuspended in 4 mL of buffer A (50 mM N-cyclohexyl-3-aminopropanesulfonic   acid   (CAPS),   25   mM   dithiothreitol,   2   mM

phenylmethylsulfonyl fluoride, 10% glycerol, pH 10.0) plus 2% (w/v) detergent sarcosyl, incubated for 45 min at room temperature and 15 min at 4^oC. Insoluble proteins are removed by centrifugation (14,000 g, 10 min). The supernatant was diluted with 6 mL of buffer B (10% glycerol, 1% TX-114) supplemented with 1 mM ATP. After 2 h incubation at 4^oC, the mixture was dialyzed against 3x300 mL (4 buffer A: 6 buffer B) (4 h, 18 h, and 4 h, respectively) to remove sarcosyl. The final dialyzed protein was supplemented with 5 mg/mL azolectin and 1 mM ATP, incubated for 2 h at 4^oC, and concentrated ~2-fold in an Ultrafree-15 centrifugal filter device (Millipore). Protein purity and concentration were analyzed using SDS-PAGE stained with Coomassie blue and a Lowry-based protein assay (Bio-Rad), respectively.

3.2.3. Reconstitution of UCPs into liposomes

Reconstitution of neuronal UCPs was achieved using the detergent-mediated reconstitution method [82]. Phospholipid (azolectin or azolectin plus CL, see below) dissolved in chloroform (100 mg/mL) was dried with N_2 gas, further dried under vacuum overnight and rehydrated in the desired buffers. Two types of lipid systems were used in this study; azolectin and azolectin with 2.5 mol% CL. For CD spectroscopic experiments, 10 mM potassium phosphate buffer at pH 7.2 was used to rehydrate the lipids. For ion transport experiments, the internal buffer (see below) containing fluorescent probe SPQ was used at pH 7.2. The detergent C_8E_4 was added to the rehydrated lipids in excess (2.5:1 w/w) to solubilize the multilamellar vesicles and form mixed lipid/detergent micelles. This ratio was pre-determined by light scattering measurement of phospholipids titrated with C_8E_4, where the weight ratio (detergent/lipid) of 2.5 yielded a minimal absorbance at 540 nm that was indicative of mixed micelle formation. Extracted UCPs were then added to the lipid preparation at a ratio that was optimal for the particular type of experiment. For CD experiments, the initial protein to lipid

molar ratio was kept at 1:500 to 1:400. For ion transport experiments, this ratio was 1:8000 (equivalent to ~1/200 protein to lipid weight ratio). No-protein controls were prepared in parallel for all experiments. The mixed lipid/detergent micelles were incubated at 4°C for 30 min. Formation of proteoliposomes was achieved through removal of detergent via SM-2 Biobeads. The lipid/protein/detergent mixture (1 mL) was incubated in 2 mL of excess SM-2 Biobeads (~40/1 beads to detergent weight ratio) for 2 h at 4°C. This detergent/protein/lipid/bead mixture was incubated in a 3-mL syringe column. The flow-through (with most detergents already removed) was collected by centrifugation at 2000 rpm for 2 min (JS13.1 rotor) and incubated in the second column of 2 mL SM-2 Biobeads (1 h, 4°C) to remove any traces of detergent. The resultant liposomes/proteoliposomes were collected by centrifugation as described above. This flow-through was ready to be used in CD spectroscopic measurements. For ion transport assays, the external fluorescent probe SPQ was removed from the proteoliposomes by gel filtration through a Sephadex G25-300 [GE Healthcare, 3 mL- column] spin column that was pre-equilibrated with internal buffer.

3.2.4. Liposome size measurement

The sizes of liposomes/proteoliposomes were determined by dynamic light scattering using a Zetasizer Nano ZS (Malvern Instruments, Worcestershire, UK). The results reported are the average of 5-10 measurements.

3.2.5. CD spectroscopy

Examination of the secondary structure content of neuronal UCPs in liposomes was achieved using CD spectroscopy on an Aviv 215 spectropolarimeter (Aviv Biomedical, Lakewood, NJ). All measurements were reported in "mean residue molar ellipticity", [θ]. All far-UV CD spectral measurements were carried out in 0.1 cm-pathlength quartz cells at 0.5 nm

resolution and 25°C. The reported spectra are an average of at least eight scans; most spectra are an average of sixteen scans. Blank-subtracted proteoliposome CD spectra were smoothed and converted to mean residue ellipticity using Aviv CDSD software. Estimation of α-helix, β-sheet, turn, and random coil contents from far-UV CD spectra was done through the deconvolution program CDSSTR (CD secondary structure). The analysis was performed on the Dichroweb website (http://dichroweb.cryst.bbk.ac.uk/htmL/home.shtmL) based on "set 7" composed of 48 reference proteins [83, 84].

3.2.6. Fluorescence measurement of ion (proton and chloride) transport

Ion flux in proteoliposomes was measured through the kinetics of the change in the fluorescence signal of SPQ using a Cary Eclipse Fluorescence spectrophotometer (Varian). Each ion transport assay was carried out in a 1-cm quartz fluorescence cuvette. The mixture of buffer and liposomes (refer to section 3.2.6.1 and 3.2.6.2 for more detail) was continuously stirred and kept at 25°C during measurements. The SPQ probe was excited at 347 nm and the fluorescence was measured at 442 nm (±5 nm). Osmotic balance was maintained in all ion flux assays, by ensuring equal total ionic strength in the internal and external media.

3.2.6.1. Proton transport measurement

In the proton flux assay, the internal medium contained 80 mM TEA_2SO_4, 30 mM TEA-TES, 1 mM EDTA and 3 mM SPQ; while the external medium contained 80 mM K_2SO_4, 30 mM K-TES, and 1 mM EDTA. The pH for both media was kept at 7.2. For each assay, 40 μl of proteoliposome solution (~0.8 mg lipid) was incubated in 1.96 mL external media. At 45 s, 4 μl of 50 mM LA (100 μM) was added into the mixture, which resulted in an increase of fluorescence intensity. Proton flux was initiated at 1 min with the addition of 2 μl of 1 mM valinomycin (val) (1 μM final concentration). The kinetics of proton transport was measured

within a 3-min interval. A schematic summary of the transport assay is outlined in Fig. 6.A. A blank liposome flux measurement was done in parallel, and the non-specific proton leak was subtracted from the signals contributed from the reconstituted protein. UCP-mediated proton transport was individually calibrated for the SPQ response, and the internal liposome volume was estimated from the volume of distribution of the fluorescent probe. These calibrations are described as follows.

Calibration of the SPQ signal in the proton flux measurement was done in the presence of 1 μM nigericin (K^+/H^+ ionophore). Introduction of nigericin allows transport of K^+ and H^+ across the membrane. For each calibration, the calibrated fluorescence was fitted to the modified Stern-Volmer equation

$$\frac{F_0}{F} = K_q\left[H^+\right] + 1 \text{ (Equation 1)}$$

Where F_0 is the initial fluorescence (in the absence of KOH), F is the fluorescence in the presence of KOH, K_q is the Stern-Volmer constant and $[H^+]$ is the change of proton concentration in the media. This fitting yielded the constant K_q to help transform the fluorescence kinetics into change of proton efflux over time.

$$\left[H^+\right] = \frac{F_0 - F}{F} \times \frac{1}{K_q} \text{ (Equation 2)}$$

The total internal volume of the proteoliposomes was also calibrated for each transport measurement. This volume was calculated by comparing the original SPQ input to the system and the final SPQ trapped in the liposomes. To estimate the concentration of trapped SPQ, a standard addition method was used. In brief, the proteoliposomes immersed in internal buffer were dissolved in 0.25% (w/v) detergent C_8E_4 and external SPQ was sequentially added. Plotting of the SPQ fluorescence signal versus [SPQ]$_{added}$ yielded the original concentration of SPQ

trapped in the liposome. The amount of SPQ present in proteoliposomes, [SPQ]$_{proteoliposome}$, was compared with the original concentration [SPQ]$_0$ = 3 mM and the included internalvolume of the proteoliposomes could be calculated as:

$$V(\mu l) = \frac{[SPQ]_{proteoliposome}}{[SPQ]_0} \text{ (Equation 3)}$$

Measurement of proton transport kinetics was obtained by measuring the initial rate of H$^+$ transport. The rate R (mM/s) was then corrected for the calibrated liposomal internal volume and transformed into R′ (nmol/s) as followed

$$R'(nmol/s) = R(mM/s) \times V(\mu l) \text{ (Equation 4)}$$

This rate of transport was then subtracted from the non-specific proton leakage in the protein-free liposomes and corrected for the protein concentration in each proteoliposome preparation. Final proton flux was reported in μmol H$^+$.min^{-1}. mg protein^{-1}. In the case of the inhibition experiments, purine nucleotides (ATP/ADP) were incubated with proteoliposomes for 2 min before the addition of LA.

Inhibition of ATP on UCP-mediated proton transport was analyzed by concentration-dependent inhibition measurements to determine their mutual affinity. The inhibitory effects of ATP on UCP-mediated proton flux were measured at nucleotide concentrations ranging from the μM to mM range. With the assumption of a simple single binding site with no cooperative effect, an inhibition plot of ATP on UCP-mediated proton transport was fitted to the Hill equation below with coefficient n=1:

$$y = V_{max} \frac{x^n}{k^n + x^n} \text{ (Equation 5)}$$

Where x is the concentration of inhibitor ATP (mM), y represents the relative proton transport rate (%), V$_{max}$ is the relative maximum transport rate when no inhibitor (ATP) was

added (100%), k is the Hill coefficient (concentration of inhibitor at which the transport rate was inhibited by 50%), and n represents the degree of cooperativity (n=1 with no cooperativity).

3.2.6.2. Chloride transport measurement

For the chloride transport assays, the internal medium contained 10 mM sodium phosphate, 100 mM TEA_2SO_4, 1 mM EDTA, 3 mM SPQ, pH 7.2; while the external medium contained 10 mM sodium phosphate, 150 mM KCl, and 1 mM EDTA, pH 7.2. The initial set-up was similar to that for the proton flux assays. No FA was required for initiation of chloride flux [85]. Chloride anion transport was triggered by the addition of 1 μM val and measured for 3 min. Kinetics of the fluorescence intensity change were compared in the absence and presence of val. A schematic summary of the chloride transport assay is outlined in Fig. 6B. UCP-mediated chloride fluxes were also calibrated for individual fluorescent SPQ probe response in the same way as the internal volume of the liposome, using the same methods as described above for the proton transport assays above. Fluorescence signal calibration, in this case, was done in the presence of a mixture of nigericin/tributyltin (0.4 μM/4 μM) and the change in signal was recorded with sequential addition of potassium chloride.

3.2.7. Protein concentration determination

Protein content from UCP extraction and final protein concentration in proteoliposomes (in CD spectroscopic measurements) were determined using a standard Lowry-based protein assay [86]. In the case of ion flux experiments, a modified Lowry protein assay was used to determine the final protein concentration in proteoliposomes because the protein concentration was so low [87]. Briefly, 100-150 μl proteoliposome samples or bovine serum albumin (BSA) standards were precipitated with trichloroacetic acid (TCA) and redissolved in 25 μl of 20% (w/v) SDS. Developing reagents (reagent A' and B, Bio-Rad) were added to each fraction. The

mixtures were incubated for 15 min at room temperature and absorbance was measured at 750 nm.

3.2.8. *Sodium dodecyl sulphate-polyacrylamide gel electrophoresis (SDS-PAGE)*

Purity of extracted protein was analyzed using 12% sodium dodecyl sulphate polyacrylamide gel electrophoresis (SDS-PAGE). Gels were stained with Coomassie Brilliant Blue R250 dye and destained with destaining solution (45% methanol, 10% acetic acid). SDS-PAGE was also used to confirm the reconstitution of UCPs into liposomes. To eliminate gel-smearing often caused by lipids, proteoliposomes were chloroform/methanol-precipitated before being loaded onto the gels. In brief, proteoliposomes were mixed with methanol/chloroform (4:1 methanol: chloroform volume ratio) and centrifuged at 14,000 rpm for 5 min. The protein layer was located between the aqueous and organic phases (top- methanol/water, bottom- chloroform). After removing the upper layer, methanol was added (same volume as the first addition) and the mixture was vortexed well. The protein was pelleted by centrifugation (10,000 rpm, 5 min), the supernatant was removed, and the protein pellet was suspended in SDS sample buffer to be loaded on the gel.
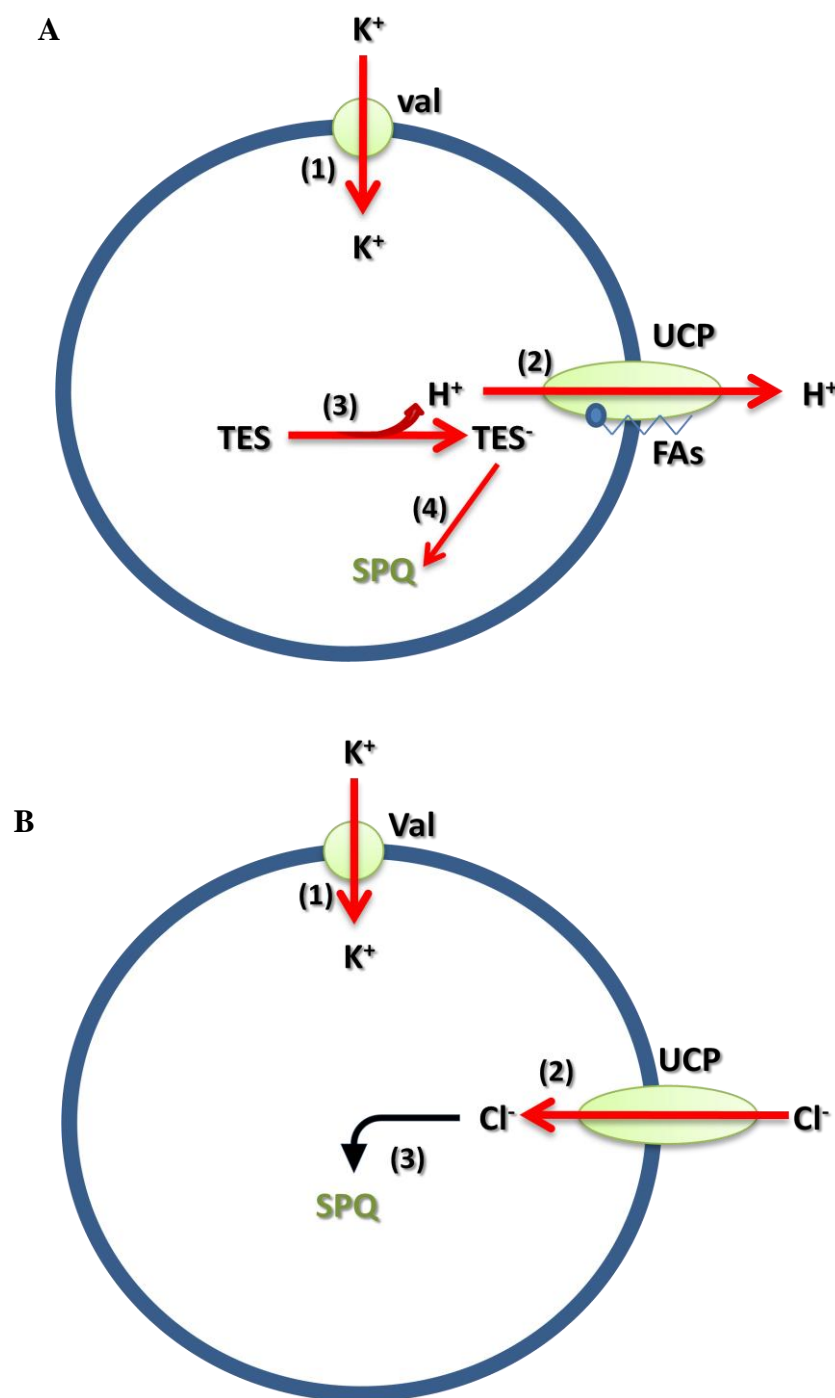
Figure 6 – Schematic of fluorescence experiments for assaying proton and chloride transport

(A) Efflux of protons (2) is driven by diffusion of K^+ (1) from the external buffer into the internal buffer with the presence of val. Proton efflux consequently shifts the equilibrium to formation of TES anion (TES$^-$) (3), which quenches the fluorescence of SPQ (4). (B) The chloride uptake assay is also driven from the diffusion of K^+ (1). In this case, SPQ fluorescence signal is quenched by chloride anions (Cl$^-$) (3). TES buffer is not used in this experiment to avoid fluorescence interference.

CHAPTER 4 – RESULTS

4.1. Protein sequence analysis and modelling of neuronal UCPs

Structure and function are two fundamental and closely related aspects of biological molecules. However, obtaining high resolution structure is often difficult, especially for membrane proteins. This problem also applies to uncoupling proteins, which has resulted in structural analyses of UCPs being done primarily through sequence alignments, molecular modelling, and mutagenesis studies [16, 20, 46, and 48]. In this study, using primary protein sequence analysis and various prediction algorithms, key amino acids and general models of neuronal UCPs have been elucidated. Previous studies have already compared all human UCP sequences with that of the prototypical UCP1 [16, 20, 46, and 48]. In the present study, a more extensive comparative sequence analysis was performed than was done previously. Sequence homologies for all UCPs were calculated and compared to each other (Table 1) [88, 89]. In addition, the sequences of five UCP homologs were compared to that of a suggested structurally similar protein, AAC. UCP2 and UCP3 shared the highest sequence homology to the prototypical UCP1 (both 59% homology), while UCP4 and UCP5 had a much lower amino acid sequence identity to UCP1 (30% and 34%, respectively). Sequence similarity between UCP4 and UCP5 was only 40%, which suggested a further difference between these two proteins. Interestingly, the sequence of AAC, whose crystal structure has been used extensively as a blueprint for UCP1-3 modelling, shared the highest sequence homology with UCP5 (28%).

Using the primary sequence alignment program (T-Coffee), identical, conserved and semi-conserved amino acid residues in UCPs were identified [77, 78]. Primary sequences of all UCPs showed a characteristic MCF sequence in three repeated regions, PxD/ExxK/RxK/R-(20-30 residues)-D/EGxxxxaK/RG [6]. Moreover, an unusually high pI (~10) was predicted for all

UCPs. This strong electrostatic character has been reported to be a common feature in most of the MCF members, which may play an important role in substrate binding and translocation, and also in anchoring the carriers to the negatively charged environment of the inner mitochondrial membrane [90]. To further understand the relations among UCPs, sequence motifs were analyzed using the pattern prediction program package MEME-MAST [91, 92]. Common motifs were searched in all five human UCP homologs, AAC, dicarboxylate carrier (DIC) and oxoglutarate/maleate carrier (OGMC). All proteins shared common MCF motifs in each repeat (Appendix 2, Table 4). Moreover, UCPs, DIC and OGMC shared two common motifs located in the intermembrane loop of the third repeat (26 residues) and at the N-terminal (10 residues) (Appendix 2, Table 4). No exclusive common motif for UCPs was found in this analysis. Instead, two additional motifs common in UCP1-3 were found and four specific UCP2/3 motifs were also determined (Appendix 2, Table 4). Interestingly, UCP2/3 did not share any specific motif with UCP4, UCP5, AAC, DIC, and OGMC. On the other hand, UCP5 and UCP4 had at least one specific shared motif with every other protein in the MCF family. Sequence alignments between all UCPs and AAC also demonstrated an interesting feature when comparing the sequences of UCP4/5 with other UCPs. The conserved/semiconserved residues in UCPs are mostly identical between UCP4 and UCP5, and are similar but not identical in UCP1-3 (e.g. I $\rightarrow$ L, D $\rightarrow$ E). Hence, protein sequence analysis here suggested the existence of three major branches of evolution of UCPs. UCP1, UCP2 and UCP3 could be grouped into one branch, where UCP2 and UCP3 share many more similarities and can potentially belong to a subgroup of this branch. Two other branches give rise to UCP4 and UCP5, respectively. This suggestion also agreed with the phylogenetic work done by Sokolova and Sokolov in 2005 [93].

Table 1 – **Primary amino acid sequence homology of UCPs and ADP/ATP carrier (AAC)**

The numbers represent the percentage of sequence identity between the two proteins. These results were obtained from the LALIGN server program with a default setup [88, 89]. Primary protein sequences of UCPs and AAC were obtained from the ExPASy Proteomics Server and the Proteomic tool ProtParam using accession numbers UCP1 (P25874), UCP2 (P55851), UCP3 (P55916), UCP4 (O95847), UCP5 (O95258), and AAC (P02722). MW = molecular weight; AA= amino acids. Net charge of proteins was calculated at physiological pH.

	Sequence homology						Primary sequence		
	UCP5	**UCP4**	**UCP3**	**UCP2**	**UCP1**	**AAC**	**MW (kDa)**	**No. of AA**	**Net charge**
UCP5		40	38	38	34	28	36.202	325	+12
UCP4			35	34	30	23	36.064	323	+6
UCP3				72	59	25	34.216	312	+11
UCP2					59	24	33.229	309	+15
UCP1						23	33.005	307	+10

3-D models of neuronal UCPs were generated in this study based on the sequence alignment and crystal structure of AAC (Fig. 7). As the models are based on the structure of a protein with only ~25% sequence identity, only highly identical/conserved characters in the models were highlighted to avoid over-analysis. All UCP models displayed a typical funnel shape that was more open at the intermembrane space (diameter ~ 20 Å) and closed at the matrix side. A uniquely long N-terminal was observed in the 3-D model of UCP5. Proline residues in the conserved MCF motifs created kinks and allowed longer TMs in the membrane. Located in the TMs, the acidic and basic residues of the PxD/ExxK/RxK/R region were suggested to interact electrostatically and participate in maintaining the kinked helices. Analysis of charge density revealed a positive cavity in 3-D models of all neuronal UCPs. This distinct richness in positive charge in UCPs' cavity could be explained by several factors. First of all, the inner mitochondrial membrane contains a specifically high amount of negatively charged lipids such

as CL [3]. Moreover, purine nucleotides (-4 or -3 charge) bind and inhibit the proton leak

mediated by UCPs [16, 20 and 48]. Finally, UCPs can also mediate transport of anions [16, 20,

and 48]. Therefore, the positive electrostatic potential of UCPs could participate in enhancing

their activity and regulation. Three conserved Arg residues located in the proposed binding

pocket were in the even-numbered TM helices (TM 2, 4, and 6) and formed a network in the

cavity of UCPs (Fig. 8). The distance between conserved Arg residues in the binding pocket of

all UCP models was measured from the carbon atoms of the guanidinium group on each Arg

(Fig. 8). In all neuronal UCPs, the average distance between two adjacent Arg residues was

approximately 10 Å. Phosphate groups of ATP were aligned in the centre of the pocket and it

was suggested that ATP might interact electrostatically with the three conserved Arg residues in

the binding pocket of all UCPs (Fig. 8). Spectroscopic evidence from our previous study

suggested that no major overall conformational change occurs upon purine nucleotide binding,

but rather changes in the microenvironment occur under these conditions [81]. Those results,

together with the modelling study from this work, suggested ATP binding to UCP might occur

locally and not induce any drastic structural changes in UCPs.

Cardiolipin, as mentioned earlier, might play an important role in the structure and

function of mitochondrial inner membrane proteins [3]. In fact, a second crystal structure of

AAC reported in 2005 was bound to three CL molecules [80]. These CL molecules could act as a

cross linkage and promote protein-protein interactions [6, 80], which could lead to the proposed

dimeric functional form of AAC [6, 80]. To observe the effect of CL on the structure of UCPs, a

second set of UCP models was generated based on the second AAC crystal structure [80]. The

overall shape of UCP models upon the introduction of CL (3 CL molecules per protein) did not

exhibit any dramatic change as compared to the earlier models. However, the nucleotide binding

pocket of UCP in the presence of CL was slightly increased in size (Fig. 9). This could potentially affect the binding affinity between UCPs and purine nucleotides.

4.2. Extraction of overexpressed neuronal UCPs from inclusion bodies

Previous studies demonstrated successful expression and purification of recombinant versions of UCP homologs in *E. coli* using hexa-histidine tags for affinity chromatography [46, 81]. Although present, the poly-histidine tags were not used in this study to purify the proteins. To compensate for the absence of this purification step, the inclusion bodies were washed carefully several times in mild detergents and in a low concentration of sarcosyl (refer to section 3.2.2) to obtain adequately pure proteins. In addition, dialysis helped remove low molecular weight proteins. All UCPs extracted from inclusion bodies were obtained in high purity as revealed by SDS-PAGE analysis (Fig. 10). A non-His tagged version of UCP2 was expressed and isolated in parallel for comparative conformational and functional studies. Final extraction of UCP4 contained a small amount of a high molecular weight protein (~100 kDa). This component was also observed previously in the IMAC-purified fractions [81]. Migration behaviour of extracted UCPs on SDS-PAGE were consistent with previous studies (Fig. 10) [81]. The His-tagged version of UCP5 (37.9 kDa) showed an apparent molecular weight similar to that of UCP2 (34.9 kDa) on the 12% SDS-PAGE gel (Fig. 10), which might be due to several reasons. First of all, all UCPs have a relatively large number of basic residues that lead to their highly positive charge at physiological pH. Although all proteins are subjected to a denaturing environment such as SDS, these positive electrostatic charges could contribute to protein-SDS complex formation, and might affect their electrophoretic mobility in gels. In addition, specific conformations of UCP5 could contribute to its distinct migration behaviour on PAGE gel compared to other UCPs (refer to section 4.5)
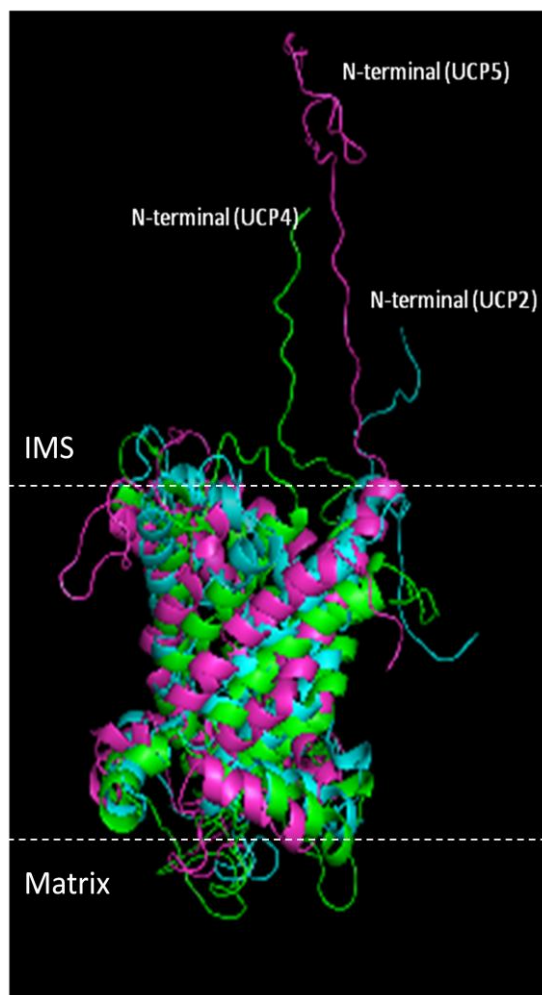
Figure 7 – Overlap of 3-D models of UCP2, UCP4, and UCP5

The models were constructed from sequence alignment (T-Coffee) and modelling program (MODELLER) using the crystal structure of AAC complexed with CATR (PBD ID: 1OKC) as a blueprint. All N- and C- termini were located on the intermembrane space (IMS), while the three hydrophilic loops in each UCP were located on the matrix side of the membrane. UCP2 is shown in cyan cartoon, UCP4 is shown in green and UCP5 is shown in magenta [77-79].
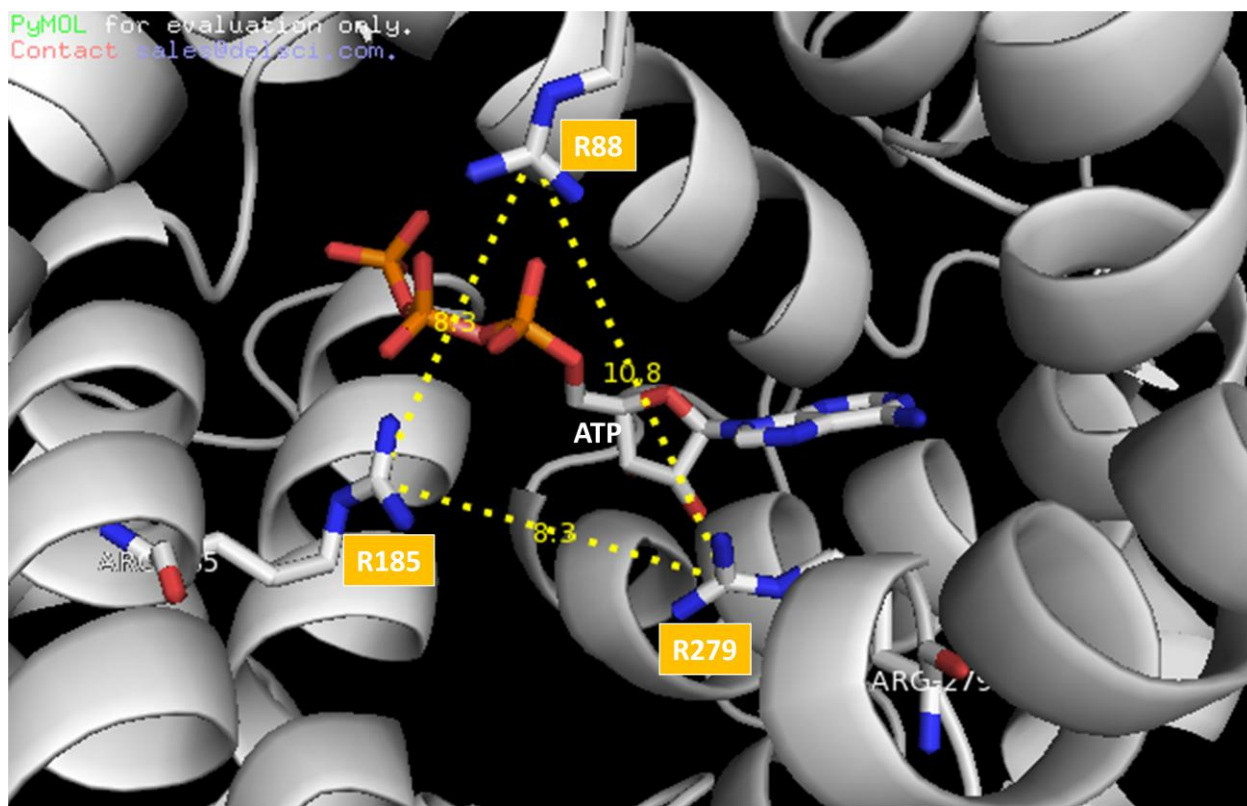
Figure 8 – Proposed ATP binding pocket of UCP2

The model was built in Pymol after sequence alignment (T-Coffee) using AAC (PDB ID: 1OKC) as blueprint (MODELLER). Distances (in Å) between R88, R185, and R279 were measured from the carbon of the capped guanidinium group in each Arg residue. An ATP molecule was placed in the centre of the proposed nucleotide binding pocket composed of R88, R185, and R279 [22, 77-79].
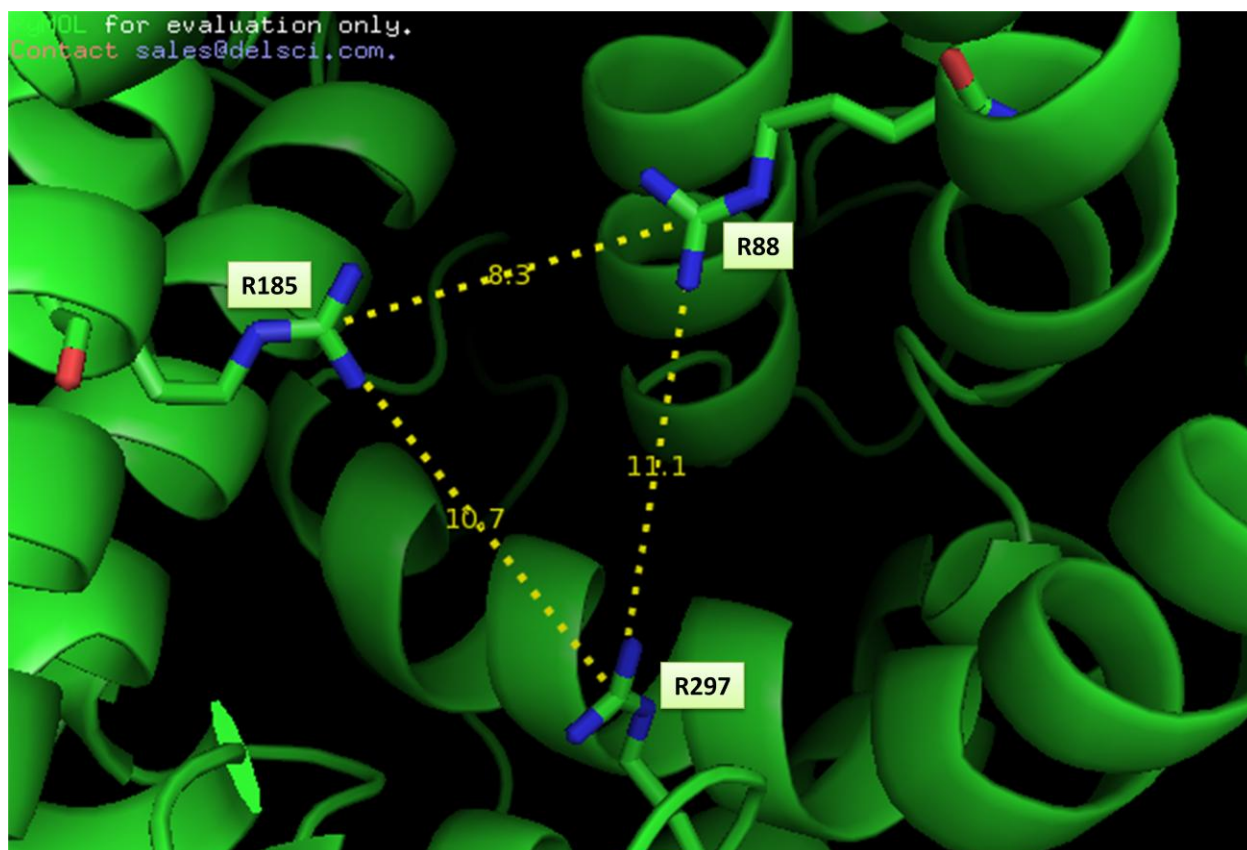
Figure 9 – Proposed ATP binding pocket of UCP2 in the presence of CL

The model was built in Pymol after sequence alignment (T-Coffee) using AAC (PDB ID: 2C3E) as blueprint (MODELLER). In this model, three CL molecules were bound to the protein's residues located closed to the matrix loop. Distances (in Å) between the three Arg residues (R88, R185, and R279) in the nucleotide binding pocket were measured from the carbon of the capped guanidinium group in each Arg residue [77-80]. CL molecules are not shown in this figure.
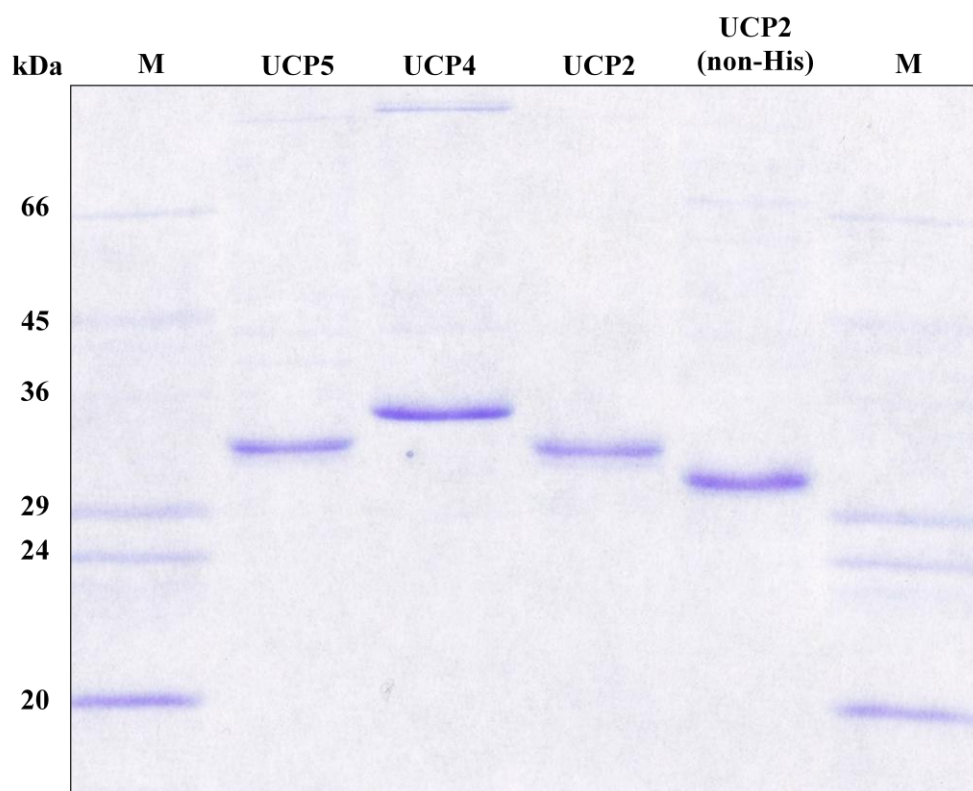
Figure 10 – Extraction of recombinant neuronal UCP homologs resolved using SDS-PAGE

Proteins were run on a 12% resolving gel, and stained with Coomassie Brilliant Blue. Extracted UCP5, UCP4, UCP2 and UCP2 (non-His) (2-5 μg) were loaded on the gel. M, molecular weight markers are indicated in kDa.

4.3. Size and morphology analysis of proteoliposomes

Unlike many other reconstitution studies, the properties of the proteoliposomes were characterized in this work. Dynamic light scattering experiments confirmed mono-disperse proteoliposomes after the detergent-mediated reconstitution procedure. All liposomes/ proteoliposomes displayed a single size population. Azolectin vesicles (without any protein) were 100 nm (± 5 nm) in radius, which is in the range of large unilamellar vesicles (Table 2). The proteoliposomes reconstituted with UCPs were stable for at least 5 h during measurement. This stability allowed reproducibility in collecting transport data. Addition of CL into the phospholipid system slightly enhanced the radius of the liposomes (Table 2). Having a unique structure that comprises four alkyl chains and an intrinsic curvature, CL has been suggested in different studies to promote organization in the inner mitochondrial membranes [94]. In the current study, CL was supplemented in the phospholipid vesicles at 2.5 mol%, compared to its approximately 10 mol% concentration in inner mitochondrial membrane. A higher content of CL is expected to cause more drastic effects on the overall size and morphology of liposomes.

Table 2 – Sizes of UCP proteoliposomes determined by dynamic light-scattering

The reported liposome sizes are averages of 5-10 measurements. Vesicles' sizes were measured for ion transport assays.

	Average radius of liposomes (nm)	
	Azolectin vesicles	**Azolectin vesicles (with 2.5 mol% CL supplement)**
No UCP	96 ± 4	103 ± 9
UCP2 (non-His)	80 ± 9	88 ± 5
UCP2	84 ± 2	95 ± 8
UCP4	69 ± 7	132 ± 8
UCP5	85 ± 5	104 ± 6

While embedding UCP into the lipid bilayers did not disturb liposome homogeneity, proteoliposomes were generally of a similar size or smaller than the protein-free liposomes, with the exception of UCP4 proteoliposomes supplemented with 2.5 mol% CL. Azolectin proteoliposomes containing UCP4 displayed the smallest size (69 nm in radius). However, in the presence of CL, UCP4 proteoliposome size was approximately doubled, to a radius of 132 nm (compared to 103 nm for the protein-free azolectin + CL liposome) (Table 2). This result aligned well with the different behaviour of UCP4-mediated proton transport compared to UCP2 and UCP5 (Refer to section 4.4). Images of liposomes obtained by electron microscopy also showed changes in liposome appearance upon the insertion of UCPs (data not shown). The images were not well defined; and this issue is anticipated to be resolved in future studies by using cryo-EM, a more suitable technique for liposome imaging.

4.4. UCP-mediated ion (proton and chloride) transport in proteoliposomes

4.4.1. Proteoliposome and trapped SPQ fluorescence signal calibrations

The use of the SPQ fluorescent probe was advantageous in that this probe could be used as a detector of both proton and chloride transport across the membrane as shown in Fig. 6. As mentioned previously, chloride flux was measured by direct quenching of SPQ fluorescence, and proton transport was monitored indirectly through quenching of SPQ by anionic TES buffer. Fluorescence experiments confirmed a strong decrease of SPQ fluorescence intensity (excited at 347 nm, $\lambda_{max} \sim 444$ nm) in the presence of either chloride or TES anions (Appendix 4, Fig. 27).

In order to convert the fluorescence kinetics to a transport rate, the response of the fluorescent signal of SPQ at 444 nm was calibrated in each ion flux measurement (refer to section 3.2.6). Calibration of the SPQ signal was done in the presence of 1 μM nigericin (K^+/H^+ ionophore) for proton transport, and in the presence of a mixture of nigericin/tributyltin (0.4

μM/4 μM) for chloride transport (Appendix 4, Figs. 28 and 29). The SPQ fluorescence signal responses in proton concentration were 0.026 ± 0.003 mM^{-1}, and were consistent for both types of phospholipid vesicles (azolectin with and without 2.5 mol% CL). The SPQ fluorescence signal responses in chloride concentration measurements were 0.083 ± 0.004 mM^{-1}.

Calibration of the internal liposome volume (refer to section 3.2.6) was achieved by the standard addition method to determine the concentration of SPQ trapped in the liposome in comparison with the original [SPQ] (Appendix 4, Fig. 30). The average liposomal internal volume for reconstituted UCPs in azolectin was 1.2 ± 0.4 μl/0.8 mg lipid, while that of reconstituted UCPs in azolectin supplemented with 2.5 mol% CL was 1.5 ± 0.7 μl/0.8 mg lipid. These results showed an increase in size in the presence of cardiolipin, which were consistent with the results from the light-scattering experiments.

4.4.2. UCP-mediated proton transport across phospholipid membranes

Proton transport mediated by reconstituted neuronal UCPs was measured in two phospholipid systems, azolectin with and without 2.5 mol% CL. In addition, the inhibition effects of purine nucleotides (ATP, ADP) on transport were also examined. The final protein content in proteoliposomes (determined by a modified Lowry assay, refer to section 3.2.7) varied in the range 2.5 μg-5 μg per mg of lipid. This protein/lipid ratio, when converted to a molar ratio was in the range of 1/18000 to 1/9000. All phospholipids were assumed to be retained after reconstitution and lipid content analysis was not performed. The presence of purified UCPs in proteoliposomes was further confirmed by SDS-PAGE (Fig. 11).

4.4.2.1. Proton transport rate of UCPs in phospholipid vesicles (azolectin with and without CL)

All neuronal UCPs, after being reconstituted, conducted positive proton transport across the phospholipid bilayer, as shown qualitatively in Fig. 12. All measurements showed that efflux

of protons occurred in the first 15-20 s after the addition of the K^+-ionophore valinomycin to trigger transport. The calculated UCP-mediated transport rate was then subtracted from the non-specific proton leak (from protein-free blank liposome) and corrected for the final protein content in each proteoliposome. The corrected proton flux ($\mu mol.min^{-1}.mg$ $protein^{-1}$) for all reconstituted UCPs was positive; this is especially noteworthy for UCP4 and UCP5, which have not been shown to have proton transport activity before (Fig. 13). Overall, all neuronal UCPs displayed comparative transport rates in azolectin vesicles (1-2 $\mu mol.min^{-1}.mg$ $protein^{-1}$) (Fig. 13A). The rate of proton transport mediated by UCP2 was relatively lower compared to data reported in other studies [44, 82]. This could be due to specific experimental conditions (i.e. buffer condition, quality of proteins, phospholipids, instrument sensitivity). The calculated transport rate also demonstrated similar proton flux mediated by non-His tagged UCP2 and His-tagged UCP2 (Fig. 13 and 14).

Addition of CL (2.5 mol%) to the phospholipid vesicles had a strong effect on the proton transport of all UCPs. Proton transport by UCP2 (His and non-His tagged) and UCP5 was more than doubled in azolectin vesicles with 2.5 mol% CL (3.5-5 $\mu mol.min^{-1}.mg$ $protein^{-1}$, Fig. 13B). On the other hand, UCP4-mediated proton flux was decreased in the second phospholipid system to about 0.6 $\mu mol.min^{-1}.mg$ $protein^{-1}$. The non-specific basal proton leak was, however, not affected. It is important to mention that the proton flux reported in the current study was specific to experiments using 100 μM of LA as the inducer of activity. In future studies, LA concentration dependence of H^+ fluxes mediated by neuronal UCPs will be performed to determine the V_{max} value of the transport.
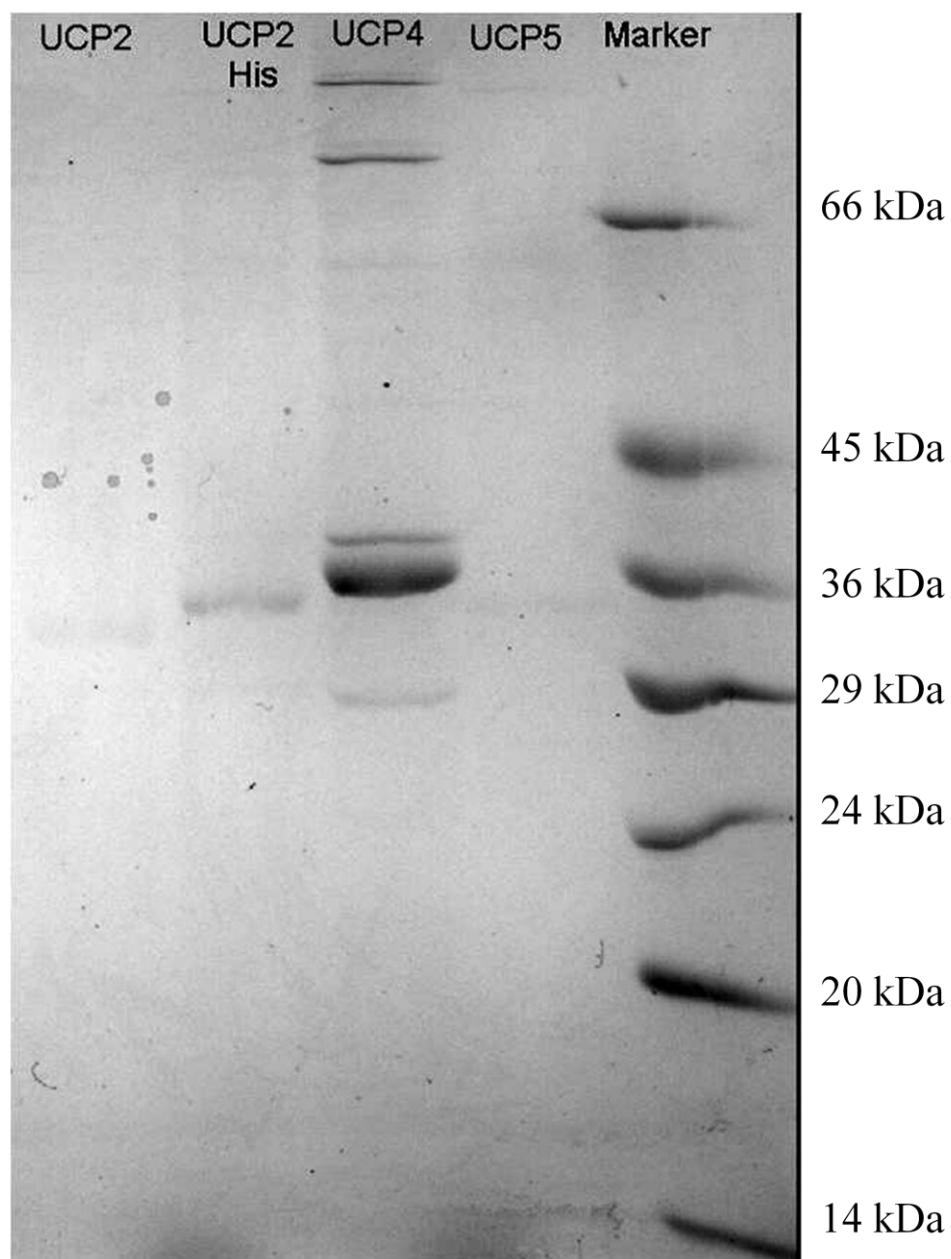
Figure 11 – Delipidated UCP proteoliposomes resolved using SDS-PAGE

Phospholipids in UCP proteoliposomes were removed by a chloroform-methanol precipitation method (refer to section 3.2.8), and the protein pellets were redissolved in 20% SDS, and subsequently loaded on an SDS-PAGE gel. Proteins were run on a 12% resolving gel, and stained with Coomassie Brilliant Blue. Some protein bands were faint due to the protein loss during the methanol-chloroform precipitation.
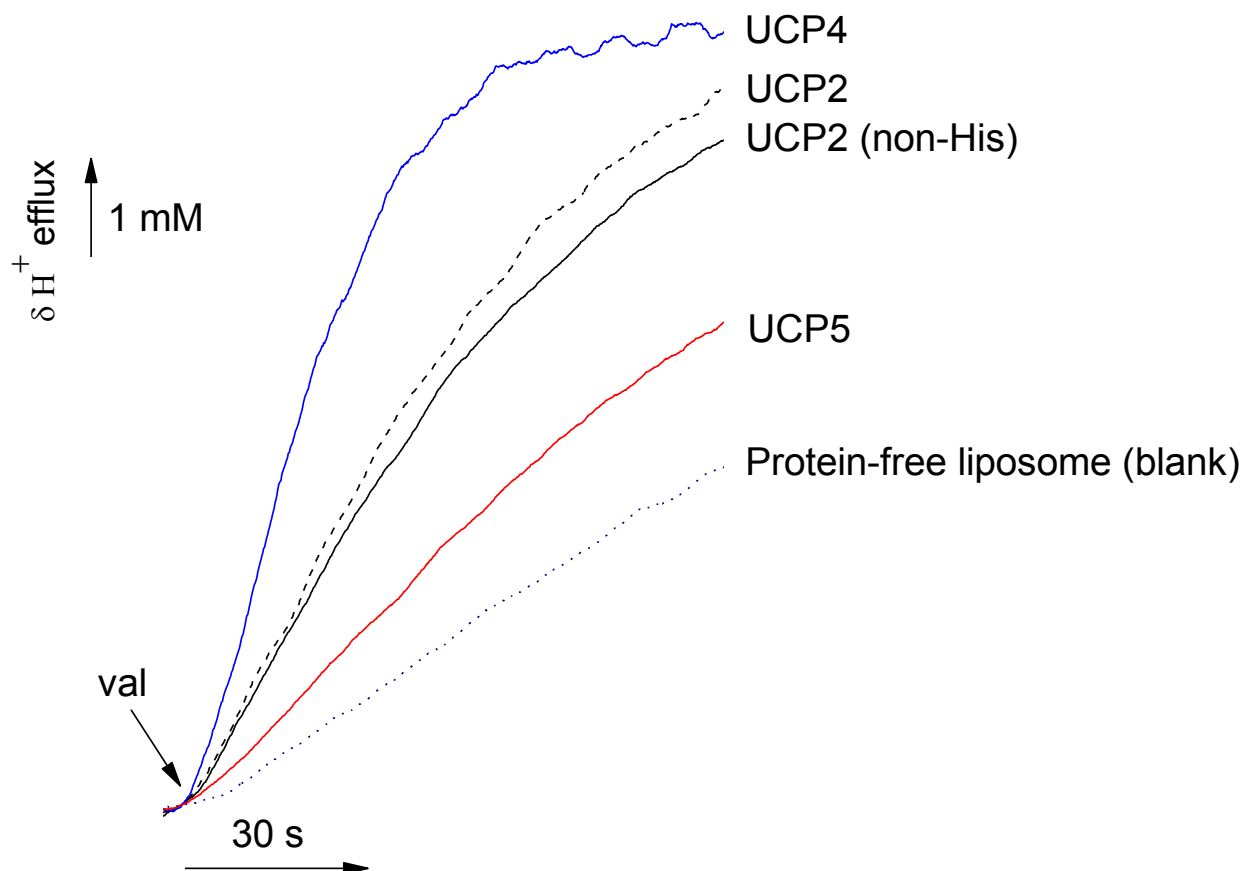
Figure 12 – UCP-mediated proton transport across azolectin vesicles

H^+ efflux through phospholipid vesicles reconstituted with all neuronal UCPs was recorded. Val was added at the concentration of 1 μM to trigger proton transport. Protein-free liposome blank showed proton efflux with a much lower magnitude compared to UCP - mediated transport. All the fluxes shown in the figure were activated with 100μM LA. A representative set of traces of at least 3 experiments is shown.
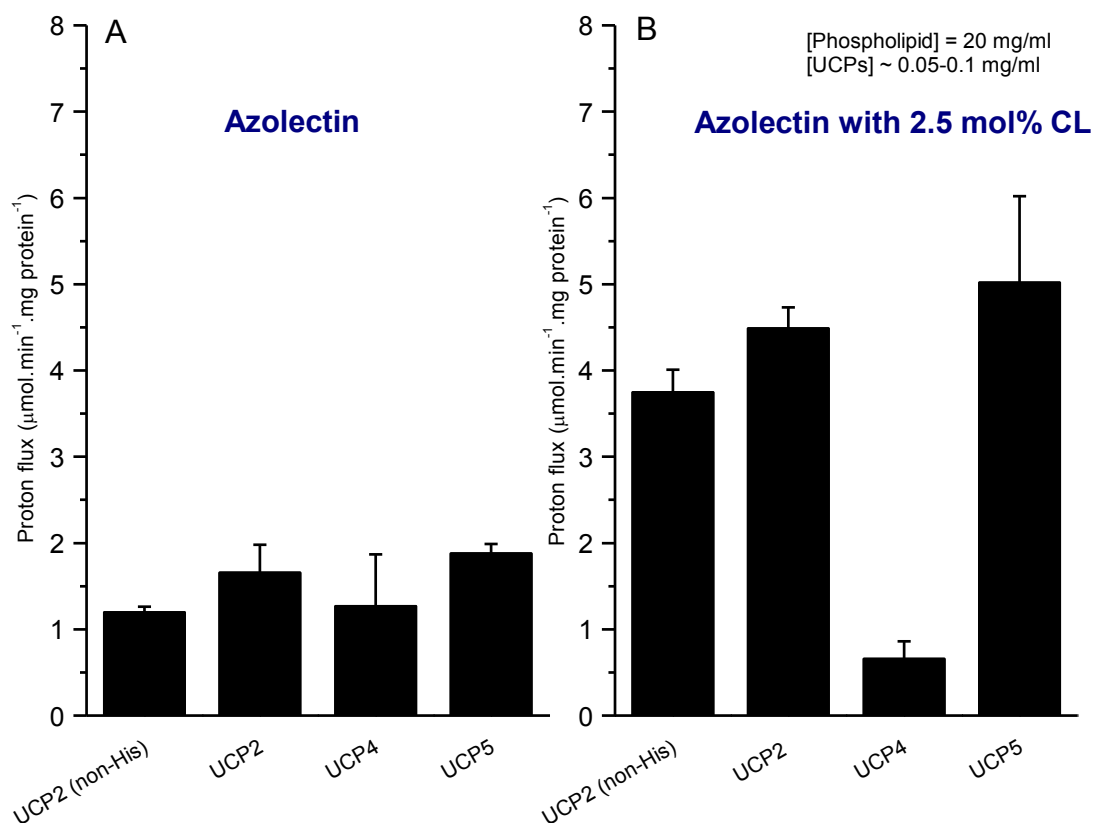
Figure 13 – **Average corrected proton transport mediated by neuronal UCPs in two phospholipid systems: (A) azolectin and (B) azolectin supplemented with 2.5 mol% CL**

Proton transport rates mediated by UCPs in azolectin vesicles are the average of 10 measurements, while those in azolectin vesicles supplemented with 2.5 mol% CL are an average of 15 measurements. Error bars are shown as standard deviation.

4.4.2.2. Inhibition of UCP-mediated proton flux by purine nucleotides (ATP and ADP)

The presence of either ATP or ADP resulted in a decrease of UCP-mediated proton transport in liposomes containing only azolectin (Fig. 14). However, each purine nucleotide might interact differently with each UCP and result in a different degree of proton flux inhibition. At 500 μM, ATP inhibited proton flux through UCP2 more strongly than ADP (Fig. 14A). The opposite occurred with UCP5 proteoliposomes, where inhibition of proton transport by ADP was stronger than that of ATP (Fig. 14C). Interestingly, both ATP and ADP showed similar inhibitory effects at 500 μM on UCP4-mediated proton transport (Fig. 14B). This difference in inhibition by ATP vs. ADP on neuronal UCPs could be related to the specificity of UCP for each type of purine nucleotide. For example, a study by Echtay *et al.* in 1999 showed that UCP3 displayed a much higher affinity for ADP vs. ATP (K_i^{ATP}/K_i^{ADP} = 2.95) [44]. The different responses of UCP3 to the di- and triphosphates were suggested by the authors to be related to the expression of UCP3 in skeletal muscle, in which the main function is energy transfer by ATP to muscle contraction [44]. Therefore, during high muscle activity (ATP/ADP ratio decreases), all oxidative energy should be converted to ATP and little diverted to uncoupling. In the resting stage, when a high ATP/ADP ratio is maintained, UCP3 was activated to generate additional heat since muscle activity cannot fulfil the heat demand [44].

The inhibition constants (K_i) between ATP and all UCPs were calculated to be approximately 10 μM (Fig. 15 and 16). These values lie between the results reported in the studies of Klingenberg *et al.* [35, 36, and 44] (~1 μM) and the studies of Ježek *et al.* and Jabůrek *et al.* (~100 μM) [34, 57, and 82]. In azolectin vesicles, K_i of ATP for UCPs varied between 9-13 μM (Fig. 15). In addition, a similar to slightly enhanced inhibition strength between UCPs and ATP was observed in the azolectin vesicles supplemented with 2.5 mol% CL (Fig. 16). In

addition, inhibition effect of ATP on UCP-mediated proton transport was examined from both sides of the proteoliposome (internal buffer and external buffer) (Fig. 17). The proton flux mediated by UCP2 was similarly inhibited by 500 μM ATP from either inside or outside the liposome.

4.4.3. UCP-mediated chloride transport across azolectin vesicles

The ability to transport anions has been analyzed for UCP1-3 and has often been used to discover other functions of UCPs. At the same time, anion transport mediated by UCPs has also been used to help elucidate the molecular mechanism of uncoupling by UCPs [35, 42, and 45]. While UCP1-3 showed anion transport properties, the relevance of this function to their ability to also transport protons has yet to be determined [35, 42, and 45]. As mentioned previously, no functional work on UCP4 and UCP5 has been done to date. All UCPs were reconstituted in azolectin-only liposomes. The ionophore valinomycin was used to trigger chloride influx mediated by UCPs, thus quenching the SPQ fluorescence signal, resulting in a decrease in fluorescence intensity. The measurements of chloride transport in this study serve as the first report of anion transport activity for neuronal UCPs, especially UCP4 and UCP5.

Preliminary transport data confirmed positive chloride fluxes in UCP2 and UCP4 proteoliposomes, while no clear chloride flux was detected in the case of UCP5 proteoliposomes (Fig. 18). In the presence of 1 μM val, the fluorescence signal of trapped SPQ in UCP2 and UCP4 proteoliposomes decreased much more drastically than that in the absence of the ionophore. On the other hand, UCP5 proteoliposome showed an insignificant change in SPQ fluorescence signal upon the addition of val. Due to insufficient replicates, the quantitative results of transport rate have not been reported in this study. This issue will be studied in more detail in the near future.
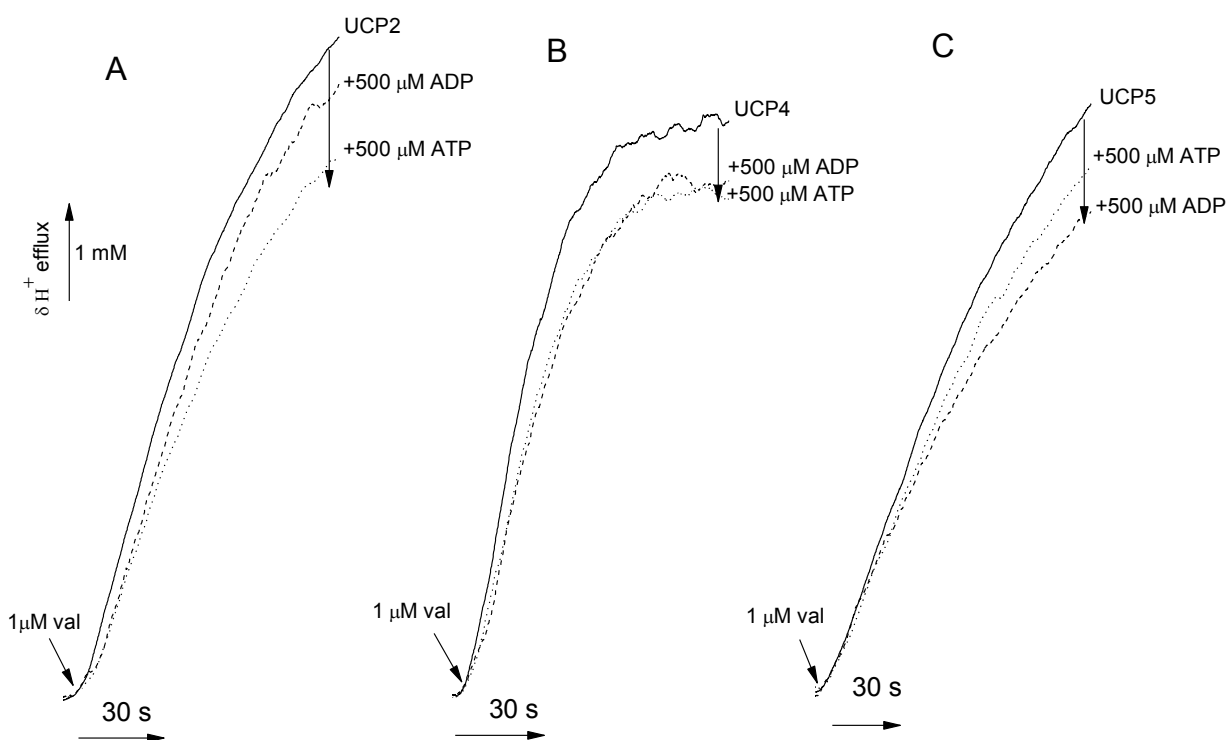
Figure 14 – Inhibition effects of ATP and ADP on proton transport mediated by (A) UCP2, (B) UCP4, and (C) UCP5 in azolectin vesicles

Azolectin concentration was kept at 20 mg/mL, while final protein content in proteoliposome was fluctuated from 0.05-0.1 mg/mL. The purine nucleotides were incubated 2 min with proteoliposomes prior to initiation of proton flux by val. The proton flux was activated by 100 μM LA and initiated with 1 μM val. A representative set of traces from 2 experiments is shown (refer to Fig. 12 for a representative of the protein-free liposome trace)
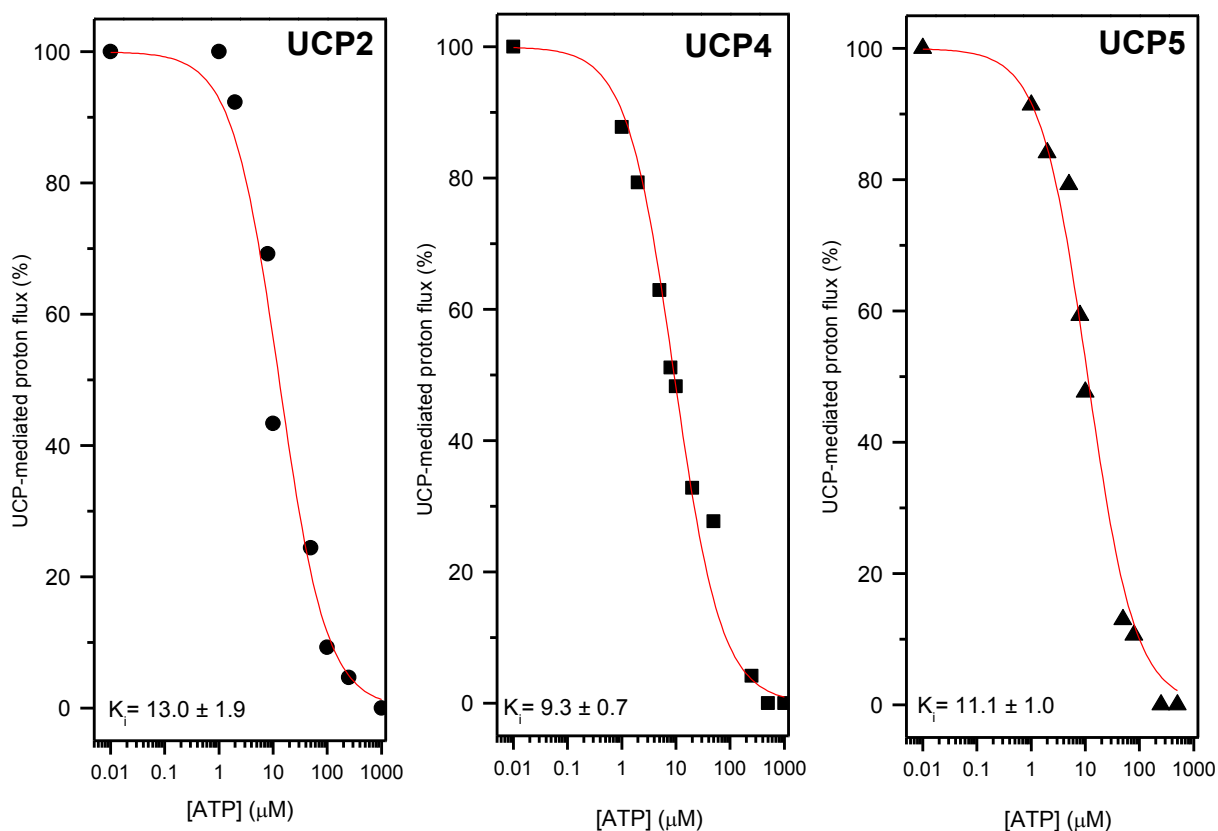
Figure 15 – ATP inhibition effects on UCP-mediated proton transport in azolectin vesicles

Lipid concentration was kept at 20 mg/mL, while protein content in liposome fluctuated from 0.05-0.1 mg/mL. Concentrations of external ATP were varied from 0.01 µM to 1 mM. The data represented in the figure are the average results from 9 measurements. The Hill equation (no cooperativity, n=1) was used to fit the inhibition curve and the K_i was estimated.
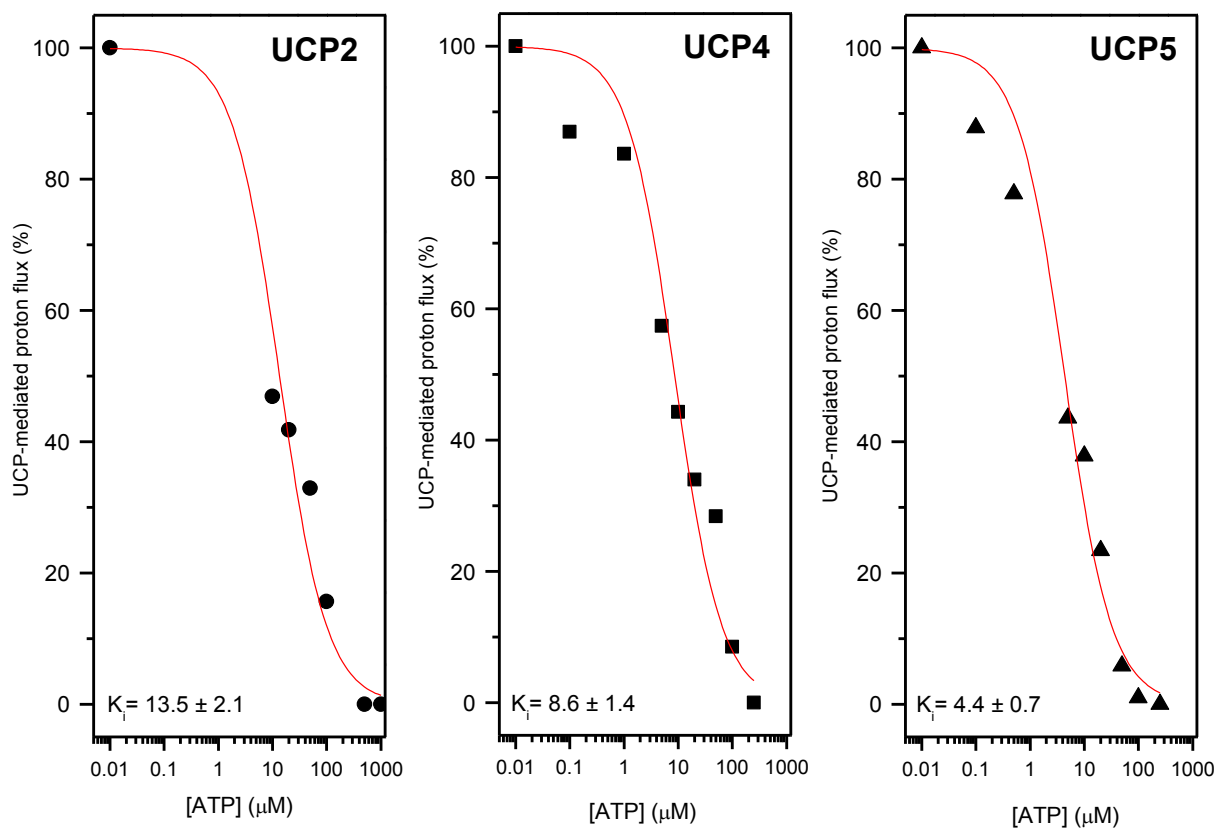
Figure 16 – ATP inhibition effects on UCP-mediated proton transport in azolectin vesicles supplemented with 2.5 mol% CL

Lipid concentration was kept at 20 mg/mL, while protein content in liposomes was 0.05-0.1 mg/mL. Concentrations of external ATP were varied from 0.01 μM to 1 mM. The data represented in the figure are the average results from 6 measurements. The Hill equation (no cooperativity, n=1) was used to fit the inhibition curve and K_i was estimated.
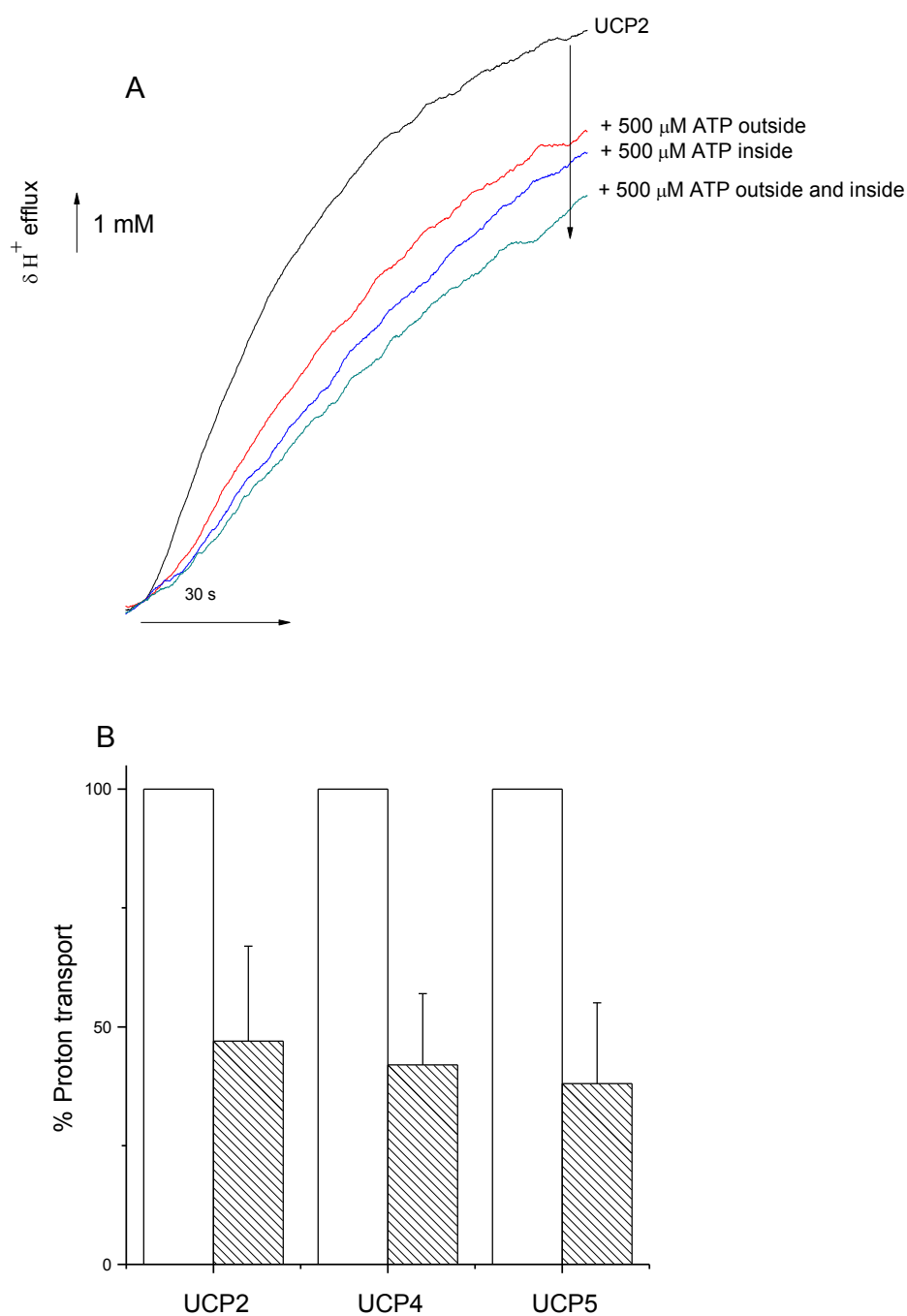
Figure 17 – Random orientation of reconstituted UCPs demonstrated through proton flux assay in azolectin vesicles

(A) Proton flux in UCP2 proteoliposomes was compared with that in the presence of 500 μM ATP on either the inner, outer leaflet or both sides of the membrane. (B) Inhibition of proton flux by external ATP at the concentration of 100 μM (shaded bars).
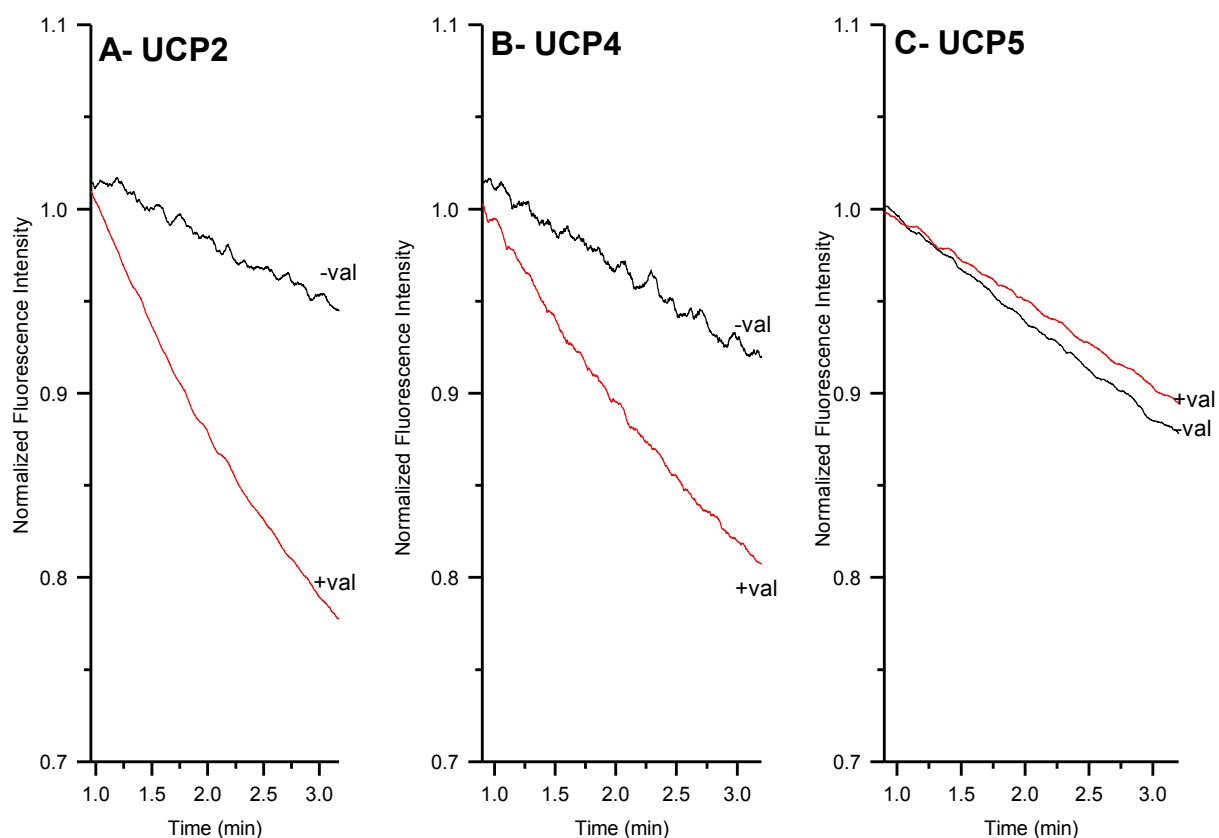
Figure 18 – Qualitative chloride influxes mediated by neuronal UCPs in azolectin vesicles

Fluorescence signal of SPQ at 444 nm (±5 nm) were normalized at 1 min, when the val was initially added. Difference in normalized fluorescence intensity of SPQ trapped in UCP proteoliposomes in the presence and absence of val were plotted. UCP2 (A) and UCP4 (B) showed positive chloride influx in the presence of val, while UCP5 (C) showed no change in SPQ fluorescence signal. Lipid concentration was kept at 20 mg/mL while lipid/protein (w/w) ratio is ~ 200/1.

4.5. Conformation of reconstituted neuronal UCPs

4.5.1. CD spectra of neuronal UCPs in phospholipid vesicles

CD spectra of all reconstituted UCPs were measured in the far-UV range (190-260 nm). The comparative CD spectra of UCPs in two phospholipid vesicles (azolectin and azolectin with 2.5 mol% CL) are depicted in Fig. 19. Three challenges were posed in the CD spectroscopic measurements, including the signal detection limit (minimum protein concentration is typically 0.5-1 μM), noise contribution from lipids, and maintaining similar protein/lipid ratio as in the ion transport assays (~1/10000 molar ratio). Taking all of these restrictions into consideration, the protein/lipid molar ratio in the CD spectroscopic experiments were kept as low as 1/1000 and protein concentration of the proteoliposome sample was maintained at ~1 μM (Fig. 19).

In azolectin vesicles, both UCP2 and UCP4 displayed high α-helical content in their far-UV CD spectra (Table 3 and Fig. 19A). The far-UV CD spectra of UCP2 contained two negative maxima (at ~220 nm and ~210 nm) and a positive maximum at 192 nm (Fig. 19A). Spectra of UCP4 displayed one local minimum at ~220 nm, a shoulder at ~210 nm and a local maximum at 194 nm. Both UCP2 and UCP4 showed typical helical conformation spectra with the ratio between positive maximum and negative maximum close to 1:2. UCP5, on the other hand, showed a much lower alpha helical content (Table 3 and Fig. 19). In addition, determination of α-helical content in UCP5 was more challenging due to the low positive maximum ellipticities and noisy signals (Fig. 19A). Estimation of secondary structure (Dichroweb, CDSSTR algorithm, reference set 7) resulted in helical contents of UCP2 and UCP4 at 52% and 51%, respectively (Table 3) [83, 84]. In contrast, UCP5 was as low as 8% helical (Table 3). It is noteworthy to mention that the reference data sets used in the available CD deconvolution methods are mainly based on known structures of soluble globular proteins and thus can only

provide estimations at a certain accuracy level, especially for membrane proteins. In addition, conformation of UCP2 and UCP2 (His-tag) were comparatively examined in 20 mM denaturing detergent SDS (Fig. 20). Both of these proteins exhibited very similar far-UV CD spectra with high α-helical content (42% α-helix).

Addition of CL at 2.5 mol% to the phospholipid vesicles induced changes in the overall secondary structures of all reconstituted UCPs as outlined in Fig. 19B and Appendix 3. Both reconstituted UCP2 and UCP4 proteins experienced a decrease in their helical content. While UCP4 experienced a slight drop in helical content (5% decrease), UCP2 demonstrated a more significant change in its secondary structure in azolectin vesicles supplemented with 2.5 mol% CL (18% decrease in helical content) (Table 3). The far-UV CD spectra of these proteins, however, still displayed dominantly helical structures (negative maxima ~220 nm and ~210 nm, positive maximum at ~190 nm, and positive maximum to negative minimum ratio of ~2). In contrast to UCP2 and UCP4, UCP5 reconstituted into azolectin-based proteoliposomes in the presence of CL exhibited an enhancement of estimated helical content (15% helix, Table 3). Yet, the far-UV CD spectra of UCP5 did not show any drastic change in overall appearance compared to the previous profile in azolectin-only vesicles (Fig. 19B). Overall, a general trend was observed, that is, addition of CL at 2.5 mol% did not cause any extreme structural changes. In addition, models of UCPs with and without CL did not show any drastic changes in their overall structures (section 4.1). Therefore, the changes in secondary structures of UCPs in proteoliposomes containing CL might be attributed to protein association, helix packing, and structural organization. The role of CL will be discussed in more detail in the discussion section.

4.5.2. Interaction of reconstituted UCPs with the purine nucleotide ATP

Interactions between the purine nucleotide ATP and reconstituted UCPs were monitored by far-UV CD spectroscopy. Similarities in spectral profiles were observed for all UCPs in both of the phospholipid systems (azolectin and azolectin with 2.5 mol% CL) (Fig. 20 and 21). These results agreed with the previous conformational study by Ivanova *et al.* in POPC/POPG vesicles [81]. The previous study, however, also detected changes in the microenvironment through near-UV CD spectra. In the current study, CD deconvolution of UCP2 and UCP4 showed a similarity or slight increase in overall helical content of both proteins in the presence of ATP (Appendix 3). On the contrary, addition of ATP yielded a small increase in helical content of UCP5 in both phospholipid systems. CD spectra of reconstituted UCP5 and ATP showed a sharper and more defined local maximum at 195 nm (Fig. 20 and 21).

Table 3 – Secondary structure composition of neuronal UCPs in lipid vesicles

Deconvolution of the CD spectra was performed using CDSSTR program on the Dichroweb website (see section 3.2.4) [83, 84]. The values represent the percentage of secondary structure composition based on the averaged CD spectra. NRMSD, normalized root mean square deviation, shows the difference between values of the fitting and the actual values, denoting the best fit between the calculated and the experimental CD spectra.

	Protein	α-helix	β-strand	Turn	Random	NRMSD
Azolectin vesicles	UCP2	52	16	17	15	0.016
	UCP4	51	12	17	20	0.015
	UCP5	8	32	23	38	0.017
Azolectin vesicles with 2.5 mol% CL	UCP2	34	22	19	24	0.026
	UCP4	46	19	17	18	0.013
	UCP5	15	32	22	31	0.022
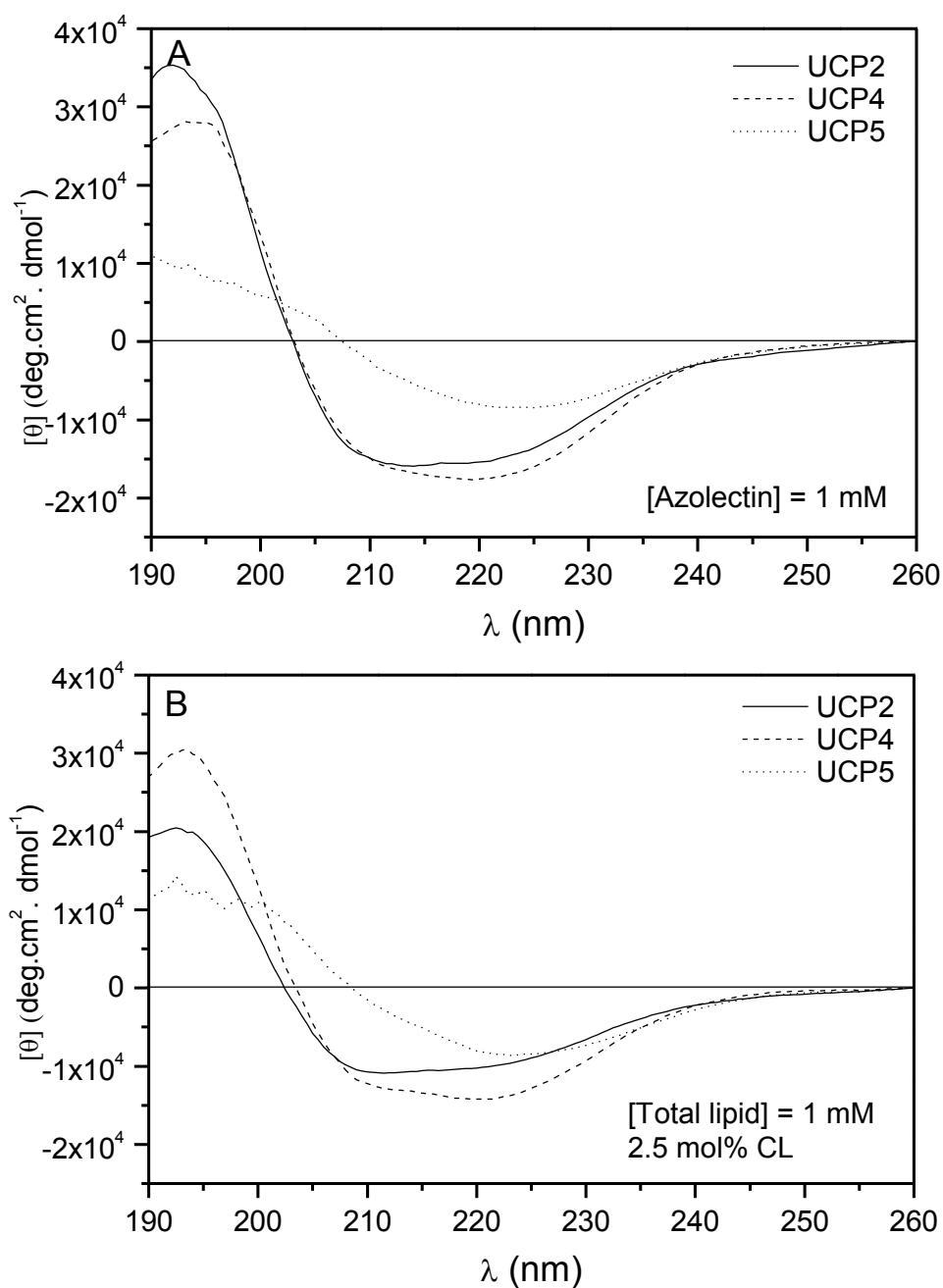
Figure 19 – Comparative far-UV CD spectra of neuronal UCPs in liposomes

The proteins were reconstituted in 1 mM of azolectin (A) or azolectin supplemented with 2.5 mol% CL (B). The protein concentrations in azolectin vesicles were 1 μM (UCP2), 0.8 μM (UCP4), 1.3 μM (UCP5) while these in the second phospholipid system were 1.6 μM (UCP2), 1 μM (UCP4), and 1.3 μM (UCP5).
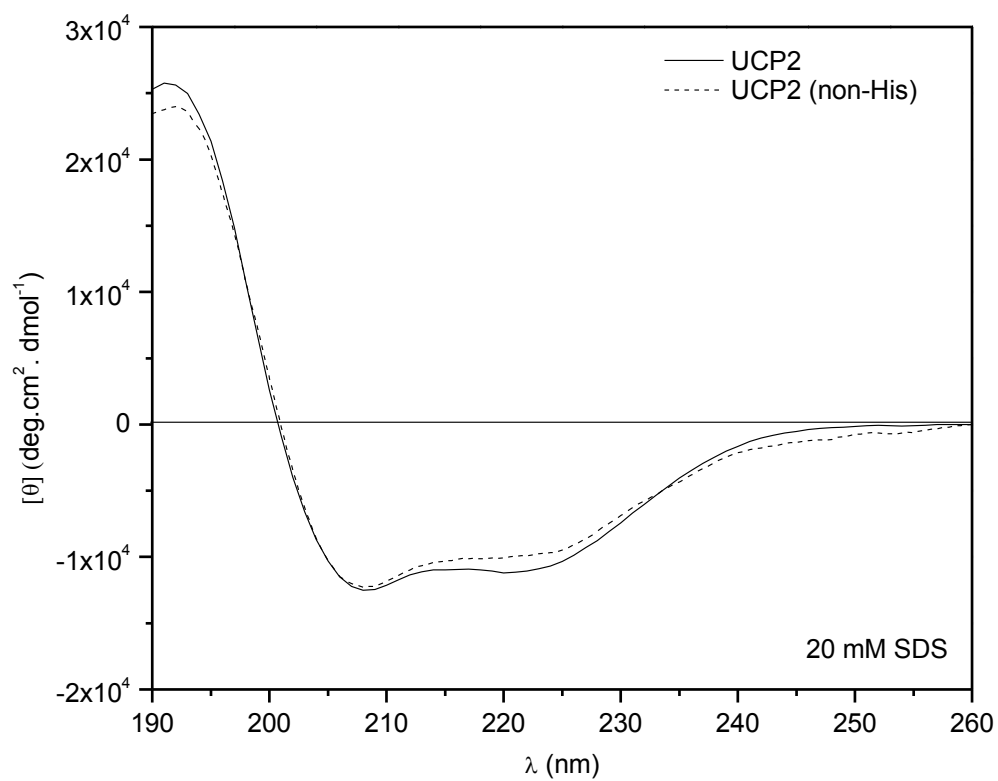
Figure 20 – Comparative far-UV CD spectra of UCP2 with and without His tag in 20 mM anionic detergent sodium dodecyl sulphate (SDS)

The protein concentrations were 4.6 μM (UCP2-His) and 2.5 μM (UCP2-non His).
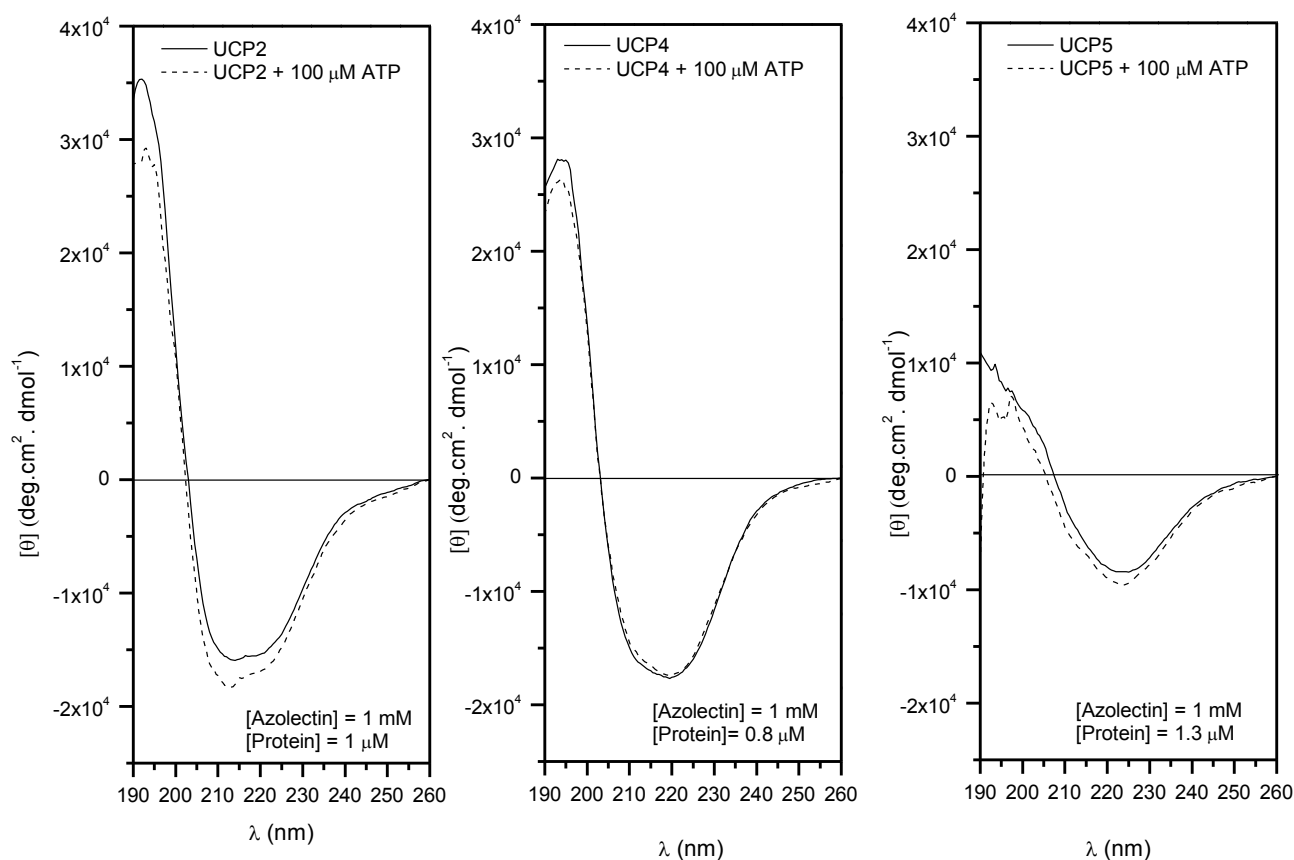
Figure 21 – Far-UV CD spectra of reconstituted neuronal UCPs in azolectin vesicles with and without the addition of 100 µM inhibitor ATP

The concentration of azolectin vesicles was kept at 1 mM, while the protein concentrations were 1 µM (UCP2), 0.8 µM (UCP4), and 1.3 µM (UCP5).
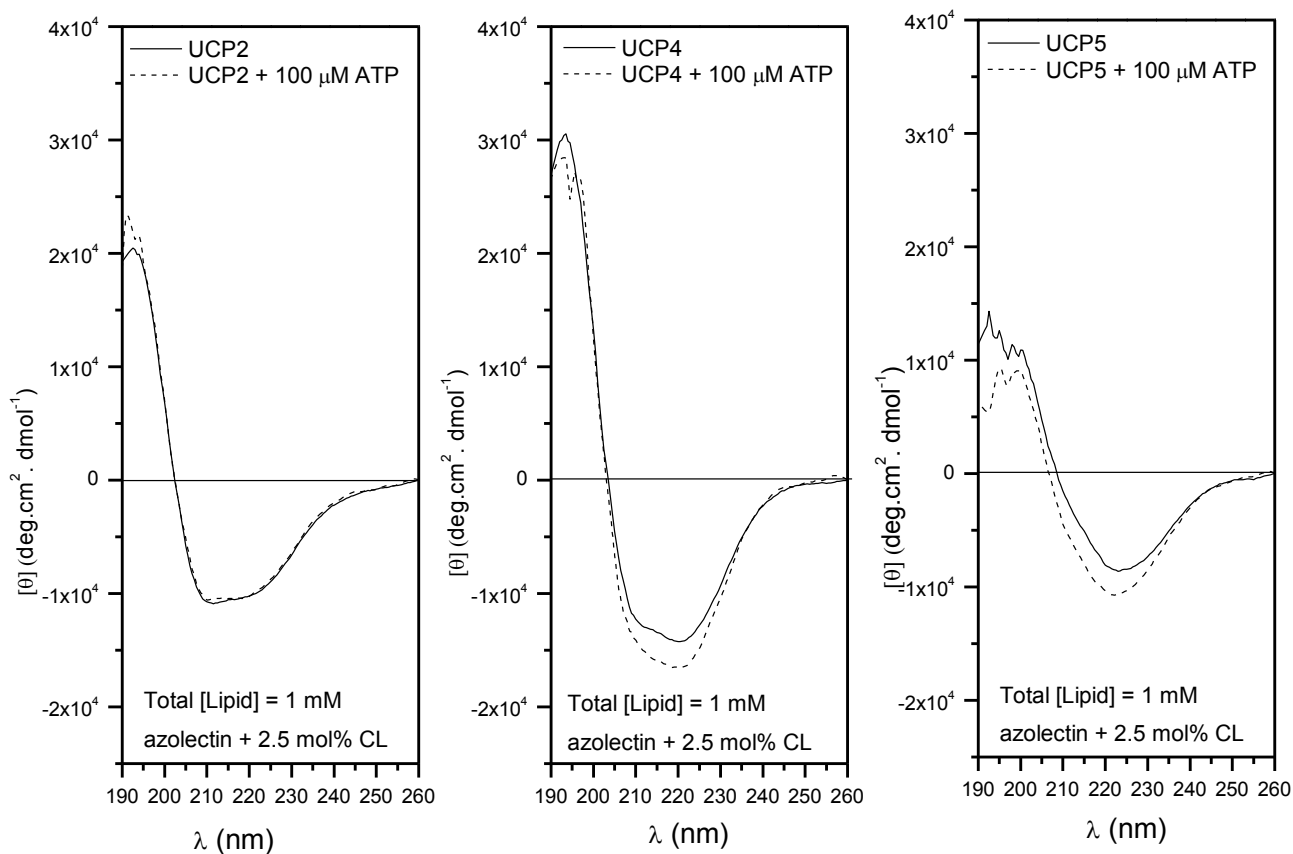
Figure 22 – Far-UV CD spectra of reconstituted UCPs in liposomes (azolectin with 2.5 mol% CL) with and without the addition of 100 µM inhibitor ATP

The total concentration of phospholipid vesicles was 1 mM, while protein concentrations were 1.6 µM (UCP2), 1 µM (UCP4), and 1.3 µM (UCP5).

CHAPTER 5 – DISCUSSION

5.1 Detergent-mediated reconstitution of membrane proteins

Obtaining correctly folded proteins is essential for all *in vitro* research on the structure and function of proteins. In the study of membrane proteins, reconstitution methods play a key role in this folding process, where the protein is eventually embedded in a lipid bilayer environment. However, it is difficult to insert directly a membrane protein into a liposome in its native structural and functional forms. Most membrane proteins, when expressed in a recombinant form in *E. coli*, are produced as insoluble inclusion body proteins. They are typically solubilized in mild detergents prior to being transferred to a native-like lipid environment [95]. Recently, a new method has been discovered to facilitate the production of proteins directly into membranes using nanodisc technology [96]. This reconstitution technique is currently in development and is hoped to become more routine in the near future. In this study, UCP2 expression was also attempted in a cell-free medium; however, optimization is still needed. Currently, conventional reconstitution is still used most commonly in research labs studying membrane proteins. The quality of membrane proteins prepared using this method, however, depends heavily on experimental conditions such as the detergents used, the phospholipid composition of the liposomes, and the nature of the membrane proteins themselves. Unlike most current reconstitution studies, the folding of neuronal UCPs into phospholipid bilayers in this study was examined in different experiments. First of all, liposome formation and size were monitored by light scattering measurements. Multilamellar phospholipids (turbid) were completely solubilized by the mild detergent C_8E_4 to form mixed micelles (transparent). The amount of detergent required for mixed micelle formation was calibrated spectroscopically at 540 nm. Dynamic light scattering analysis confirmed a homogenous and comparatively small

population of these mixed micelles (~30 nm diameter). In the final stage of reconstitution, removal of detergents allows phospholipid molecules to come together spontaneously and form unilamellar vesicles embedding the membrane proteins of interest. In this study, SM-2 Biobeads were used to quickly remove detergents (C_8E_4 and TX-114), after which the successful formation of liposomes was verified by size measurements. The final liposomes were mono-disperse, unilamellar vesicles of ~100 nm in radius (refer to section 4.3). Incorporation of UCPs into the phospholipid vesicles affected both the liposomal size (refer to section 4.3) and morphologies (data not shown). Successful refolding of UCPs in liposomes was demonstrated using conformational and functional experiments. CD spectra of reconstituted UCPs showed that the proteins had taken on significant secondary structure, and that they interacted with the known UCP regulatory ligand ATP (and ADP) (Figs. 19-22). In addition, all reconstituted UCPs exhibited transmembrane positive proton fluxes that are regulated by fatty acids and purine nucleotides (Figs. 12-16). Thus, according to these criteria, renaturation of reconstituted UCPs was successfully achieved in this study.

Besides correct refolding, the orientation of reconstituted proteins in liposomes is another important consideration in reconstitution experiments. UCP orientation in this study was assumed to be symmetrical in nature, implying that both C- and N-termini of 50% of the reconstituted proteins were oriented towards either the outer or inner leaflet of the lipid vesicles without any specific preference. This hypothesis was further supported by analyzing the inhibition effect of purine nucleotides on UCP-mediated proton transport from both the internal and external side of the lipid bilayers. The results showed that, in fact, the reconstituted UCPs were in approximately symmetrical orientation in phospholipid vesicles (Fig. 17). The proton flux of UCP2 was similarly inhibited by 500 μM ATP either on the inside or outside of the

liposome, and this inhibition was further enhanced by having ATP on both sides of the membrane leaflets (Fig. 17A). Moreover, it was also shown that the saturation of proton transport inhibition was reached at ~100 μM external ATP, where the proton transport of all reconstituted UCPs were approximately 50% compared to the basal proton flux (Fig. 17B). Therefore, supported by experimental evidence, neuronal UCPs in this study were shown to be reconstituted in an approximately symmetrical orientation across the lipid bilayers.

5.2. Impacts of a poly-histidine tag on conformation and function of recombinant UCPs

To facilitate the purification of recombinant UCPs, during molecular design and cloning, a hexahistidine tag was incorporated into the N-terminus of each protein. This addition was expected to have negligible impact on the structure and function of UCPs. Indeed, insignificant changes in both conformation and ion transport ability were observed in the His-tagged version of UCP2 as compared to the untagged version of the protein. In the functional study, untagged UCP2 and His-tagged UCP2 transported protons at similar rates in both types of lipid vesicles (refer to section 4.4.2). Both types of proteoliposomes also shared similarities in size (refer to section 4.3). Finally, both His-tagged and non-His tagged versions of UCP2 exhibited similar conformations in the presence of 20 mM SDS (42% helical content, refer to section 4.5) (Fig. 20) [81]. Therefore, in total, the data indicate that the incorporation of a polyhistidine tag at the N-terminus has a minimal impact on the overall structure and function of recombinant UCPs.

5.3 Cardiolipin influences the structure and function of neuronal UCPs

In the membrane, lipids not only act as a semi-permeable barrier, but also as an important interacting partner with many other components of the membrane, including membrane proteins. Each cellular membrane has a distinct composition of proteins and lipids. Therefore, the lipid composition plays an important role in defining the characteristics (structure and function) of

biomolecules associated with any given membrane. The composition of lipids, however, is complex and difficult to quantify and replicate *in vitro*. Studies of membrane proteins, when using different lipid bilayer environments, could result in different structures/functions of the membrane proteins. This was demonstrated when comparing the conformations of neuronal UCPs determined in this study to the ones in our previous work [81]. Specifically, in the conformational study of Ivanova *et al.* in 2010, the neuronal UCPs were placed in negatively charged synthetic POPC/POPG (7/3 molar ratio) SUV phospholipids, and yielded a helical content of ~ 35% [81]. UCP4 reconstituted into proteoliposomes consisting of the same lipid mixture displayed a slightly different far-UV CD spectrum compared to other UCPs in that study [81]. In the current study, all UCPs were reconstituted in the natural phospholipid azolectin extracted from egg yolk, containing mostly phosphatidylcholine (at least 60%), phosphatidylethanolamine, and other phospholipids such as triglycerides and cholesterol. This difference in phospholipid content led to conformational differences in all reconstituted neuronal UCPs as compared to the earlier study (refer to section 4.4 and 4.5) [81]. Significant increases in helical content were observed for both UCP2 and UCP4 proteoliposomes (~50% helix, compared to ~35% in POPC/POPG). In contrast, UCP5 proteoliposomes in the current study had a very different far-UV CD spectrum than UCP5 in the previous study, suggesting a conformation that consisted mostly of β-sheet, rather than α-helix. Thus, lipid compositions strongly affect the conformations of reconstituted UCPs.

Cardiolipin has been claimed in many recent reports to play a pivotal role in overall mitochondrial inner membrane organization and dynamics [4-9, 80, 97]. This dimeric phospholipid is abundant in the inner mitochondrial membrane (~20% w/w) and has an unusual structure consisting of four acyl chains, in comparison with more typical lipids with only two

acyl chains [98, 99]. Although little is known about the exact impact of CL on the organization

of mitochondrial membrane components, this phospholipid has been demonstrated to bind rather

tightly to certain mitochondrial protein surfaces and affect their conformation and folding. For

instance, AAC, a structural model for UCPs, was shown to be tightly bound to CL [70]. In

addition, recent cryoelectron tomogram work by Acehan *et al*. suggested that CL promotes the

ribbon-like assembly of ATP synthase dimers and affects lateral organization and morphology of

the crista membrane [97]. The overall consensus leans toward CL having the role in promoting

protein-protein interactions and protein oligomerization.

Our data in this study further confirm the role of CL on the structure and function of

neuronal UCPs. Addition of CL at 2.5 mol% of the total phospholipid enlarged the liposomal

size and induced changes in both UCP conformations and ion transport rates (refer to section 4.3,

4.4, and 4.5). These effects caused by CL were distinct for each UCP, which could be due to

specific interactions of each UCP with CL molecules. In addition, a similar (UCP2 and UCP4) to

slightly stronger (UCP5) inhibition of ATP on UCP-mediated proton transport was observed in

the presence of 2.5 mol% CL (refer to section 4.4). Given a high positive potential in all UCPs

and the negative charge in CL, it is highly plausible that these molecules interact

electrostatically. Molecular modelling of UCPs based on the second crystal AAC (bound with 3

CL molecules) also revealed a slightly larger nucleotide binding pocket as compared to the one

that did not bind to CL (refer to section 4.1). Therefore, the presence of CL can potentially

induce structural changes of UCPs and their functions (proton transport rate and binding to the

inhibitor molecule ATP). As shown in the 3D models of UCPs, the proposed nucleotide binding

pocket is located in the middle of the funnel-shaped UCP structure (Fig. 23). On the other hand,

CL was shown in the second model to interact strongly with amino acid residues (hydrophobic,

H-bond, and electrostatic interactions) that are situated towards the inner leaflet of the membrane and partially nested in small grooves formed by the matrix loops [6]. Therefore, the interaction sites between CL and UCPs are located a few Å below the purine nucleotide binding pocket (Fig. 23). Piecing all of the above information together, a suggested mechanism of interactions between CL and UCPs was drawn from this study (Fig. 23). In brief, negatively charged phospholipid CL interacts with amino acids located close to the matrix loops, causing minor structural changes and consequently inducing a slightly more open binding pocket, allowing for a better interaction between UCPs and purine nucleotides. These CL molecules could also act as a link for protein-protein interactions that promote a more functional form of UCPs.

Overall, it seems clear that CL is an essential component in defining structures and functions of inner mitochondrial membrane proteins, especially UCPs. In the current study, CL was supplemented at 2.5 mol% of total phospholipids. This is approximately four times less than the average content of CL in the mitochondrial inner membrane (~20% weight ratio, ~10% mol ratio). Therefore, a higher content of CL is expected to cause an even more dramatic effect on the structures and functions of UCPs. It is also important to note that mitochondria from different cells or tissues contain different levels of CL [67]. For example, mitochondria from rat brain were observed in one study to contain markedly lower amounts of this phospholipid [100]. Therefore, UCP expressed in different tissues can behave differently based on the varying amounts of CL in these tissues. Another notable concern is the acyl chain composition of CL. Recent studies found that unlike the majority of mammalian tissues, tetralinoleoyl CL is not the predominant form of CL in the brain. Instead, stearic (18:0), oleic (18:1), cervonic (22:6), and arachidonic acid (20:4) were found to contribute equally (~20% each) to the acyl chain of CL in mouse brain [101]. Linoleic acid (18:2) was only found to contribute ~5% of the total brain CL

[102, 103]. This difference in acyl chain composition of brain CL could be significant for the interactions of CL with other mitochondrial membrane proteins. CL used in the current study contains only oleic acyl chains.

5.4. Linking conformation and ion transport of neuronal UCPs to their physiological roles in the CNS

As previously mentioned, many studies have been done on different aspects of UCPs in the past decade; however, a clear picture of their functional role has not yet emerged, with the exception of UCP1. A relatively new area of UCP research focuses on their roles in the CNS. These roles have become especially relevant after the discovery of UCP2, UCP4 and UCP5 expression profiles in the brain. Nevertheless, many uncertainties remain, and the relative lack of clear structural information for these proteins has caused difficulties in defining the functions of the CNS UCPs. On the basis of the results obtained in this study integrated with data from other recent studies, an attempt will be made to unravel some of the potential roles of neuronal UCPs (especially UCP4 and UCP5) in the CNS.

UCP4 and UCP5 display UCP1-like biochemical properties

Although listed under the generic name UCP, both UCP4 and UCP5 have not garnered much attention from UCP researchers due to their low sequence homology to other UCPs. After their discovery, studies have been done to evaluate their uncoupling effects in cells [29, 30, 60, 104, 105]. However, their relation to the UCP family has been questioned in many studies [16, 20]. In his review in 2007, Echtay mentioned that the question as to whether UCP4 and UCP5 are natural mitochondrial UCPs remains to be proven, since the typical UCP1-like biochemical properties of these proteins (such as sensitivity to regulation by FAs and nucleotides) have not yet been demonstrated [16].
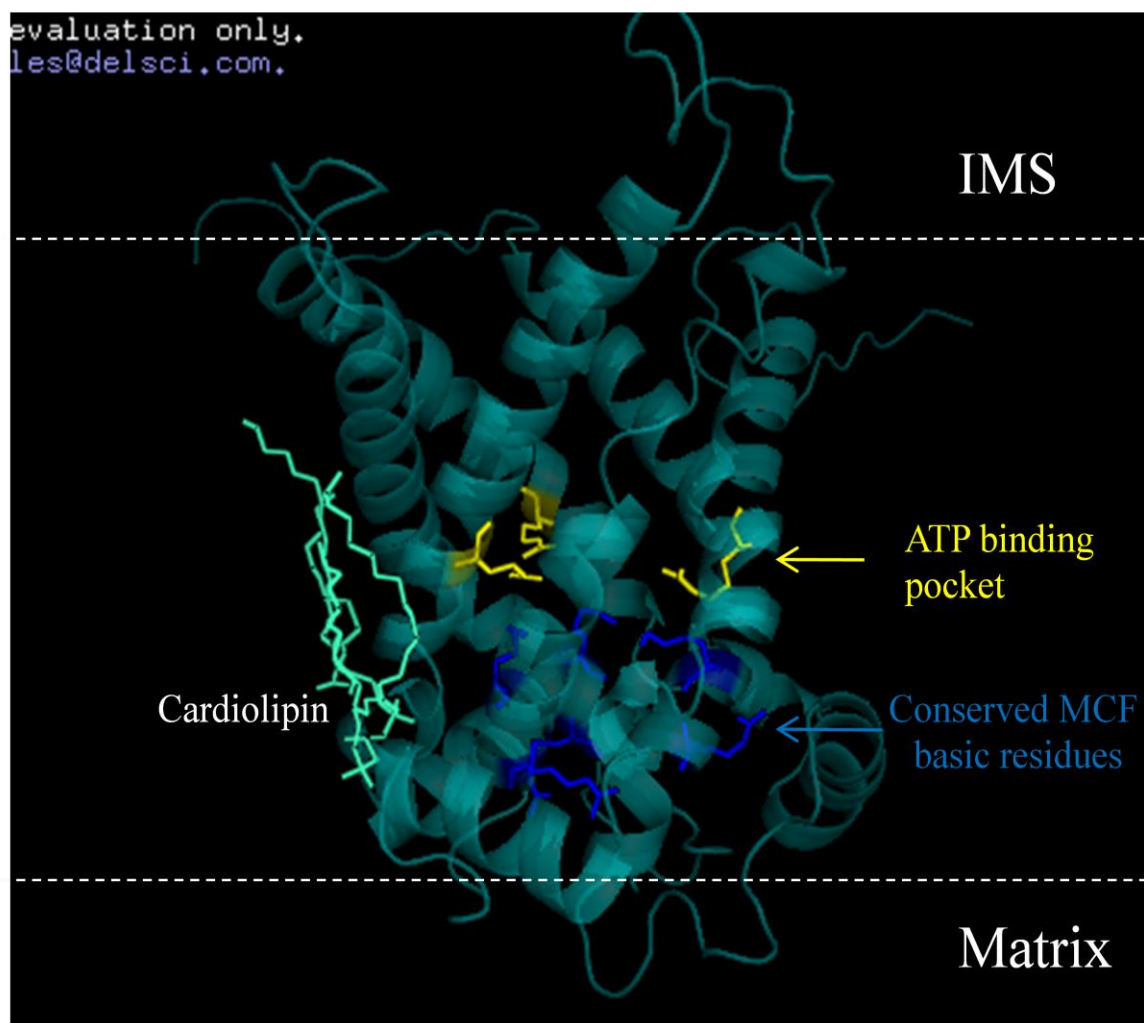
Figure 23 – Proposed model mechanism of UCP2 and CL interaction

CL molecules bind strongly to residues located on the inner leaflet of membrane closed to the matrix loop (only one of three CL molecules is shown), thus inducing the 3-D change in the ATP binding pocket (three Arg residues are represented as yellow sticks). The basic residues (K and R) of the conserved MCF motifs located closed to the CL binding sites are shown in blue sticks. The model was built in Pymol after sequence alignment (T-Coffee) using ADP/ATP carrier (PDB ID: 2C3E) as blueprint (MODELLER) [77-80].

Under our experimental conditions, all neuronal UCPs displayed proton transport in both types of phospholipid vesicles tested (azolectin with and without 2.5 mol% CL) (refer to section 4.4). The proton transport rates for all neuronal UCPs were comparable in the azolectin vesicles (1-2 $\mu mol.min^{-1}.mg$ protein^{-1}), while those in the second phospholipid system varied within a larger range (0.6-5 $\mu mol.min^{-1}.mg$ protein^{-1}). Moreover, the proton flux mediated by UCP2, UCP4 and UCP5 followed a similar pattern to that of prototypic UCP1. In these experiments, proton transport was only activated in the presence of FAs (LA, 100 μM in this case) and inhibited by purine nucleotides (both ATP and ADP) at relatively low concentrations ($K_i \sim$ 10 μM). In the presence of CL, changes were consistently observed in the conformation and transport properties of all neuronal UCPs. Thus, based on the results of the current study, despite their low sequence homology to the prototypical protein UCP1, UCP4 and UCP5 share common structural and functional features with the other members of the UCP family (UCP1, 2, and 3) and can therefore be considered as genuine members of this family of mitochondrial proteins.

In addition to proton transport, based on the results of this study, UCP2 and UCP4 also transport chloride anions. UCP5, on the other hand, did not show any significant chloride transport activity (refer to section 4.4). This is the first time that anion transport has been examined for UCP4 and UCP5 in proteoliposomes. Although no quantitative work has been done, the results show that future experiments focusing on anion transport are warranted. The quantitative analysis of chloride transport (with and without the presence of CL) will help clarify the mechanism of ion transport in neuronal UCPs, especially with the less studied UCP4 and UCP5.

Suggested physiological roles for neuronal UCPs in the CNS

Thermogenesis

Uncoupling-induced thermogenesis by UCP1 has been well understood for some time [20, 69]. Given their similarities in biochemical properties, all other UCPs are suggested to also generate a certain amount of heat through uncoupling actions. This also applies to all neuronal UCPs, where their expressions are mainly in the CNS, with the exception of the ubiquitously expressed UCP2. Interestingly, brown adipose tissues are located close to the CNS and their tissue expression is controlled by the temperature-sensing system in the CNS [106]. Therefore, UCP1 highly expressed in this tissue might have a close connection with the brain UCPs (UCP4 and UCP5). Given their lower expression level in the brain, neuronal UCPs could contribute partly to the localized temperature control in the CNS, which is essential for communications between neurons (thermal synapses) [48].

Transport of FAs

Another possible role of UCPs, based on the fatty acid-cycling model, is to transport FA anions out of the mitochondria and protect the organelles from toxic effects caused by FA anions and peroxides. FAs play an important role in β-oxidation pathways. When FA supply exceeds the oxidation rate, accumulation of unesterified FAs could produce toxic effects. Therefore, a role of UCP will be to export these FA anions from the matrix into the cytosol to prevent any mitochondrial damage. In fact, mRNA levels of UCP3 in muscle, in both mice and rats, were observed to markedly increase after fasting, acute exercises, and high-fat diet feeding [107-112]. In the CNS, FAs also play an important role. They participate mainly in CNS membrane biogenesis. Moreover, the protective myelin in the brain contains 70% lipids [113]. One of the most common FAs in myelin is oleic acid [113]. Therefore, the brain UCPs (UCP2, 4, and 5)

could also be anticipated to reduce the toxic effects caused by FA anions. This protective mechanism could be achieved by transporting directly FA anions (UCP2 and UCP4 demonstrated the chloride anion transport ability in this study). On the other hand, accumulation of FAs in the matrix could increase the risk of mitochondrial lipid peroxidation, which is also harmful. Therefore, another pathway of neuronal UCPs against the FA anion-induced toxic effects is to mediate proton flux to reduce the membrane potential across the inner mitochondrial membrane, thus lowering superoxide production. This mechanism is discussed in more detail below.

Control of reactive oxygen species (ROS) production

Mitochondria serve as production sites for both ATP and superoxide. Superoxide production is detrimental to tissue survival and can lead to many neurodegenerative diseases [16, 20, and 48]. Besides the antioxidant defence systems discussed in Chapter 1, uncoupling could also help lower the superoxide production in mitochondria by reducing the membrane potential across the inner mitochondrial membrane. Stress-induced expression of neuronal UCPs has been observed in different studies [29, 30, 60, 104, 105]. Therefore, neuronal UCPs are currently hypothesized to participate in attenuating mitochondrial production of free radicals and thus protecting against oxidative damage [16, 20, 48]. This hypothesis could be generally applied to all UCPs. A question posed for this function of UCPs is whether they require a specific regulator to optimize their proton transport rate. A study done in 2000 by Etchay *et al.* defined CoQ as an obligatory cofactor for proton transport mediated by UCP1-3 [114]. Given the different expression level in various tissues, it is plausible that each UCP in different cell types could require its own specific activator for proton transport. Various superoxides have been examined in the role of activating transport mediated by UCPs [16, 115]. Therefore, it is worthwhile to

focus future studies on the crucial ROS-induced proton flux mediated by neuronal UCPs, especially UCP4 and UCP5.

Is uncoupling a main function of UCPs?

The uncoupling function of UCP1 has a well-established physiological role. However, whether the uncoupling action is the main function for other UCPs is still a question that remains to be answered. It has been shown that other proteins in the MCF could also mediate a proton leak [116]. An example of a protein that can catalyze an uncoupling function is the AAC. This protein is far more abundant than other carrier proteins [117]. Except for the case of BAT where UCP1 is highly expressed, AAC is constantly present at ~10% total mitochondrial protein [117]. Thus, this protein could mediate a significant amount of proton leak as well. Therefore, the remaining question is whether UCPs carry out proton leak as their main function, or like other proteins in the MCF, if the uncoupling function is a side function of these proteins. If the latter is true, then the next question is, should these proteins even be called uncoupling proteins?

<u>CHAPTER 6</u> – CONCLUSION and FUTURE STUDIES

A general reconstitution protocol has been developed in the current study, which allowed formation of LUVs for the study of the structure and function of UCPs from the mitochondrial inner membrane. More importantly, this work has provided important insights into the conformations and ion transport activity of all neuronal UCPs reconstituted into liposomes, especially UCP4 and UCP5, which have not been examined before. Under our experimental conditions, all reconstituted neuronal UCPs showed clear proton transport activity, and were regulated in a similar way (i.e. activated by FAs and inhibited by purine nucleotides) to the prototypical protein UCP1. Thus, the results of this study confirm the similar transmembrane conductance of protons in all neuronal UCPs despite their differences in primary sequence, and partly answer the question of whether UCP4 and UCP5 belong to the family of mitochondrial UCPs [16]. Finally, the important role of CL in the structure and function of mitochondrial membrane proteins such as UCPs was demonstrated in this study. A suggested interaction mechanism between UCPs and CL was drawn based in part by molecular models that were generated for these proteins, in which CL interacts with residues located in the inner leaflet of the membrane, allowing UCP monomer interactions and the formation of a more optimal binding pocket for purine nucleotides.

Further research is needed to reveal the true physiological role of neuronal UCPs in the CNS. Strong evidence from recent studies suggests a possible superoxide activation pathway for neuronal UCPs [104, 105, and 115]. Therefore, an objective for future studies in our laboratories is to investigate the positive protective roles of neuronal UCP homologs against oxidative stress in the CNS using proteoliposome systems. Attempts should be focused on generating *in situ* lipid peroxidation processes to evaluate the proton transport activity of UCPs in the presence of mixed

oxidation products. It is also important to note that the recent structural study of UCP2 by NMR molecular fragment searching demonstrated striking similarities between UCP2 and AAC despite only 20% sequence identity [118]. However, in that study, UCP2 was placed in a mixed micelle environment and overall structure determination was only determined by piecing together molecular fragments from the Protein Data Bank that best fit experimental residual dipolar couplings (RDCs) from samples weakly aligned in a DNA nanotube liquid crystal. Therefore, solid-state NMR techniques are currently in development to obtain a high resolution structure of neuronal UCPs in native-like lipid bilayer environments. The results from these studies will provide additional insight into the structure-function relationship of neuronal UCPs. Ultimately, these findings will clarify the role of neuronal UCPs in protection against neurodegenerative diseases in the CNS, and may play an important part in designing successful treatment strategies against neuropathological conditions.

REFERENCES

1. Becker, W. M., Kleinsmith, L. J., and Hardin, J. (2005) The World of The Cell, 6th Ed, Chapter 10: Chemotrophic Energy Metabolism: Aerobic Respiration.

2. Scheffler, I. E. (1999) Mitochondria. Chapter 3, John Wiley and Sons, New York.

3. Haines, T. H. (2009) A new look at cardiolipin. *Biochim.Biophys. Acta* **1788**, 1997-2002.

4. Robinson, N. C. (1993) Functional binding of cardiolipin to cytochrome c oxidase. *J. Bioenerg. Biomembr*. **25**, 153-163.

5. Dale, M. P., and Robinson, N. C. (1988). Synthesis of cardiolipin derivatives with protection of the free hydroxyl: its application to the study of cardiolipin stimulation of cytochrome c oxidase. *Biochemistry* **27**, 8270-8275.

6. Nury, H., Dahout-Gonzalez, C., Trezeguet, V., Lauquin, G. J. M., Brandolin, G., and Pebay-Peyroula, E. (2006) Relations between structure and function of the mitochondrial ADP/ATP carrier. *Annu. Rev. Biochem*. **75**, 713-741.

7. Eble, K. S., Coleman, W. B., Hantgan, R. R., and Cunningham, C. C. (1990) Tightly associated cardiolipin in the bovine heart mitochondrial ATP synthase as analyzed by ^{31}P nuclear magnetic resonance spectroscopy. *J. Biol. Chem*. **265**, 19434-19440.

8. Kaplan, R. S., Pratt, R. D., and Pedersen, P. L. (1986) Purification and characterization of the reconstitutively active phosphate transporter from rat liver mitochondria. *J. Biol. Chem*. **261**, 12767-12773.

9. Pfeiffer, K., Gohli, V., Stuart, R. A., Hunte, C., Brandt, U., Greenberg, M. L., and Schagger, H. (2003) Cardiolipin stabilizes respiratory chain supercomplexes. *J. Biol. Chem*. **278**, 52873-52880.

10. Mitchell, P. (1961) Coupling of phosphorylation to electron and hydrogen transfer by a chemi-osmotic type of mechanism. *Nature* **191**, 144-148.

11. Voet, D., and Voet, J. G. (2004) Biochemistry, 3rd Ed, Volume 1: Biomolecules, Mechanisms of Enzyme Action and Metabolism. John Wiley and Sons, Inc., NJ, USA, chapters 1, 4, 16, 17, 22.

12. Hirono-Hara, Y., Noji, H., Nishiura, M., Muneyuki, E., Hara, K. Y., Yasuda, R., Kinosita, K., and Yoshida, M. (2001) Pause and rotation of F_1-ATPase during catalysis. *Proc. Natl Acad. Sci. U.S.A* **98**, 13649-13654.

13. Brand, M. D., Pakay, J. L., Ocloo, A., Kokoszka, J., Wallace, D. C., Brookes, P. S., and Cornwall, E. J. (2005) The basal proton conductance of mitochondria depends on adenine nucleotide translocase content. *Biochem J*. **392**, 353-362.

14. Samartsev, V. N., Smirnov, A. V., Markova, O. V., Mokhova, E. N., and Skulachev, V. P. (1997) Involvement of aspartate/glutamate antiporter in fatty acid-induced uncoupling of liver mitochondria. *Biochim. Biophys. Acta.* **1319**, 251-257.

15. Hunter, D. R., Haworth, R. A., and Southard, J. H. (1976) Relationship between configuration, function, and permeability in calcium-treated mitochondria. *J. Biol. Chem.* **251**, 5069-5077.

16. Echtay, K. S. (2007) Mitochondrial uncoupling proteins – what is their physiological role? *Free Radical Biol. Med.* **43**, 1351-1371.

17. Rolfe, D. F., and Brand, M. D. (1996) Contribution of mitochondrial proton leak to skeletal muscle respiration and to standard metabolic rate. *Am. J. Physiol*. **271**, C1380-C1389.

18. Hansford, R. G., Hogue, B. A., and Mildaziene, V. J. (1997) Dependence of H_2O_2 formation by rat heart mitochondria on substrate availability and donor age. *J. Bioenerg. Biomembr*. **29**, 89-95.

19. Skulachev, V. P. (1997) Membrane-linked systems preventing superoxide formation. *Biosci. Rep*. **17**, 347-366.

20. Krauss, S., Zhang, C. Y., and Lowell, B. B. (2005) The mitochondrial uncoupling protein homologs. *Nat. Rev. Mol. Cell Biol*. **6**, 248-26.

21. Borecky, J., Maia, I. G. and Arruda, P. (2001) Mitochondrial uncoupling proteins in mammals and plants. *Biosci. Rep*. **21**, 201–212.

22. Pebay-Peyroula, E., Dahout-Gonzalez, C., Kahn, R., Trézéguet, V., Lauquin, G.J-M. and Brandolin, G. (2003) Structure of mitochondrial ADP/ATP carrier in complex with carboxyatractyloside. *Nature* **426**, 39-44.

23. Nicholls, D. G., Bernson, V. S., and Heaton, G. M. (1978) The identification of the component in the inner membrane of brown adipose tissue mitochondria responsible for regulating energy dissipation. *Experientia Suppl.* **32**: 89–93.

24. Bossa, O., Samecb, S., Paoloni-Giacobinoc, A., Rossierc, C., Dulloob, A., Seydouxb, J., Muzzina, P., and Giacobinoa, J-P. (1997) Uncoupling protein-3: a new member of the mitochondrial carrier family with tissue-specific expression. *FEBS Lett.* **408**, 39-42.

25. Vidal-Plug, A., Solanes, G., Grujic, D., Flier, J. S., and Lowell, B. B. (1997) UCP3: an uncoupling protein homolgoue expressed preferentially and abundantly in skeletal muscle and brown adipose tissue. *Biochem. Biophys. Res. Commun*. **235**, 79-82.

26. Gong, D. W., He, Y., Karas, M., and Reitman, M. (1997) Uncoupling protein-3 is a mediator of thermogenesis regulated by thyroid hormone, β3-adrenergic agonist, and leptin. *J. Biol. Chem.* **272**, 24129-24132.

27. Sivitz, W. I., Fink, B. D., and Donohoue, P. A. (1999) Fasting and leptin modulate adipose and muscle uncoupling protein: divergent effects between messenger ribonucleic acid and protein expression. *Endocrinology* **140**, 1511–1519.

28. Pecqueur, C., Alves-Guerra, M-C., Gelly, C., Levi-Meyrueis, C., Couplan, E., Collins, S., Ricquier, D., Bouillaud, F., and Miroux, B. (2001) Uncoupling protein 2, *in vivo* distribution, induction upon oxidative stress, and evidence for translational regulation. *J. Biol. Chem.* **276**, 8705–8712.

29. Mao, W., Yu, X.X., Zhong, A., Li, W., Brush, J., Sherwood, S.W., Adams, S.H. and Pan, G. (1999) UCP4, a novel brain-specific mitochondrial protein that reduces membrane potential in mammalian cells. *FEBS Lett.* **443**, 326-330.

30. Sanchis, D., Fleury, C., Chomiki, N., Goubern, M., Huang, Q., Neverova, M., Grégoire, F., Easlick, J., Raimbault, S., Lévi-Meyrueis, C., Miroux, B., Collins, S., Seldin, M., Richard, D., Warden, C., Bouillaud, F. and Ricquier, D. (1998) BMCP1, a novel mitochondrial carrier with high expression in the central nervous system of humans and rodents, and respiration uncoupling activity in recombinant yeast. *J. Biol. Chem.* **273**, 34611-34615.

31. Ježek, P., and Garlid, K. D. (1990) New substrates and competitive inhibitors of the Cl translocating pathway of the uncoupling protein of BAT mitochondria. *J. Biol. Chem.* **265**, 19303-19311.

32. Ježek, P., Orosz, D. E., and Garlid, K. D. (1990) Reconstitution of the uncoupling protein of brown adipose tissue mitochondria; demonstration of GDP-sensitive halide anion uniport. *J. Biol. Chem.* **265**, 19296-19302.

33. Jabůrek, M., Vařecha, M., Ježek, P., and Garlid, K. D. (2001) Alkylsulfonates as probes of uncoupling protein transport mechanism. *J. Biol. Chem.* 276, 31897-31905.

34. Ježek, P., Modrianský, M., and Garlid, K. D. (1994) Transport of anions and protons by the mitochondrial uncoupling protein and its regulation by nucleotides and fatty acids. *J. Biol. Chem.* **269**, 26184-26190.

35. Echtay, K. S., Winkler, E., Bienengraeber, M., and Klingenberg, M. (2000) Site-directed mutagenesis identifies residues in uncoupling protein (UCP1) involved in three different functions. *Biochemistry* **39**, 3311-3317.

36. Echtay, K. S., Bienengraeber, M., and Klingenberg, M. (1997) Mutagenesis of the uncoupling protein of brown adipose tissue. Neutralization of E190 largely abolishes pH control of nucleotide binding. *Biochemistry* **36**, 8253-8260.

37. Nicholls, D. G. (2001) A history of UCP1. *Biochem. Soc. Trans.* **29**, 751-755.

38. LaNoue, K. F., Koch, C. D., and Meditz, R. B. (1982) Mechanism of action of norepinephrine in hamster brown adipocytes. *J. Biol. Chem.* **257**, 13740-13748.

39. Arechaga, I., Ledesma, A., and Rial, E. (2001) The mitochondrial uncoupling UCP1: a gated pore. *IUBMB Life* **52**, 165-173.

40. Klingenberg, M., Echtay, K. S., Bienengraeber, M., Winkler, E., and Huang, S. G. (1999) Structure-function relationship in UCP1. Int. J. *Obes. Relat. Metab. Disord.* **23** (Suppl. 6), S24-S29.

41. Modrianský, M., Murdza-Inglis, D. L., Patel, H. V., Freeman, K. B., and Garlid, K. D. (1997) Identification by site-directed mutagenesis of three arginines in uncoupling protein that are essential for nucleotide binding and inhibition. *J. Biol. Chem*. **272**, 24759-24762.

42. Klingenberg, M., and Echtay, K. (2001) Uncoupling proteins: the issues from a biochemist point of view. *Biochim. Biophys. Acta.* **1504**, 128-143.

43. Huang, S.G., and Klingenberg, M. (1996) Chloride channel properties of the uncoupling protein from brown adipose tissue mitochondria: a patch-clamp study. *Biochemistry* **35**, 16806-16814.

44. Echtay, K. S., Liu, Q., Caskey, T., Winkler, E., Frischmuth, K., Bienengraber, M., and Klingenberg, M. (1999) Regulation of UCP3 by nucleotides is different from regulation of UCP1. *FEBS Lett.* **450**, 8-12.

45. Garlid, K. D., Orosz, D. E., Modrianský, M., Vassanelli, S., and Ježek, P. (1996) On the mechanism of fatty acid-induced proton transport by mitochondrial uncoupling protein. *J. Biol. Chem*. **271,** 2615-2620.

46. Jelokhani-Niaraki, M., Ivanova, M. V., McIntyre, B. L., Newman, C. L., McSorley, F. R., Young E. K., and Smith, M. D. (2008) A CD study of uncoupling protein-1 and its transmembrane and matrix-loop domains. *Biochem. J*. **411**, 593-603.

47. Yamaguchi, H., Jelokhani-Niaraki, M., and Kodama, H. (2004) Second transmembrane domain of human uncoupling protein 2 is essential for its anion channel formation. *FEBS Lett.* **577**, 299-304.

48. Andrews, Z. B., Diano, S., and Horvarth, T. L. (2005) Mitochondrial uncoupling proteins in the CNS: in support of function and survival. *Nat. Rev. Neurosci*. **6**, 829-840.

49. Nedergaard, J., Ricquier, D. and Kozak, L.P. (2005) Uncoupling proteins: current status and therapeutic prospects. *EMBO Rep.* **6**, 917-921.

50. Bo, H., Jiang, N., Ma, G., Qu, J., Zhang, G., Cao, D., Wem, L., Liu, S., Ji, L.L. and Zhang, Y. (2008) Regulation of mitochondrial uncoupling respiration during exercise in rat heart: Role of reactive oxygen species (ROS) and uncoupling protein 2. *Free Radical Biol. Med.* **44**, 1373-1381.

51. Harper, M.E. and Gerrits, M.F. (2004). Mitochondrial uncoupling proteins as potential Targets for pharmacological agents. *Curr. Opin. Pharmacol*. **4**, 603-607.

52. Derdak, Z., Mark, N.M., Beldi, G., Robson, S.C., Wands, J.R. and Baffy, G. (2008). The mitochondrial uncoupling protein-2 promotes chemoresistance in cancer cells. *Cancer Res*. **68**, 2813-2819.

53. Ricquier, D. and Bouillaud, F. (2000). Mitochondrial uncoupling proteins: from mitochondria to the regulation of energy balance. *J. Physiol.* **529**, 3-10.

54. Chan, C. B., Leo, D. D., Josheph, J. W., McQuaid, T. S., Ha, X. F., Xu F., Tsushima, R. G., Pennefather, P. S., Salapatek, A. M. F., and Wheeler, M. B. (2001) Increased uncoupling protein-2 levels in β-cells are associated with impaired glucose-stimulated insulin secretion: mechanism of action. *Diabetes* **50**, 1302-1310.

55. Chan, C. B., McDonald, P. E., Saleh, M. C., Johns, D. C., Marban, E., and Wheeler M. B. (1999) Overexpression of uncoupling protein 2 inhibits glucose-stimulated insulin secretion from rat islets. *Diabetes* **48**, 1482-1486.

56. Fleury, C., Neverova, M., Collins, S., Raimbault, S., Champigny, O., Levi-Meyrueis, C., Bouillaud, F., Seldin, M. F., Surwit, R. S., Ricquier, D., and Warden, C. H. (1997) Uncoupling protein-2: a novel gene linked to obesity and hyperinsulinemia. *Nat. Rev. Genet.* **15**, 269-272.

57. Jabůrek, M., Vařecha, M., Gimeno, R. E., Dembski, M., Ježek, P., Zhang, M., Burn, P., Tartaglia, L. A., and Garlid, K. D. (1999) Transport function and regulation of mitochondrial uncoupling proteins 2 and 3. *J. Biol. Chem.* **274**, 26003-26007.

58. Zhang, M., Wang, B., Ni, Y., Liu, F., Fei, L., Pan, X., Guo, M., Chen, R. and Guo, X. (2006) Overexpression of uncoupling protein 4 promotes proliferation and inhibits apoptosis and differentiation of preadipocytes. *Life Sci.* **79**, 1428-1435.

59. Fridell, Y. W., Sanchez-Blanco, A., Silvia, B. A., and Helfand, S. L. (2004) Functional characterization of a *Drosophila* mitochondrial uncoupling protein. *J. Bioenerg. Biomembr*. **36**, 219-228.

60. Yu, X. X., Mao, W., Zhong, A., Schow, P., Brush, J., Sherwood, S. W., Adams, S. H., and Pan, G. (2000) Characterization of novel UCP5/BMCP1 isoforms and differential regulation of UCP4 and UCP5 expression through dietary or temperature manipulation. *FASEB J.* **14**, 1611-1618.

61. Ledesma, A., Lacoba, D. G., and Rial, E. (2002) The mitochondrial uncoupling proteins. *Genome Biol.* **3**, 3015.1-3015.9.

62. Banerjee, R. K., and Datta, A. G. (1983) Proteoliposome as the model for the study of membrane-bound enzymes and transport proteins. *Mol. Cell. Biochem.* **50**, 3-15.

63. Rigaud, J. L., Pitard, B., and Levy, D. (1995) Reconstitution of membrane proteins into liposomes: application to energy-transducing membrane proteins. *Biochim. Biophys. Acta.* **1231**, 223-246.

64. Sharom, F. J., and Eckford, P. D. (2003) Reconstitution of membrane transporters. *Methods Mol. Biol.* **227**, 129-154.

65. Hoffmann, B., Stockl, A., Schlame, M., Beyer, K., and Klingenberg, M. (1994) The reconstituted ADP/ATP carrier activity has an absolute requirement for cardiolipin as shown in cysteine mutants. *J. Biol. Chem.* **269**, 1940-1944.

66. Claypool, S. M., Oktay, Y., Boontheung, P., Loo, J. A., and Koehler, C. M. (2008) Cardiolipin defines the interactome of the major ADP/ATP carrier protein of the mitochondrial inner membrane. *J. Cell. Biol.* **182**, 937-950.

67. Klingenberg, M. (2009) Cardiolipin and mitochondrial carriers. *Biochim. Biophys. Act.* **1788**, 2048-2058.

68. Holloway, P. W. (1973) A simple procedure for removal of Triton X-100 from protein samples. *Anal. Biochem.* **53**, 304-308.

69. Rigaud, J. L., Levy, D., Mosser, G., and Lambert, O. (1998) Detergent removal by non-polar polystyrene beads. Applications to membrane protein reconstitution and two-dimensional crystallization. *Eur. Biophys. J.* **27**, 305-319.

70. Kelly, S. M., and Price, N. C. (2000) The use of circular dichroism in the investigation of protein structure and function. *Curr. Protein Pept. Sci.* **14**, 349-384.

71. Greenfield, N. J. (2007) Using circular dichroism spectra to estimate protein secondary structure. *Nat. Protoc.* **1**, 2876-2890.

72. Winkler, E., and Klingenberg, M. (1994) Effect of fatty acids on H^+ transport activity of the reconstituted uncoupling protein. *J. Biol. Chem.* **269**, 2508-2515.

73. Klingenberg, M., and Winkler, E. (1985) The reconstituted isolated uncoupling protein is a membrane potential driven H^+ translocator. *EMBO J.* **4**, 3087-3092.

74. Winkler, E., and Klingenberg, M. (1992) An improved procedure for reconstitution of the uncoupling protein and in-depth analysis of H^+/OH^- transport. *Eur. J. Biochem.* **207**, 135-145.

75. Seigneuret, M., and Rigaud, J-L. (1985) Use of the fluorescent pH probe pyranine to detect heterogeneous directions of proton movement in bacteriorhodopsin reconstituted large liposomes. *FEBS Lett.* **188**, 101-106.

76. Orosz, D. E., and Garlid, K. D. (1993) A sensitive new fluorescence assay for measuring proton transport across liposomal membranes. *Anal. Biochem.* **210**, 7-15.

77. Poirot, O., O'Toole, E., and Notredame, C. (2003) Tcoffee@igs: A web server for computing, evaluating and combining multiple sequence alignments. *Nucleic Acids Res.* **31**, 3503-3506.

78. Notredame, C., Higgins, D. G., and Heringa, J. (2000) T-Coffee: A novel method for fast and accurate multiple sequence alignment. *J. Mol. Biol.* **302**, 205-217.

79. Sali, A., Potteron, L., Yuan, F., Van Vlijimen, H., and Karplus, M. (1995) Evaluation of comparative protein modelling by MODELLER. *Proteins* **23**, 318-326.

80. Nury, H., Dahout-Gonzalez, C., Trezeguet, V., Lauquin, G., Brandolin, G., and Pebay-Peyroula, E. (2005) Structural basis for lipid-mediated interactions between mitochondrial ADP/ATP carrier monomers. *FEBS Lett.* **579**, 6031-6036.

81. Ivanova, M.V., Hoang, T., McSorley, F. R., Krnac, G., Smith, M. D., and Jelokhani-Niaraki, M. (2010) A comparative study on conformation and ligand binding of the neuronal uncoupling proteins. *Biochemistry* **49**, 512-521.

82. Jabůrek, M., and Garlid, K.D. (2003) Reconstitution of recombinant uncoupling proteins: UCP1, -2, and -3 have similar affinities for ATP and are unaffected by coenzyme Q_{10}. *J. Biol. Chem.* **278**, 25825-25831.

83. Whitmore, L. and Wallace, B.A. (2004) DICHROWEB: an online server for protein secondary structure analyses from circular dichroism spectroscopic data. *Nucleic Acids Res.* **32**, W668-673.

84. Whitmore, L. and Wallace, B. A. (2008) DICHROWEB, accessed June 30th, 2011 < http://dichroweb.cryst.bbk.ac.uk/htmL/home.shtmL >.

85. Ježek, P., Modrianský, M., and Garlid, K. D. (1997) A structure-activity study of fatty acid interaction with mitochondrial uncoupling protein. *FEBS Lett.* **408**, 166-170.

86. Lowry, O. H., Rosebrough, N. J., Farr, A. L., and Randall R. J. (1951) Protein measurement with the folin phenol reagent. *J. Biol. Chem.* **193**, 265-275.

87. Peterson, G. L. (1997) A simplification of the protein assay method of Lowry et al. which is more generally applicable. *Anal. Biochem.* **83**, 346-356.

88. Huang, X., and Miller, M. (1991) A time-efficient, linear-space local similarity algorithm. *Adv. Appl. Math.* **12**, 337-357.

89. Huang, X., and Miller, M (1991) LALIGN- find multiple matching subsegments in two sequences, accessed June 30th, 2011 < http://www.ch.embnet.org/software/LALIGN_form.htmL >.

90. Wang, Y., and Tajkhorshid, E. (2008) Electrostatic funnelling of substrate in mitochondrial inner membrane carriers. *Proc. Natl. Acad. Sci. U.S.A.* **105**, 9598-9603.

91. Bailey, T. L., and Elkan, C. (1994) Fitting a mixture model by expectation maximization to discover motifs in biopolymers. *Proc. Second Intl. Conf. Intell. Syst. Mol. Biol.* pp. 28-36. Menlo Park, Calif. AAAI Press.

92. Bailey, T. L., and Gribskow, M. (1998) Combining evidence using p-values: application to sequence homology searches. *Bioinformatics* **14**, 48-54.

93. Sokolova, I. M., and Sokolov, E. P. (2005) Evolution of mitochondrial uncoupling proteins: novel invertebrate UCP homologs suggest early evolutionary divergence of the UCP family. *FEBS Lett.* **579**, 313-317.

94. Huang, K. C., Mukhopadhyaym R., and Wingreen, N. S. (2006) A curvature-mediated mechanism for localization of lipids to bacterial poles. *PLoS Comput. Biol.* **2**, e151.

95. Seddon, A. M., Curnow, P., and Booth, P. J. (2004) Membrane proteins, lipids and detergents: not just a soap opera. *Biochim. Biophys. Act.* **1666**, 105-117.

96. Popot, J-L. (2010) Amphipols, nanodisc, and fluorinated surfactants: three nonconventional approaches to studying membrane proteins in aqueous solution. *Annu. Rev. Biochem.* **79**, 737-775.

97. Acehan, D., Malhotra, A., Xu, Y., Ren, M., Stokes, D. L., and Schlame, M. (2011) Cardiolipin affects the supramolecular organization of ATP synthase in mitochondria. *Biophys. J.* **100**, 2184-2192.

98. Daum, G. (1985) Lipids of mitochondria. *Biochim. Biophys. Acta* **822**, 1-42.

99. Meer, G., Voelker, D. R., and Feigenson, G. W. (2008) Membrane lipids: where they are and how they behave. *Nat. Rev. Mol. Cell Biol.* **9**, 112-124.

100. Biran, L. A., and Bartley, W. (1961) Distribution of fatty acids in lipids of rat brain, brain mitochondria and microsomes. *Biochem. J.* **79**, 159-176.

101. Sullivan, P. G., Rippy, N. A., Dorenbos, K., Concepcion, R. C., Agarwal, A. K., and Rho, J. M. (2004) The ketogenic diet increases mitochondrial uncoupling protein levels and activity. *Ann. Neurol.* **55**, 576-580.

102. Ellis, C. E., Murphy, D. C., Golovko, M. Y., Scaglia, F., Bacerlo-Coblijin, G. C., and Nussbaum, R. L. (2005) Mitochondrial lipid abnormality and electron transport chain impairment in mice lacking alpha-synuclein. *Mol. Cell. Biol.* **25**, 10190-10201.

103. Bayir, H., Tyurin, V. A., Tyurina, Y. Y., Viner, R., Ritov, V., Amoscato, A. A., Zhao, Q., Zhang, X. J., Janesko-Feldman, K. L., Alexander, H., Basova, L. V., Clark, R. S., Kochanek, P. M., and Kagan, V. E. (2007) Selective early cardiolipin peroxidation after traumatic brain injury: antioxidative lipidomics analysis. *Ann. Neurol.* **62**, 154-169.

104. Chu, A. C. Y., Ho, P. W. L, Kwok, K. H. H., Ho, J. W.M., Liu, H. F., Chan, K. H., Kung, M. H. W., Ramsden, D. B., and Ho, S. L. (2009) Mitochondrial UCP4 attenuates MPP$^+$ and dopamine-induced oxidative stress, mitochondrial depolarization, and ATP deficiency in neurons, and is interlinked with UCP2 expression. *Free Radic. Biol. Med*. **46**, 810-820.

105. Kwok, K. H. H., Ho, P. W. L., Chu, A. C. Y., Ho, J. W. M., Liu, H. F., Yiu, D. C. W., Chan, K. H., Kung, M. H. W., Ramsden, D. B., and Ho, S. L. (2010) Mitochondrial UCP5 is neuroprotective by preserving mitochondrial membrane potential, ATP level, and reducing oxidative stress in MPP$^+$ and dopamine toxicity. *Free Radic. Biol. Med*. **49**, 1023-1035.

106. Enerback, S. (2010) Human brown adipose tissue. *Cell Metab.* **11**, 248-252.

107. Boss, O., Samec, S., Kuhne, F., Bijlenga, P., Assimacopoulos-Jeannet, D., Seydoux, J., Giacobino, J. P., and Muzzin, P. (1998) Uncoupling protein-3 expression in rodent skeletal muscle is modulated by food intake but not by changes in environmental temperatures. *J. Biol. Chem*. **273**, 5-8.

108. Millet, L., Vidal, H., Andreelli, F., Larrouy, D., Riou, J. P., Ricquier, D., Laville, M., and Lagin, D. (1997) Increased uncoupling protein-2 and -3 mRNA expression during fasting in obese and lean humans. *J. Clin. Invest*. **100**, 2665-2670.

109. Tsuboyama-Kasaoka, N., Tsunoda, N., Maruyama, K., Takahashi, M., Kim, H., Ikenmoto, S., and Ezaki, O. (1998) Upregulation of uncoupling protein 3 (UCP3) mRNA by exercise training and down-regulation of UCP3 by denervation in skeletal muscle. *Biochem. Biophys. Res. Commun*. **247**, 498-503.

110. Schrauwen, P., Hesselink, M. K., Vaartjes, I., Kornips, E., Saris, W. H., Giacobino, J. P., and Russel, A. (2000) Effect of acute exercise on uncoupling protein 3 is a fat metabolism-mediated effect. *Am. J. Physiol. Endocrinol. Metab*. **282**, E11-E17.

111. Matsuda, J., Hosoda, K., Itoh, H., Son, C., Doi, K., Tanaka, T., Fukunaga, Y., Inoue, G., Nishimura, H., Yoshimasa, Y., Yamori, Y., and Nakao, K. (1997) Cloning of rat uncoupling protein-3 and uncoupling protein-2 cDNAs: their gene expression in rats fed high-fat diet. *FEBS Lett*. **418**, 200-204.

112. Schrauwen, P., Hoppeler, H., Billeter, R., Bakker, A. H., and Pendergast, D. R. (2001) Fiber type dependent upregulation of human skeletal muscle UCP2 and UCP3 mRNA expression by high-fat diet. *Int. J. Obes. Relat. Metab. Disord*. **25**, 449-456.

113. Morell, P. (1984) Myelin. Plenum Press, New York.

114. Etchay, K. S., Winkler, E., and Klingenberg, M. (2000) Coenzyme Q is an obligatory cofactor for uncoupling protein function. *Nature* **408**, 609-613.

115. Brand, M. D., Affourtit, C., Esteves, T., Green, K., Lambert, A. J., Miwa, S., Pakay, J. L., and Parker, N. (2004) Mitochondrial superoxide: production, biological effects, and activation of uncoupling proteins. *Free Radic. Biol. Med*. **37**, 755-767.

116. Azzu, V., and Brand, M. D. (2010) The on-off switches of the mitochondrial uncoupling proteins. *Trends Biochem. Sci*. **25**, 298-307.

117. Trezeguet, V., Pelosi, L., Lauquin, G. J. M., and Brandolin, G. (2008) The mitochondrial ADP/ATP carrier: functional and structural studies in the route of elucidating pathological aspects. *J. Bioenerg. Biomembr*. **40**, 435-443.

118. Berardi, M., Shih, W M., Harrison, S. C., and Chou, J. J. (2011) Mitochondrial uncoupling protein 2 structure determined by NMR molecular fragment searching. *Nature* **476**, 109-113.

APPENDICES

APPENDIX 1 – Structure, physical and chemical properties of detergents and phospholipids used in this study

Detergents

	Class of detergents	Structure	MW (g/mol)	CMC (mM)	Cloud point (^{o}C)
TX-100	Non-ionic		625	0.2-0.9	65
TX-114	Non-ionic		537	0.2	23
C_8E_4	Non-ionic		306	7.2	
Sarcosyl	Anionic		293	14.6	----
SDS	Anionic		289	7-10	>100

Lipids

	Class of phospholipid	Structure	MW (g/mol)
1,1',2,2' Tetraoleoyl Cardiolipin	Anionic/ synthetic		1500
Azolectin	Mixed/ natural lipids		avg.768

APPENDIX 2 – Protein sequence analysis and models of neuronal UCPs

```
UCP5_HUMAN    MGIFP-GIILIFLRVKFATAAVIVSGHQKSTTVSHEMSGLNWKPFVYGGL
UCP4_HUMAN    MSVPEEEERLL--------------------PLTQRWPRASKFLLSGC
UCP2_HUMAN    MVGFKATDV----------------------PPTATVKFLGAGT
UCP3_HUMAN    MVGLKPSDV----------------------PPTMAVKFLGAGT
UCP1_HUMAN    MGGLTASDV----------------------HPTLGVQLFSAGI
ADT1_BOVIN    M-----SDQ----------------------ALSFLKDFLAGGV
                      *                              :. .*

UCP5_HUMAN    ASIVAEFGTFPVDLTKTRLQVQGQSIDAR-----FKEIKYRGMFHALFRI
UCP4_HUMAN    AATVAELATFPLDLTKTRLQMQGEAALARLGDGARESAPYRGMVRTALGI
UCP2_HUMAN    AACIADLITFPLDTAKVRLQIQGESQGPV---RATASAQYRGVMGTILTM
UCP3_HUMAN    AACFADLVTFPLDTAKVRLQIQGENQA-V---QTARLVQYRGVLGTILTM
UCP1_HUMAN    AACLADVITFPLDTAKVRLQVQGECP-------TSSVIRYKGVLGTITAV
ADT1_BOVIN    AAAISKTAVAPIERVKLLLQVQHASKQ------ISAEKQYKGIIDCVVRI
              *: .:.   . *:: .* **:*          *:*:.     :

UCP5_HUMAN    CKEEGVLALYSGIAPALLRQASYGTIKIGIYQSLKRLFVERLED-E-TLL
UCP4_HUMAN    IEEEGFLKLWQGVTPAIYRHVVYSGGRMVTYEHLREVVFGKSEDEHYPLW
UCP2_HUMAN    VRTEGPRSLYNGLVAGLQRQMSFASVRIGLYDSVKQFYTK-GSEH-ASIG
UCP3_HUMAN    VRTEGPCSPYNGLVAGLQRQMSFASIRIGLYDSVKQVYTPKGADN-SSLT
UCP1_HUMAN    VKTEGRMKLYSGLPAGLQRQISSASLRIGLYDTVQEFLTA-GKETAPSLG
ADT1_BOVIN    PKEQGFLSFWRGNLANVIRYFPTQALNFAFKDKYKQIFLGG-VDRHKQFW
               . :*     : * . : *        .:   :   :..      :    :

UCP5_HUMAN    I----NMICGVVSGVISSTIANPTDVLKIRMQAQGSL--------FQGSM
UCP4_HUMAN    K----SVIGGMMAGVIGQFLANPTDLVKVQMQMEGKRKLEGKPLRFRGV-
UCP2_HUMAN    S----RLLAGSTTGALAVAVAQPTDVVKVRFQAQARAGG---GRRYQST-
UCP3_HUMAN    T----RILAGCTTGAMAVTCAQPTDVVKVRFQASIHLGPSRSDRKYSGT-
UCP1_HUMAN    S----KILAGLTTGGVAVFIGQPTEVVKVRLQAQSHLHG--IKPRYTGT-
ADT1_BOVIN    RYFAGNLASGGAAGATSLCFVYPLDFARTRLAADVGKGA--AQREFTGL-
                       :   *  :*  .      * :. : ::  .            :.

UCP5_HUMAN    IGSFIDIYQQEGTRGLWRGVVPTAQRAAIVVGVELPVYDITKKHLILSGM
UCP4_HUMAN    HHAFAKILAEGGIRGLWAGWVPNIQRAALVNMGDLTTYDTVKHYLVLNTP
UCP2_HUMAN    VNAYKTIAREEGFRGLWKGTSPNVARNAIVNCAELVTYDLIKDALLKANL
UCP3_HUMAN    MDAYRTIAREEGVRGLWKGTLPNIMRNAIVNCAEVVTYDILKEKLLDYHL
UCP1_HUMAN    YNAYRIIATTEGLTGLWKGTTPNLMRSVIINCTELVTYDLMKEAFVKNNI
ADT1_BOVIN    GNCITKIFKSDGLRGLYQGFNVSVQGIIIYRAAYFGVYDTAKGML-----
               .   *    *  **: *    .    :    . .** *  :

UCP5_HUMAN    MGDTILTHFVS----SFTCGLAGALASNPVDVVRTRMMNQRA-IVGHVDL
UCP4_HUMAN    LEDNIMTHGLS----SLCSGLVASILGTPADVIKSRIMNQPRDKQGRGLL
UCP2_HUMAN    MTDDLPCHFTS----AFGAGFCTTVIASPVDVVKTRYMNSALG------Q
UCP3_HUMAN    LTDNFPCHFVS----AFGAGFCATVVASPVDVVKTRYMNSPPG------Q
UCP1_HUMAN    LADDVPCHLVS----ALIAGFCATAMSSPVDVVKTRFINSPPG------Q
ADT1_BOVIN    -PDPKNVHIIVSWMIAQTVTAVAGLVSYPFDTVRRRMMMQSG-RKGADIM
                *       *       :              . * *.:: * : .

UCP5_HUMAN    YKGTVDGILKMWKHEGFFALYKGFWPNWLRLGPWNIIFFITYEQLKRL----------QI
UCP4_HUMAN    YKSSTDCLIQAVQGEGFMSLYKGFLPSWLRMTPWSMVFWLTYEKIREMS------GVSPF
UCP2_HUMAN    YSSAGHCALTMLQKEGPRAFYKGFMPSFLRLGSWNVVMFVTYEQLKRALMAACTSREAPF
UCP3_HUMAN    YFSPLDCMIKMVAQEGPTAFYKGFTPSFLRLGSWNVVMFVTYEQLKRALMKVQMLRESPF
UCP1_HUMAN    YKSVPNCAMKVFTNEGPTAFFKGLVPSFLRLGSWNVIMFVCFEQLKRELSKSRQTMDCAT
ADT1_BOVIN    YTGTVDCWRKIAKDEGPKAFFKGAWSNVLR-GMGGAFVLVLYDEIKKF----------V
               *  .          **  ::** .. **    . ... : ::::::.
```
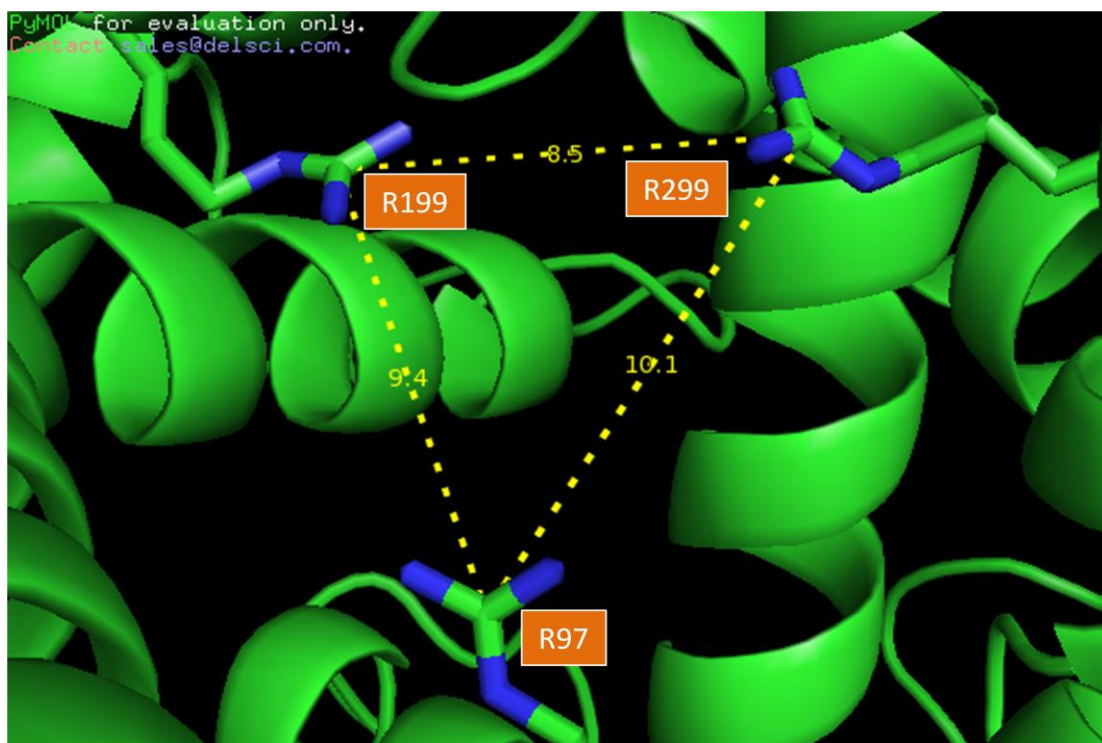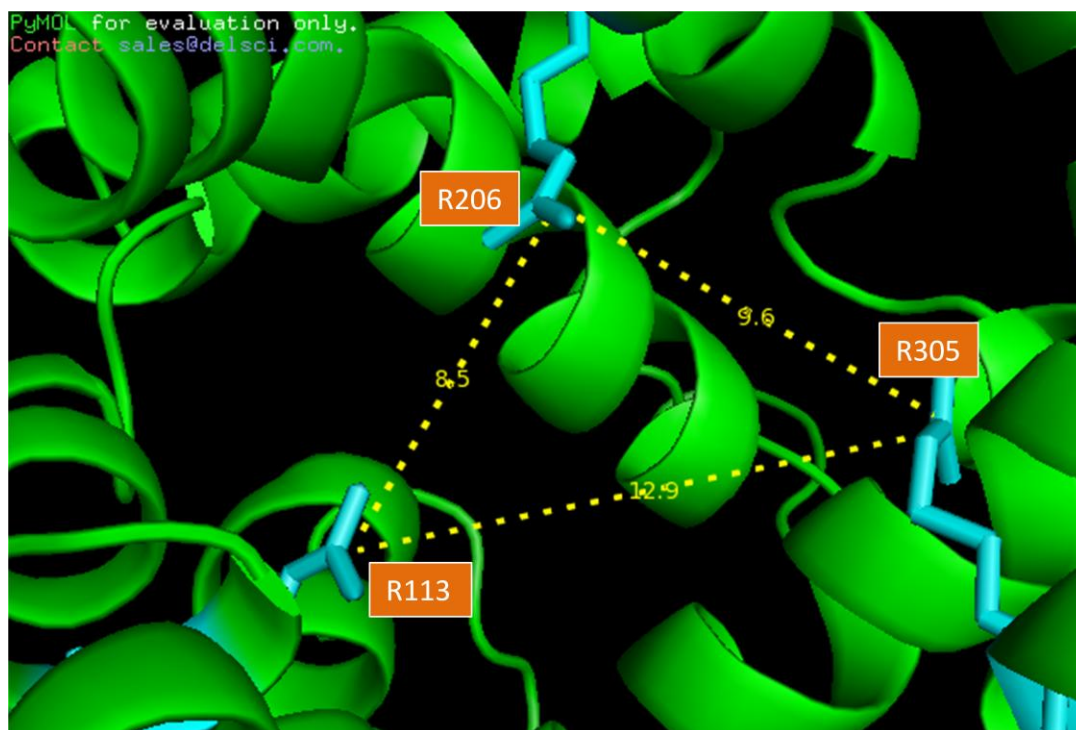
Figure 24 – Sequence alignment of UCPs and AAC.

Sequences of UCP5 (O95258), UCP4 (O95847), UCP3 (P55916), UCP2 (P55851), UCP1 (P25874), and ADP/ATP carrier (P02722) were aligned using T-Coffee program [62, 63]. The identical residues are denoted by "*", the conserved substitutions by ":", and the semi-conserved substitutions by ".". Identical residues in UCPs are underlined, while conserved residues in UCP4 and UCP5 that are modified in UCP1-3 are highlighted.

Figure 25 – Hypothetical ATP binding pocket of UCP4

The model was built in Pymol after sequence alignment (T-coffee) using AAC as blueprint (MODELLER). Distance between R97, R199, and R299 were measured from the carbons of the capped guanidinium group in each Arg residue.
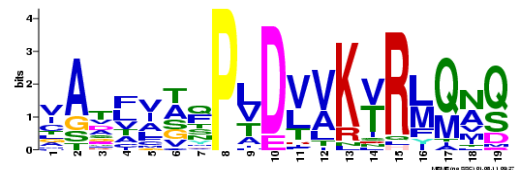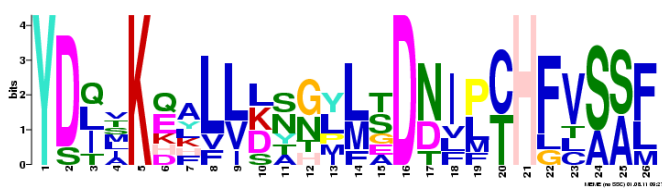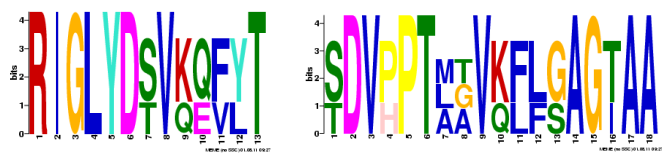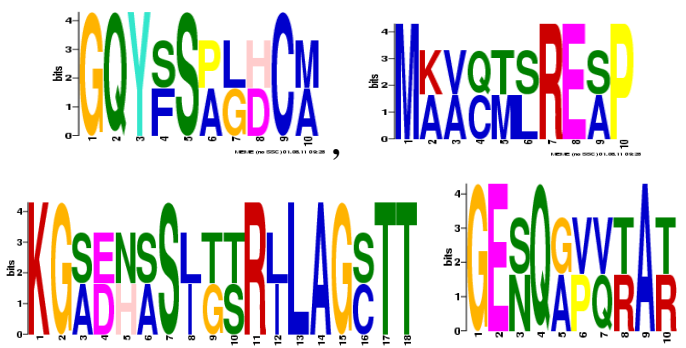
Figure 26 – Hypothetical ATP binding pocket of UCP5

The model was built in Pymol after sequence alignment (T-coffee) using AAC as blueprint (MODELLER). Distance between R113, R206, and R305 were measured from the carbons of the capped guanidinium group in each Arg residue.

Table 4 – Some common motifs among MCF members*

UCP5 (O95258), UCP4 (O95847), UCP3 (P55916), UCP2 (P55851), UCP1 (P25874), ADP/ATP carrier (1OKC), DIC (Q9UBX3), and OGMC (Q02978) were analyzed using the pattern prediction program package MEME-MAST (at least 10 residues in each motif)

Specificity	Detailed motifs	Motif length (amino acids)
All MCF members		**26**
		19
UCP1-5, DIC, and OGMC		**26**
		10
UCP1-3		**13, 18**
UCP2 and UCP3		**10, 10 18, 10**

<u>APPENDIX 3</u> – Secondary structure composition of UCP proteoliposomes with and without 100 µM ATP

Deconvolution of the CD spectra was performed using CDSSTR program on the Dichroweb website (see section 3.2.4). The values represent the percentage of secondary structure composition. NRMSD, normalized root mean square deviation, denotes the best fit between the calculated and the experimental CD spectra.

		Protein	α-helix	β-strand	Turn	Random	NRMSD
Azolectin vesicles	UCP2	No ATP	52	16	17	15	0.016
		+100 µM ATP	54	13	17	18	0.020
	UCP4	No ATP	51	12	17	20	0.015
		+100 µM ATP	51	13	18	19	0.015
	UCP5	No ATP	8	32	23	38	0.017
		+100 µM ATP	24	23	17	35	0.031
Azolectin vesicles with 2.5 mol% CL	UCP2	No ATP	34	22	19	24	0.026
		+100 µM ATP	34	23	20	23	0.031
	UCP4	No ATP	46	19	17	18	0.013
		+100 µM ATP	51	13	18	18	0.023
	UCP5	No ATP	15	32	22	31	0.022
		+100 µM ATP	21	28	20	32	0.017

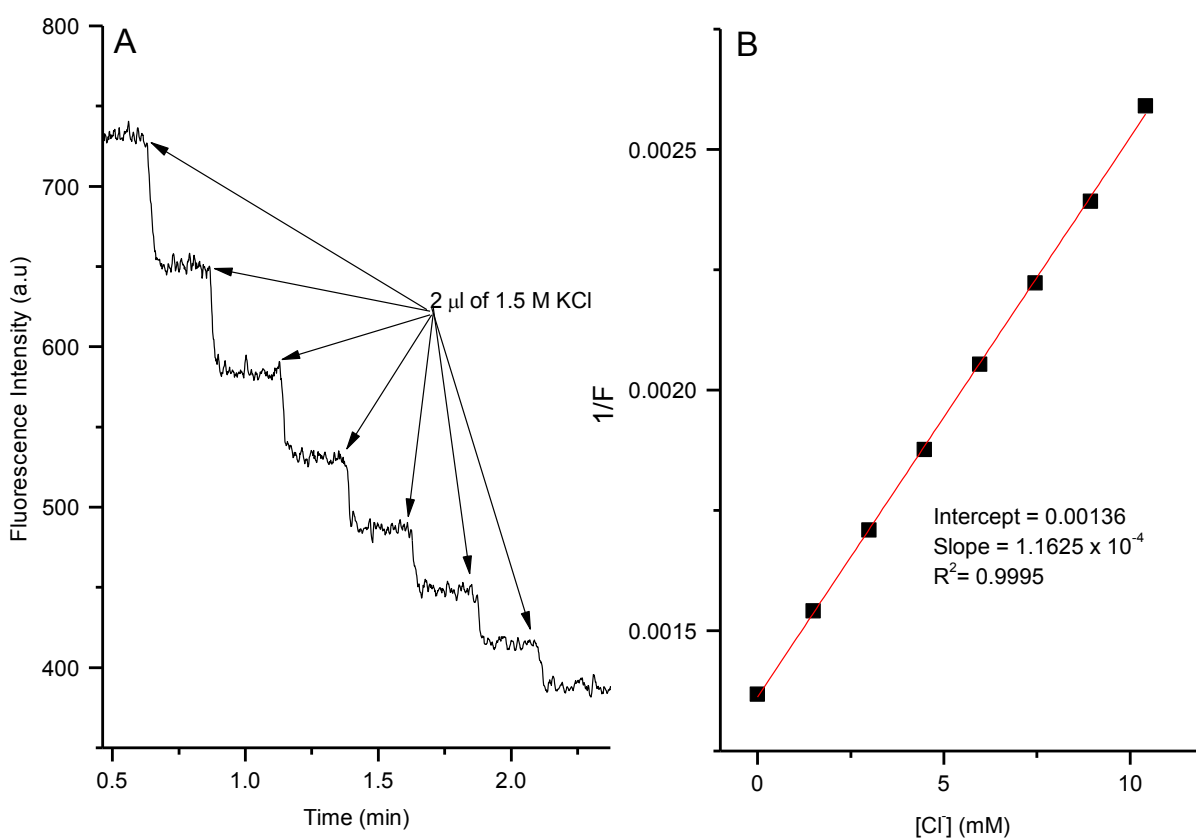# APPENDIX 4 – Calibration of SPQ fluorescence signals and liposome internal volumes
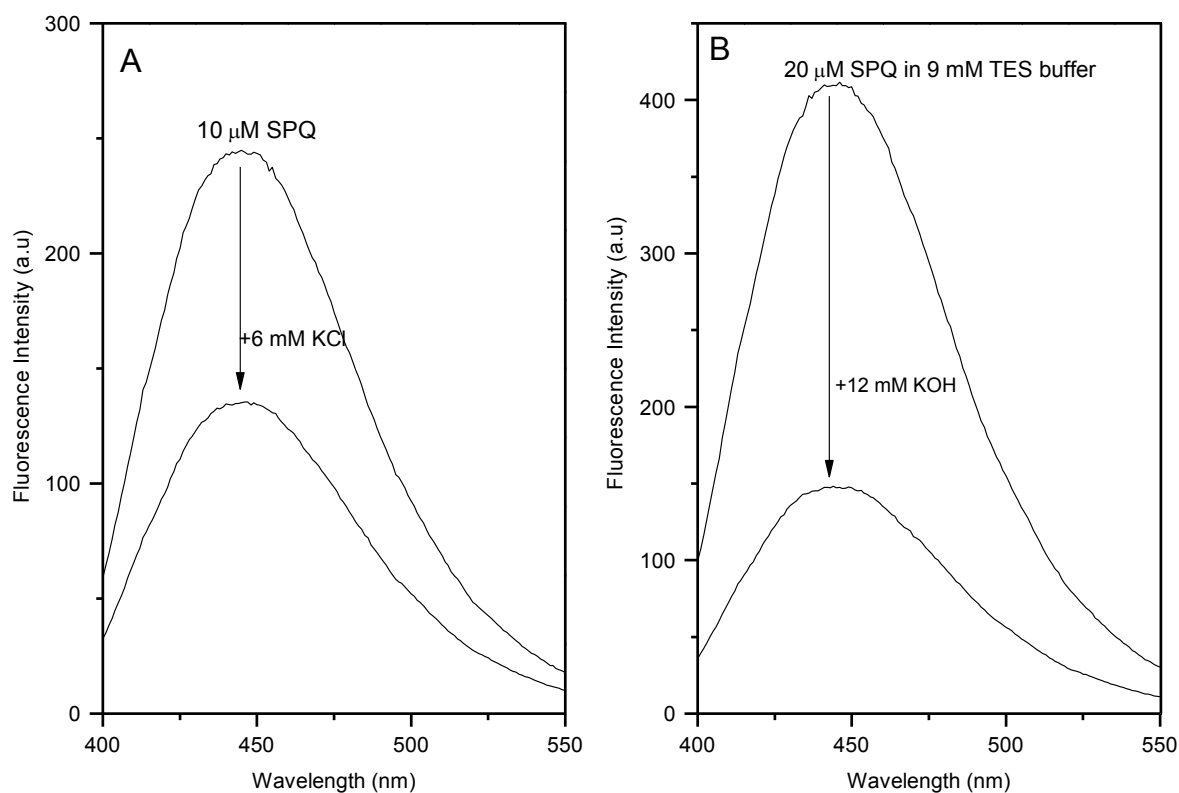
Figure 27 – Fluorescence quenching of SPQ by KCl (A) and TES anion buffer (B)

SPQ fluorescent probe was excited at 347 nm and its emission intensity (λ_{max} = 444 nm) was decreased by 6 mM KCl (A), or by 12 mM KOH (in the presence of 9 mM TES buffer) (B).
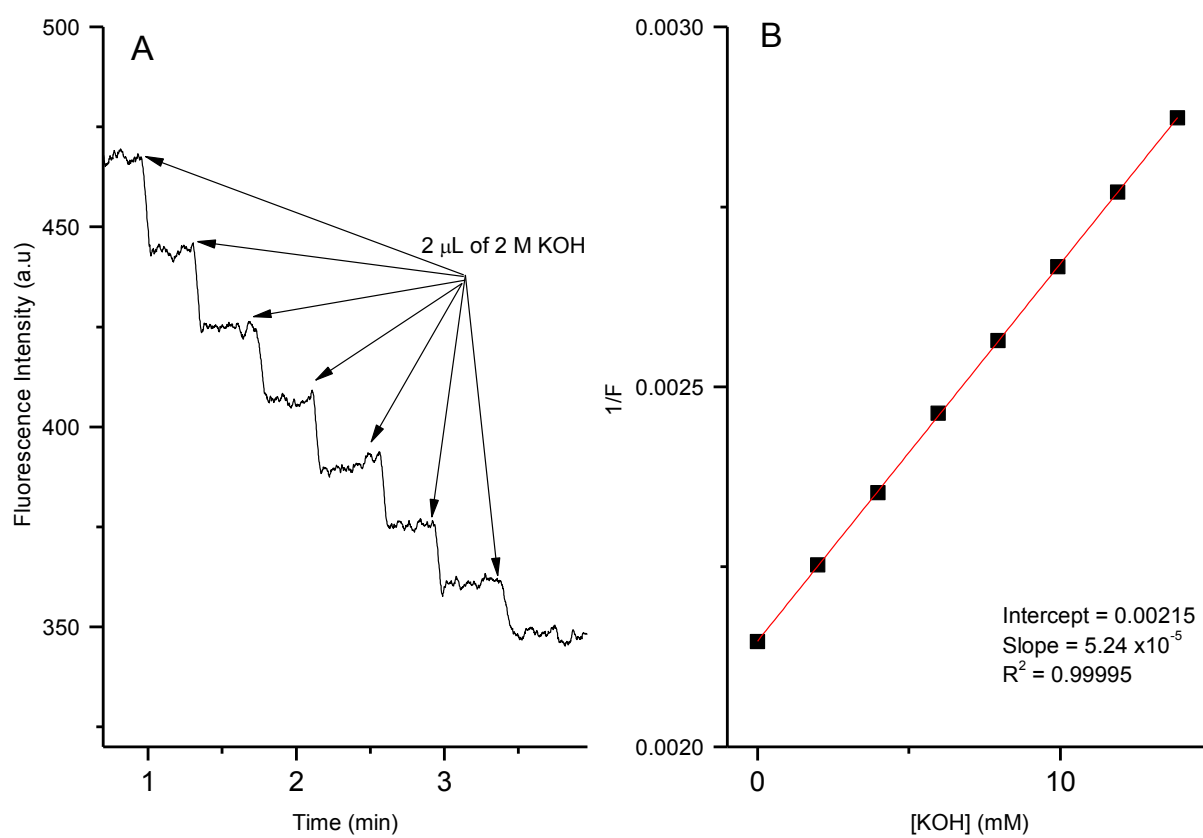
<u>Figure 28</u> – A representative of SPQ fluorescence signal calibration in proton flux assays

(A) 2 μl of 2 M KOH was added step-wise to a proteoliposome sample in internal buffer and 1 μM nigericin. (B) The Stern-Volmer constant was determined by a linear plot of 1/F vs. [KOH].

Figure 29 – An example of SPQ fluorescence signal calibration in chloride transport assays

(A) 2 μl of 1.5 M KCl was added step-wise to a proteoliposome sample in internal buffer and mixture nigericin/tributyltin (0.4 μM/ 4 μM). (B) The Stern-Volmer constant was determined by a linear plot of 1/F vs. [KCl].
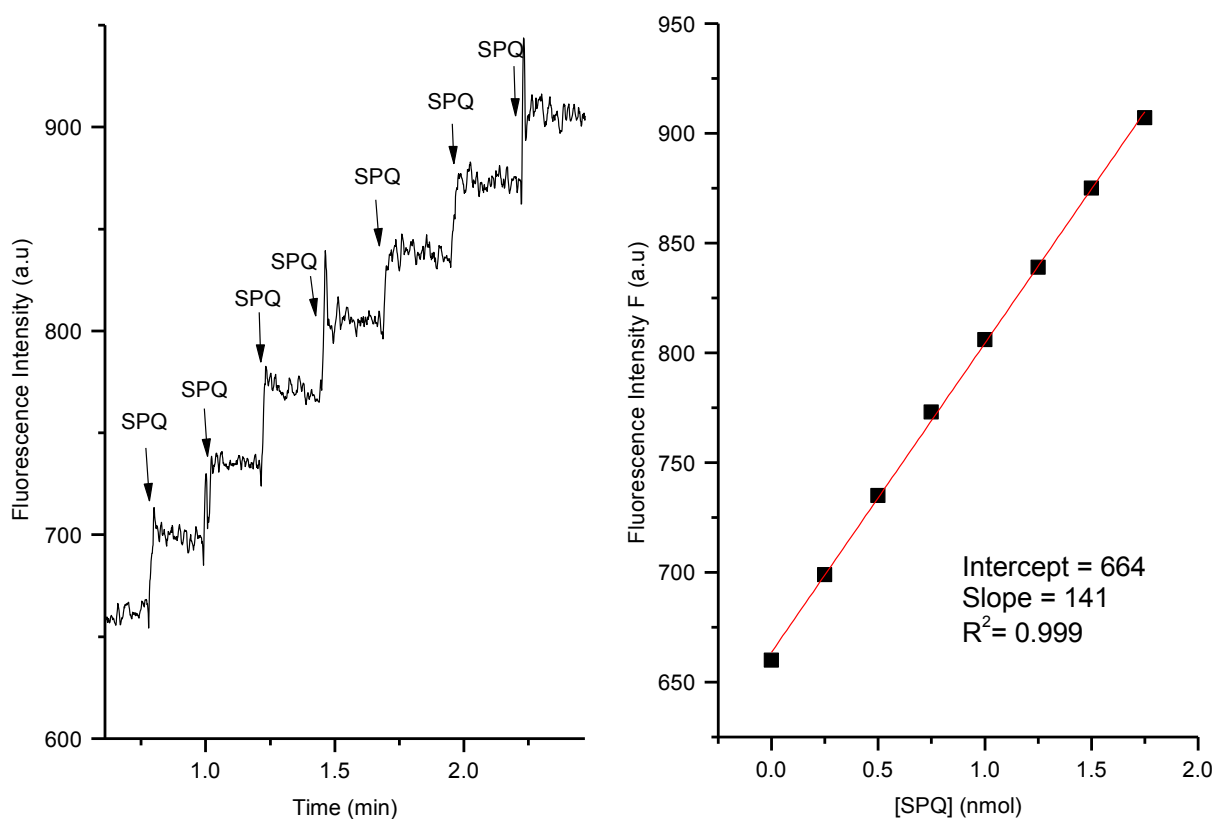
<u>Figure 30</u> – An example of liposomal volume calibration in ion transport measurement

(A) Fluorescent probe SPQ was added sequentially to liposome that was already dissolved in 0.25 % (w/v) C_8E_4. (B) Standard addition of SPQ yielded a linear relationship with fluorescence intensity at 442 nm, which helped determine the concentration of trapped SPQ.